SMIP2000

SMIP2000 SEMINAR ON
UTILIZATION OF STRONG-MOTION DATA

Sacramento, California
September 14, 2000

PROCEEDINGS

Sponsored by

California Strong Motion Instrumentation Program
Division of Mines and Geology
California Department of Conservation

Supported in Part by

California Seismic Safety Commission
Federal Emergency Management Agency

The California Strong Motion Instrumentation Program (CSMIP) is a program within the Division of Mines and Geology of the California Department of Conservation and is advised by the Strong Motion Instrumentation Advisory Committee (SMIAC), a committee of the California Seismic Safety Commission. Current program funding is provided by an assessment on construction costs for building permits issued by cities and counties in California, with additional funding from the California Department of Transportation, the Office of Statewide Health Planning and Development, and the California Department of Water Resources.

In January 1997, a joint project, TriNet, between CDMG, Caltech and USGS was funded by the Federal Emergency Management Agency (FEMA) through the California Office of Emergency Services (OES). The goals of the project are to record and rapidly communicate ground shaking information in southern California, and to analyze the data for the improvement of seismic codes and standards.

DISCLAIMER

SMIP2000

SMIP2000 SEMINAR ON
UTILIZATION OF STRONG-MOTION DATA

Sacramento, California
September 14, 2000

PROCEEDINGS

Edited by

Moh Huang

Sponsored by

California Strong Motion Instrumentation Program
Division of Mines and Geology
California Department of Conservation

Supported in Part by

California Seismic Safety Commission
Federal Emergency Management Agency

PREFACE

The California Strong Motion Instrumentation Program (CSMIP) in the Division of Mines and Geology of the California Department of Conservation promotes and facilitates the improvement of seismic codes and design practices through the Data Interpretation Project. The objective of this project is to increase the understanding of earthquake strong ground shaking and its effects on structures through interpretation and analysis studies of strong-motion data. The ultimate goal is to accelerate the process by which lessons learned from earthquake data are incorporated into seismic code provisions and seismic design practices.

Since the establishment of CSMIP in the early 1970s, over 800 stations have been installed, including 550 ground-response stations, 162 buildings, 20 dams and 60 bridges. Significant strong-motion records have been obtained from many of these stations. One of the most important sets of strong-motion records is from the 1994 Northridge earthquake. During this earthquake strong-motion records were obtained from 116 ground-response stations and 77 extensively-instrumented structures. In addition to these records, CSMIP in cooperation with the City of Los Angeles and other agencies, collected and archived accelerograms recorded at over 300 high-rise buildings during the Northridge earthquake. These buildings were instrumented by the building owners as required by the City's Building Code. The strong-motion records from the Northridge earthquake have been and will be the subject of CSMIP data interpretation projects.

The SMIP2000 Seminar is the 12th in a series of annual technical seminars designed to transfer recent interpretations and findings on strong-motion data to practicing seismic design professionals and earth scientists. The goal of the Seminar is to increase the utilization of strong-motion data in improving post-earthquake response, seismic design codes and practices.

In this seminar, investigators of three CSMIP-funded data interpretation projects and invited experts will present the results from studies on data from ground response stations, steel frame buildings, bridges and downhole geotechnical arrays, on measured ground motion and observed damage in the 1999 Taiwan earthquake, and on seismic performance evaluation of transportation structures. In addition, there will be presentations on the virtual strong-motion data center of the Consortium of Organizations for Strong-Motion Observation Systems (COSMOS) and the TriNet engineering strong-motion data center. Director Darryl Young of the Department of Conservation will present a luncheon address on the importance of strong motion programs for California.

The papers in this Proceedings volume presented by the investigators of the CSMIP-funded data interpretation projects represent interim results. Following this seminar the investigators will prepare final reports with their final conclusions. These reports will be more detailed and will update the results presented here. CSMIP will make these reports available after the completion of the studies.

Moh J. Huang
Data Interpretation Project Manager

TABLE OF CONTENTS

Seminar Program

Ground Motion Amplification as a Function of Surface Geology 1
Jonathan Stewart and Andrew Liu

Recent Data Recorded from Downhole Geotechnical Arrays 23
Vladimir Graizer, Anthony Shakal and Pat Hipley

Validation of Evaluation Methods and Acceptance Criteria in Evolving Peformance-Based Seismic Codes 39
Sashi Kunnath, Quan Nghiem, Alfred John and Sherif El-Tawil

Seismic Performance Evaluation of Transportation Structures. 65
Joseph Penzien and Wen Tseng

System Identification and Modeling of Bridge Systems for Assessing Current Design Procedures 77
Yalin Arici and Khalid Mosalam

COSMOS Virtual Strong Motion Data Center 97
Ralph Archuleta

TriNet Engineering Strong Motion Data Center 115
Anthony Shakal and Criag Scrivner

SMIP2000 SEMINAR ON UTILIZATION OF STRONG-MOTION DATA

Conventional Center, Sacramento, California
September 14, 2000

FINAL PROGRAM

8:00 - 9:00 **Registration**

9:00 - 9:10 **Welcoming Remarks**
Bruce Bolt and *Ashok Patwardhan*, Strong Motion Instrumentation Advisory Committee (SMIAC)
James Davis, State Geologist, Division of Mines and Geology

9:10 - 9:20 **Introductory Remarks**
Anthony Shakal and *Moh Huang*, DMG/Strong Motion Instrumentation Program

SESSION I **GROUND MOTIONS**
Moderator: *Bruce Bolt*, UC Berkeley
Chair, SMIAC Ground Response Subcommittee

9:20 - 9:45 **Ground Motion Amplification as a Function of Surface Geology**
Jonathan Stewart and Andrew Liu, UCLA, Los Angeles

9:45 - 10:10 **Recent Data Recorded from Downhole Geotechnical Arrays**
Vladimir Graizer, Anthony Shakal, DMG/SMIP and Pat Hipley, Caltrans

10:10 - 10:30 **Questions and Answers for Session I**

10:30 - 10:50 Break

SESSION II **BUILDING RESPONSE**
Moderator: *Chris Poland*, Degenkolb Engineers
Chair, SMIAC Buildings Subcommittee

10:50 - 11:15 **Validation of Evaluation Methods and Acceptance Criteria in Evolving Performance-Based Seismic Codes**
Sashi Kunnath, Quan Nghiem, Alfred John and *Sherif El-Tawil*, University of Central Florida

11:15 - 11:40 **Observation on the Correlation between Measured Ground Motion and Observed Damage in the 1999 Taiwan Earthquake**
Chris Poland and Jon Heintz, Degenkolb Engineers

11:40 - 12:00 **Questions and Answers for Session II**

12:00 - 1:55 **Luncheon**
Introduction *James Davis*, State Geologist, Division of Mines and Geology
Speaker*: Darryl Young*, Director, Department of Conservation

SESSION III **LIFELINE STRUCTURE RESPONSE**
Moderator: *Vern Persson*
Chair, SMIAC Lifelines Subcommittee

2:00 - 2:25 **Seismic Performance Evaluations of Transportation Structures**
Joseph Penzien and *Wen Tseng*, International Civil Engineering Consultants

2:25 - 2:50 **System Identification and Modeling of Bridge Systems for Assessing Current Design Procedures**
Yalin Arici and *Khalid Mosalam*, UC Berkeley

2:50 - 3:00 **Questions and Answers for Session III**

3:00 - 3:20 Break

SESSION IV **DATA DISSEMINATION THROUGH INTERNET**
Moderator: *Wilfred Iwan*, Caltech
Chair, SMIAC Data Utilization Subcommittee

3:20 - 3:45 **COSMOS Virtual Strong Motion Data Center**
Ralph Archuleta, UC Santa Barbara;

3:45 – 4:00 **TriNet Engineering Strong Motion Data Center**
Anthony Shakal and Craig Scrivner, DMG/SMIP

4:00 - 4:10 **COSMOS Update**
Carl Stepp, COSMOS

4:10 - 4:20 **Questions and Answers for Session IV**

4:20 **Closing Remarks**

GROUND MOTION AMPLIFICATION AS A FUNCTION OF SURFACE GEOLOGY

Jonathan P. Stewart and Andrew H. Liu
University of California, Los Angeles

ABSTRACT

Empirical relationships are developed to predict amplification factors for 5% damped spectral acceleration as a function of surface geology. Amplification factors are derived for spectral periods T = 0.01 – 5 s by assigning a reference spectrum to > 700 recordings from shallow crustal earthquakes. The reference spectrum is derived from soft rock attenuation relations modified to account for event-specific source/path peculiarities and rupture directivity effects. Strong motion sites are classified according to three geologic classification schemes: age only, age + depositional environment, and age + material gradation. Within each scheme, amplification is regressed against ground motion amplitude, and for one scheme, against amplitude and duration. The material gradation scheme is found to produce the least scatter in the amplification functions. The results of the regression indicate significant nonlinear ground response effects, and pronounced variations in the levels of amplification across geological categories. Amplification is also found to be sensitive to the duration of strong shaking. Due to the soft rock reference spectra used in this study, amplification levels are smaller than had been identified in previous studies employing reference motions from relatively firm rock sites.

INTRODUCTION

It has long been recognized that geologic conditions can exert a strong influence on ground motions and structural damage patterns (e.g., Seed et al., 1972; Seed et al., 1987; Seed et al., 1991; Chang et al., 1996; Rathje et al., 2000). Quantification of site amplification effects from strong motion recordings requires the removal of source and path effects. This has typically been accomplished by one of three techniques. The first and most common technique compares rock and soil motions recorded in close proximity to each other (e.g., Borcherdt, 1970; Seed and Idriss, 1971; Idriss, 1990; Borcherdt and Glassmoyer, 1994; Dickenson and Seed, 1996; Borcherdt, 1996; Rathje et al., 2000). Comparisons of this type, performed by Borcherdt (1994) on 35 strong motion stations (with 9 accompanying reference sites) that recorded the 1989 Loma Prieta earthquake, comprise the principal empirical basis for the ground motion provisions in the 1997 Uniform Building Code (*Uniform*, 1997) and 1997 National Earthquake Hazards Reduction Program Code and Commentary (BSSC, 1998). A modified version of this approach has also been used in which rock site spectra are applied as a reference motion across a relatively broad region by correcting motions with a geometric spreading factor of 1/r (e.g., Borcherdt, 1996), or by coupling geometric spreading with a frequency-dependant attenuation model (e.g., Hartzell et al., 1996; Hartzell et al., 1997).

Alternative approaches for evaluating ground motion amplification on soil do not require the presence of a reference site. Such approaches have the distinct advantage of being able to incorporate essentially all available earthquake recordings. One such approach, termed horizontal-to-vertical spectral ratio (HVSR), involves normalizing the horizontal component

spectra for a given site by the vertical component spectra for that same site (Lermo and Chavez-Garcia, 1993). A second approach implements a generalized inversion scheme to identify source, path, and site effects for a given earthquake (Boatwright et al., 1991). While this approach, when properly implemented, can reproduce spectral ratios comparable to those observed from adjacent rock/soil sites (e.g., Field and Jacob, 1995), considerable amounts of strong motion and geologic data are needed to obtain reliable inversions. Moreover, a reliable assessment of site effects is needed *a priori*, which limits the usefulness of the approach for identifying such effects from strong motion records.

This study implements a third approach not requiring the presence of a reference site. Amplification is defined using the acceleration response spectra of recordings normalized by a reference spectrum that represents the ground motions that would have been expected at the site had the geologic condition been soft rock. The reference spectrum is defined using an attenuation relation for rock sites in active tectonic regions modified for source-specific peculiarities and rupture directivity effects. As such, this approach incorporates the observed, event-specific characteristics of source and path into the reference motions so that the ratio of recorded/reference spectra represents as cleanly as possible the effects of local geologic conditions on the ground motion. This approach is conceptually similar to that employed by Sokolov and his co-workers (e.g., Sokolov, 1997; Sokolov et al., 2000) in which spectral ratios are calculated using recordings and reference motions from attenuation models for “very hard rock” sites. The principal difference from our approach is that Sokolov uses attenuation models derived for Fourier spectra (instead of response spectra) that do not incorporate the effects of source mechanism, directivity, or event-specific source/path peculiarities. The present approach, by using response spectra in lieu of Fourier spectra, leverages significant recent developments in ground motion attenuation relationships for spectral acceleration that allow these effects to be incorporated into the estimation of reference motions.

A total of 433 recording stations were classified based on mapped surficial geology. Amplification factors are derived for each recording, and are regressed within various categories of surficial geology against ground motion amplitude. Median levels of amplification, as well as the standard error of amplification, are compiled across geologic site categories to evaluate the effect of geologic conditions on amplification and to identify the advantages of incorporating different levels of detail in geologic site classifications. This paper presents preliminary results of work in progress, as additional strong motion and geologic data is becoming available for sites that recorded the recent earthquakes in Turkey in Taiwan. Moreover, amplification factors are also being examined as a function of 30 m shear wave velocity (V_s), and geotechnical classification schemes.

STRONG MOTION DATABASE

The strong motion database includes 704 recordings from 433 stations and 44 events between 1933 and 1999. The source information for this database includes the Pacific Engineering and Analysis Strong Motion (PE&A) database, the National Geophysical Data Center database (shallow crustal events only), and data provided by the State of California (CSMIP), U.S. Geological Survey, University of Southern California (USC), and Los Angeles Department of Water and Power. Data from the 1995 Hyogo-Ken Nanbu (Kobe) earthquake, the

1999 Kocaeli and Duzce earthquakes in Turkey, and the 1999 Chi-Chi earthquake in Taiwan are not included in this compilation due to inadequate sources of geologic information for the recording station sites and a lack of uniformly processed ground motion records as of this writing.

GEOLOGIC SITE CLASSIFICATIONS

Geologic conditions at each strong motion station were classified. The level of mapping detail for Quaternary deposits is variable across California, where most of the stations are located. The geology of the entire state is documented on 27 maps at 1:250,000 scale by the California Division of Mines and Geology (CDMG, 1959-1998). These maps distinguish Quaternary deposits based on age (Holocene-Pleistocene) and generalized descriptions of depositional environment. The Southern California Aerial Mapping Project (SCAMP) is compiling more detailed geologic information for selected quadrangles in southern California. For example, data for the Santa Ana 30' x 60' quadrangle has been prepared at 1:100,000 scale by Morton et al. (1999) and was used in this study. In addition, preliminary digital geologic maps at 1:24,000 scale prepared through SCAMP of 7.5' quadrangles in Los Angeles and Orange counties have been obtained (CDMG staff, 2000). The SCAMP maps are the most detailed of the available geologic maps, providing basic information on the gradation of Quaternary deposits (e.g., coarse/fine/mixed), and detailed information on depositional environment. Information from the above sources was supplemented as necessary with field geologic classifications for strong motion stations by Geomatrix (1993) and by the authors.

Attempts were made to classify each site according to schemes that make use of different levels of detail on geologic conditions. Three different schemes were used so that the sensitivity of ground motion amplification to various mapped geologic parameters could be discerned. Criteria used for the geologic classifications are presented in Table 1. The three classification schemes are as follows: age only, age + depositional environment, age + material gradation. Length restrictions preclude a full listing of the site classifications, but these will be published in a forthcoming report.

Table 1: Criteria for geologic classifications

Age	Depositional Environment*	Material Gradation*
Holocene	Fan alluvium	Coarse
Pleistocene	Valley alluvium	Fine
	Lacustrine/Marine	Mixed
	Aeolian	
	Artificial fill	
Tertiary		
Mesozoic		

* criteria only used for Holocene and Pleistocene age groups

ANALYSIS OF AMPLIFICATION FACTORS

Site-specific amplification factors, F_{ij}, are evaluated from the geometric mean of 5% damped acceleration response spectra for the two horizontal components of shaking, S_{ij}, and the reference ground motion for the site, $(S_r)_{ij}(T)$, as follows:

$$F_{ij}(T) = S_{ij} / (S_r)_{ij} \tag{1}$$

where the indices refer to ground motion j within site category i, and T = spectral period. In Eq. (1), S_{ij} and $(S_r)_{ij}$ are computed at the same spectral period, which is varied from 0.01 to 5.0 s. $(S_r)_{ij}$ represents an estimate of the spectrum that would have been expected at the recording site had the geologic condition been soft rock.

The principal challenge in evaluating F_{ij} is the analysis of the reference ground motion spectrum, $(S_r)_{ij}$. Median spectral accelerations from the Abrahamson and Silva (1997) attenuation relationship for "rock" sites are used to provide a first-order estimate of the reference spectrum based on the following factors:

- Moment magnitude of causative event, M_w.
- Closest distance from site to source, r.
- Rupture mechanism (reverse, oblique, strike-slip, or normal).
- Location of the site on or off the hanging wall of dip slip faults.

This first-order estimate is then adjusted to correct for period-dependent deviations between event-specific attenuation and the Abrahamson and Silva (1997) model. This is accomplished with the use of "event terms" computed during the regression of the attenuation model and provided by Dr. Norman Abrahamson. For sites that may have been influenced by rupture directivity effects, a second correction is made using relations updated from those in Somerville et al. (1997).

The ground motion amplification estimate provided by $(S_r)_{ij}$ is subject to error as a result of the uncertainty associated with the modified attenuation model. Because S_{ij} is known, the standard error of the ground motion amplification for a particular site, $(\sigma_f)_{ij}$, is equivalent to the standard error of the reference motion estimate, $(\sigma_r)_{ij}$, i.e.,

$$(\sigma_f)_{ij} = (\sigma_r)_{ij} \tag{2}$$

Standard error terms from attenuation relationships are fairly large (≈0.4-0.9), and hence the uncertainty in individual estimates of amplification are also large. However, the central limit theorem in statistical theory (e.g., Ang and Tang, 1975) suggests that statistical quantities (i.e., means, standard deviations) estimated from *large* data populations are relatively insensitive to the probability density function associated with individual data points in the population. Accordingly, the errors in point estimates of amplification can be accepted because relations for amplification factors are regressed upon using a large database.

Finally, it is acknowledged that the evaluation of amplification factors in terms of response spectral ordinates is less physically based than Fourier amplitude ratios, which have generally been used in previous studies. The use of spectral ratios was prompted by two principal factors (1) state-of-the-art procedures for evaluating reference motions in terms of response spectral ordinates are more maturely developed that those for Fourier spectral ordinates, and (2) seismic hazard analyses are typically performed in terms of response spectral ordinates, and hence amplification factors expressed in term of spectral ordinates may be more useful in practice.

REGRESSION OF AMPLIFICATION AGAINST SURFACE GEOLOGY AND GROUND MOTION PARAMETERS

Regression Procedure

Site-specific amplification factors defined in Eq. 1 were sorted into site categories defined by the schemes in Table 1. For a given scheme, within a given category *i*, regression analyses were performed to relate amplification factors, F_{ij}, to ground motion amplitude as follows,

$$\ln(F_{ij}) = a + b\ln(G_{ij}) \tag{3a}$$

where a and b are regression coefficients, and G_{ij} is a parameter representing the reference ground motion for site j in units of g. This same regression equation has been used by Youngs (1993) and Bazzuro and Cornell (1999). Abrahamson and Silva (1997) added a constant term to G_{ij} as shown below.

$$\ln(F_{ij}) = a + b\ln(G_{ij} + c) \tag{3b}$$

where c=0.03 g independent of period. This form of the regression equation was also investigated here, as discussed below. Due to the incorporation of event terms into the reference motions, systematic variations of amplification factors across events are not expected, and standard nonlinear regression analyses are performed (which give equal weight to all points) in lieu of the random effects model (Abrahamson and Youngs, 1992).

The following three types of G_{ij} parameters were compiled for each reference motion and were used in the regressions:

1. Peak ground acceleration (PGA), taken as $(S_r)_{ij}$ at T = 0.01 s.
2. Spectral acceleration at the same period, T, used in the evaluation of F_{ij}, i.e., $(S_r)_{ij}(T)$.
3. Peak horizontal velocity, calculated using the attenuation relation by Campbell (1997). In these calculations of peak velocity, a soft rock site condition was assumed, and the depth to basement rock was taken as 1.0 km (Campbell, 2000).

Residuals (R_{ij}) between the amplification "prediction" of Eq. 3 and $\ln(F_{ij})$ values were evaluated for all data in category *i* to enable evaluation of the mean residual, R_i, and the standard deviation of the residual, $(\sigma_R)_i$.

$$R_i = \frac{1}{N_i}\sum_{j=1}^{N_i} R_{ij} \tag{5a}$$

$$(\sigma_R)_i = \sqrt{\frac{\sum_{j=1}^{N_i}(R_{ij} - R_i)^2}{N_i - 1}} \tag{5b}$$

where N_i = number of data points in category i. Well defined site categories would be expected to have smaller values of $(\sigma_R)_i$ than relatively broad categories.

Regressions utilizing Equations 3a and 3b were performed for several site categories. It was not possible to achieve a stable regression using Eq. 3b. However, a comparison of the residuals $(\sigma_R)_i$ obtained using Eq. 3a, and Eq. 3b with c set fixed at various values, indicated decreases of $(\sigma_R)_i$ with decreasing c down to c=0. For this reason, the analyses that follow are based on Eq. 3a as the regression equation.

Results for Age-Only Classification Scheme and G = PGA

Each site was classified for geologic age. The breakdown of sites in each of four major age categories is presented in Figure 1. Amplification of peak acceleration (PGA) and T=1.0 s spectral acceleration are presented in Figures 2 (a) and (b) for each age category. The results are regressed against reference motion parameter, G = PGA. Several trends are apparent from these data:

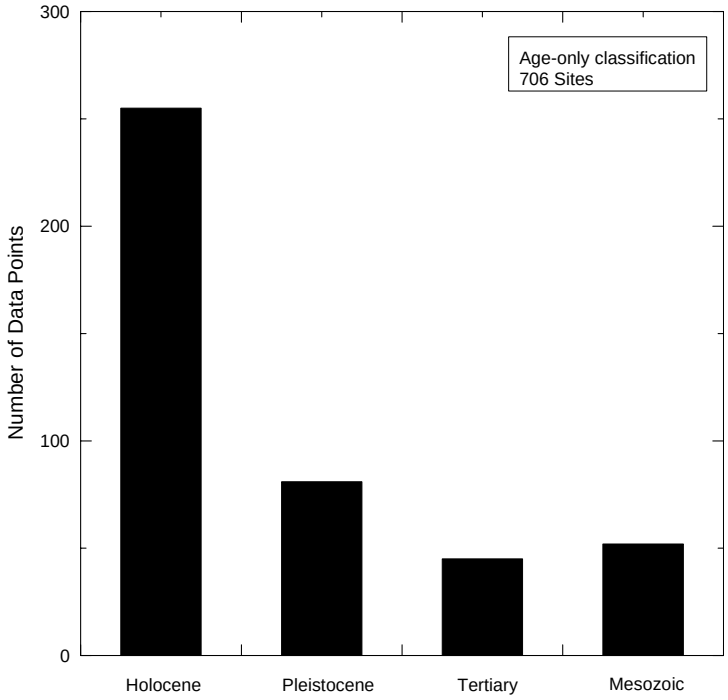

Figure 1: Data breakdown for age-only geologic classification scheme

1. Amplification was generally found to decrease with increasing peak acceleration. The amount of this change (i.e., the *b* parameter) is larger for younger, less consolidated soils. Holocene sediments exhibit amplification at low levels of shaking (PGA < 0.2g), and de-amplification for stronger shaking (PGA >~0.2g). This reduction of amplification with increasing ground motion amplitude at soil sites has previously been observed analytically from site response studies (e.g., Idriss, 1990) and empirically from comparisons of mainshock and aftershock recordings (e.g., Field et al., 1997). This reduction is a result of increases in hysteretic material damping with increasing shear strain amplitude (Seed et al., 1974).

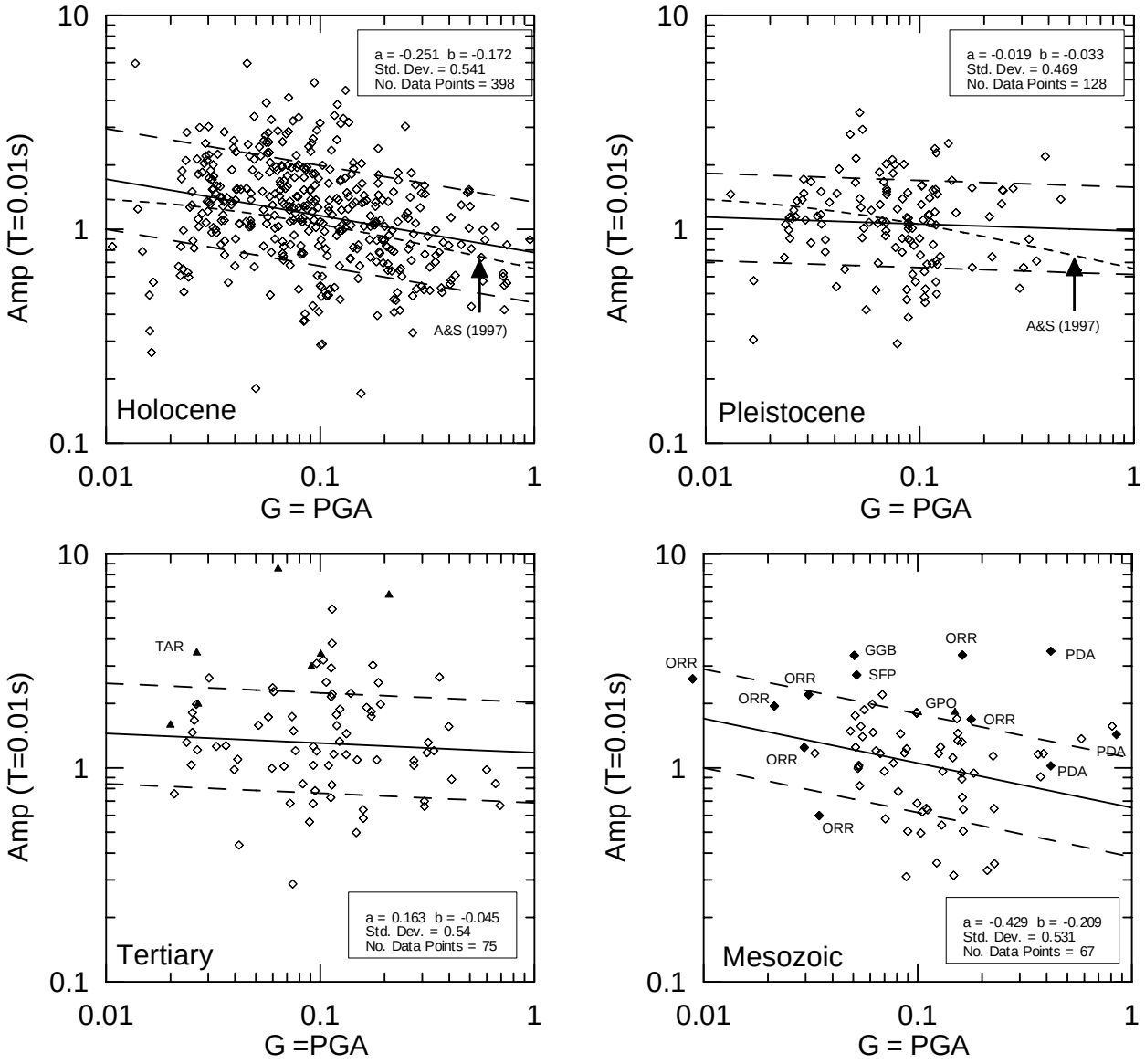

Figure 2(a): PGA amplification factors for age-only classification scheme along with Abrahamson and Silva, A&S (1997) site factor

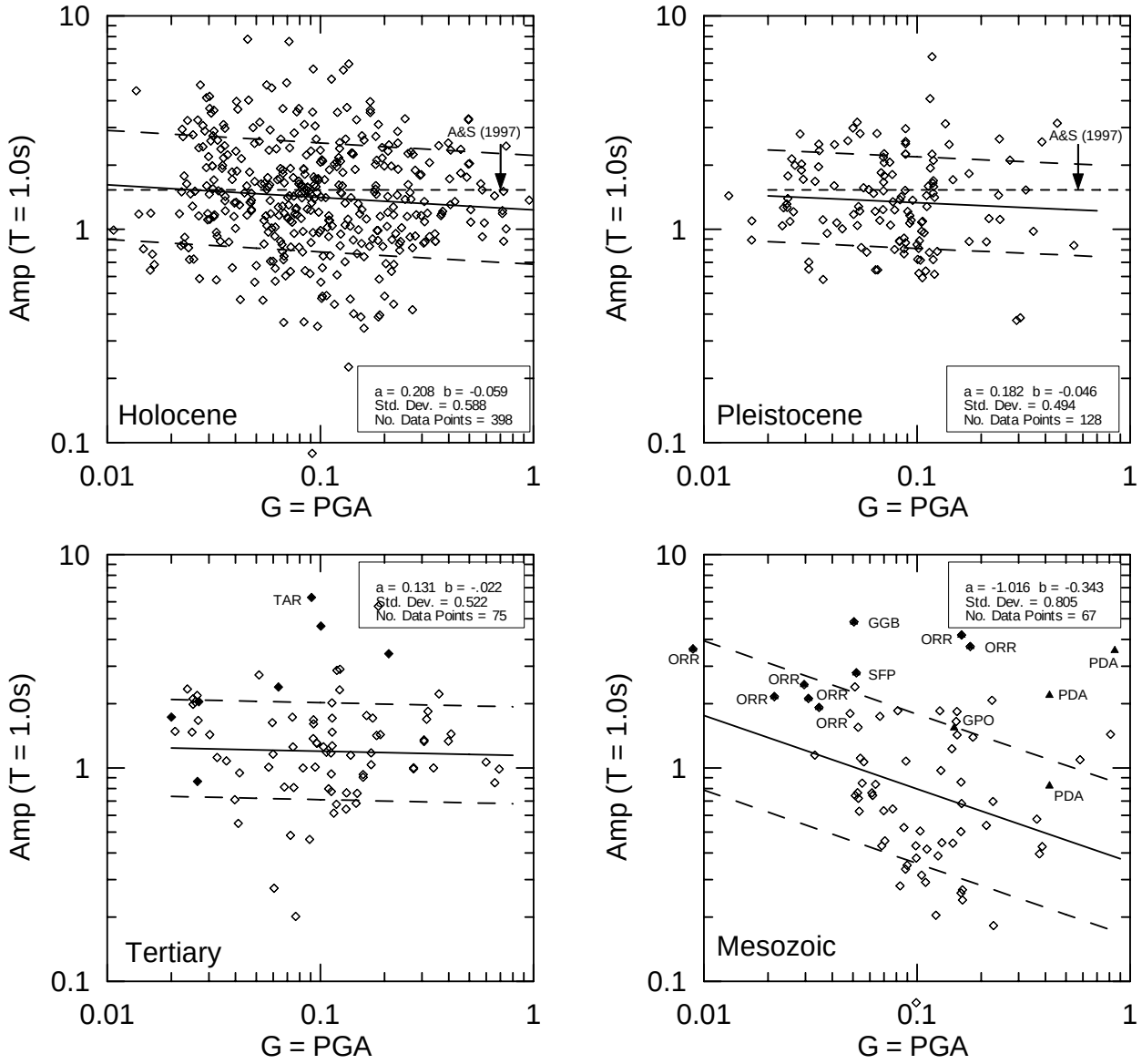

Figure 2(b): T=1.0 s spectral amplification factors for age-only classification scheme along with Abrahamson and Silva, A&S (1997) site factor

2. Amplification at low levels of shaking (i.e., PGA ≈ 0.01g) is largest for Holocene sediments, and generally decreases with increasing geologic age (with the exception of Mesozoic). The *a* parameter, which represents an index of amplification at G = 1.0 g, generally increases with geologic age. This can be attributed to the previously noted decrease of nonlinear sediment response with increasing geologic age.
3. As shown in Figure 2(c), the nonlinearity in Holocene materials (indexed by *b*) decreases with period (i.e., *b* increases). This change in *b* is sufficient that median T=1 s spectral amplification levels for Holocene materials exceed 1.0 even during strong shaking (PGA ≈ 1 g). Nonlinearity in the Pleistocene and Tertiary sediments is less period dependant up to $T \approx 1$ s, beyond which the results are subject to increased scatter and are less reliable. Values of *b* for the Mesozoic category have significant fluctuations with period, and are less reliable than other categories, as discussed further below.

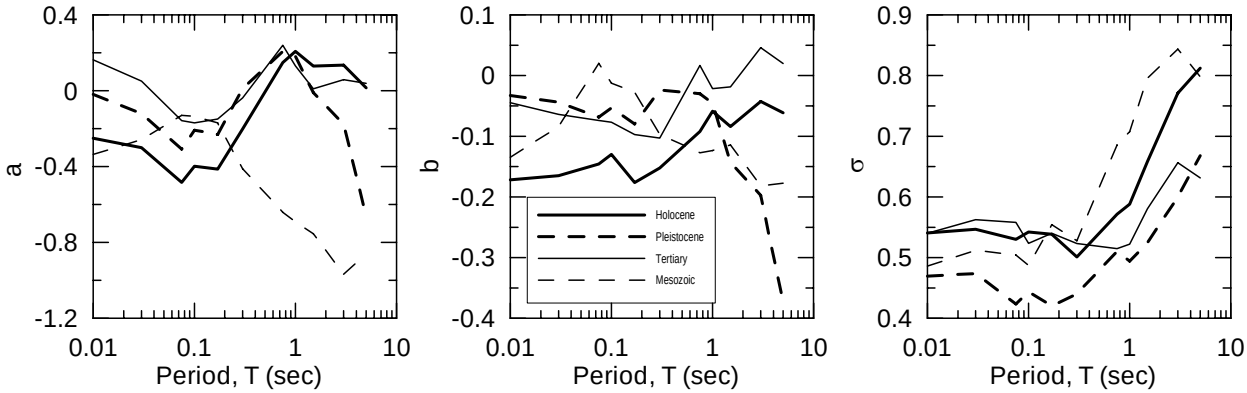

Figure 2(c): Regression parameters for age-only classification scheme

4. For T < 0.3 s, the standard deviation of the amplification levels are $(\sigma_R)_i \approx$ 0.5-0.55 for Holocene, Tertiary, and Mesozoic materials, and $(\sigma_R)_i \approx$ 0.43-0.47 for Pleistocene. Error terms in all categories increase significantly with period for $T >\sim$ 0.3-1.0 s.

The amplification factors obtained in this study are compared to the site terms developed by Abrahamson and Silva (A&S), 1997, which are shown as dotted lines in Figures 2(a) and (b). Median PGA amplification levels for Holocene sediments exceed the A&S site term, whereas Pleistocene PGA amplification is generally smaller and more linear. These results are not surprising, as the A&S site terms were developed using all "soil" sites, which generally include Holocene and Pleistocene sediments. A&S long period ($T>\sim$1 s) site terms tend to over-predict amplification levels.

It should be noted that several sites in the Tertiary and Mesozoic classification schemes may have significant topographic amplification, and were not used in the regression. One such site is Tarzana Cedar Hills Nursery (Tertiary category), which as shown in Figures 2(a) and (b), consistently shows high amplification levels across multiple events. This has been attributed to topographic amplification (Spudich et al., 1996). Sites excluded from the Mesozoic regression because of probable topographic effects include Pacoima dam abutment (PDA), Castaic Old Ridge Route (ORR), Griffith Park Observatory (GPO), San Francisco Presidio (SFP), and San Francisco Golden Gate Bridge (GGB). These sites generally have unusually large amplification levels.

The Mesozoic category shows significant non-linearity in the ground response in both PGA and T=1.0 s spectral acceleration. However, this result should be interpreted with caution, as the data is sparse (only 67 recordings), and the mapped surface geology at some Mesozoic sites is tenuous (i.e., many rock sites are found to actually have thin veneers of soil and/or weathered rock when investigated with borings).

Results for Other Classification Schemes and G=PGA

As indicated in Table 1, two additional geologic classification schemes were considered that incorporate information beyond age – depositional environment and material gradation. It was not possible to classify all sites according to these criteria due to the limited quality of geologic

mapping in some areas. The breakdown of sites in categories associated with these schemes is presented in Figure 3. Due to a paucity of data, no regression analyses were performed for Aeolian and fill categories (depositional environment scheme). Further, data for Pleistocene sites was sufficient only to define an alluvial category in the depositional environment scheme.

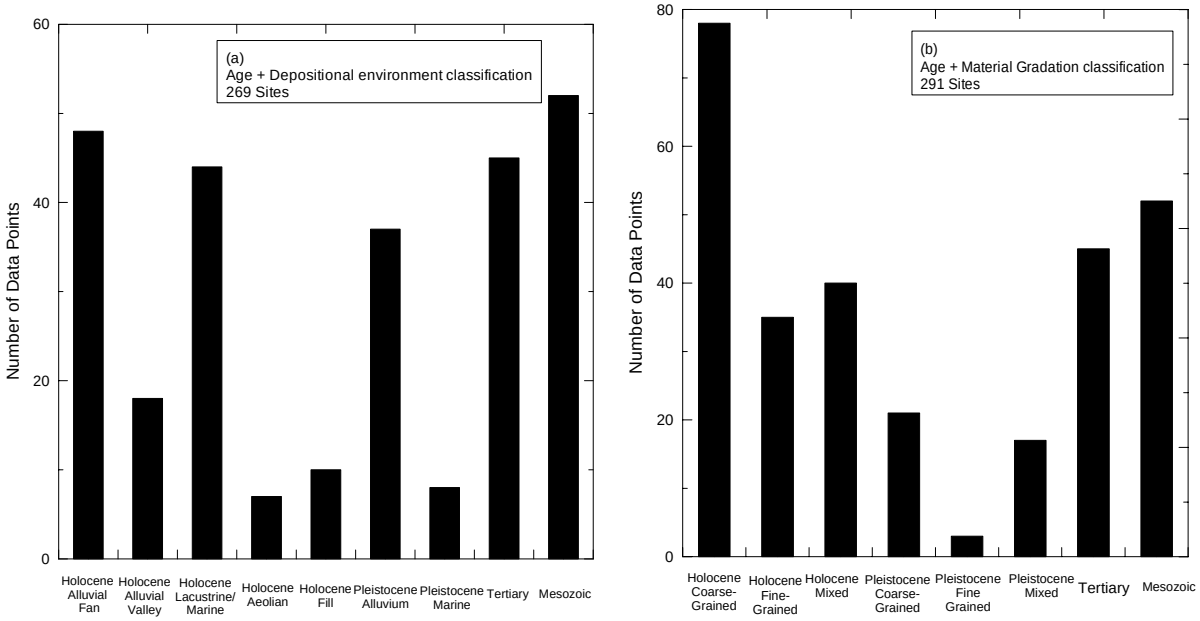

Figure 3: Data breakdown for geologic classification schemes incorporating information on depositional environment and material gradation.

Figure 4(a) presents data on PGA amplification for Quaternary sediments sorted by depositional environment. Also shown on the figure is the A&S site factor for soil sites. The highest levels of amplification and non-linearity are observed in the lacustrine/marine category, which includes a significant number of sites from Imperial Valley and San Francisco bay shore locations. The most abundant data is for Holocene alluvial fan deposits, which exhibit amplification levels consistent with the A&S site term. The data for Holocene alluvial valley deposits contains a relatively high level of scatter, and no data at strong shaking levels. Thus, it does not appear that meaningful trends can be identified for this category. The data for Pleistocene alluvium is generally similar to that for the overall Pleistocene category in the age-only scheme. Given this result and the limited available data for other Pleistocene depositional environments, sub-division of the Pleistocene age category does not appear to be justified.

The period dependence of the regression results for depositional environment is presented in Figure 4(b). The lacustrine/marine category exhibits strong period dependant non-linearity, as illustrated by the significant increases in b with period. These increases are sufficient that parameter a (representing spectral amplification at G = 1.0 g) exceeds zero for T > 1 s. The significance of the sediment response effect in the lacustrine/marine category is further illustrated by the low standard error term, which has little period dependence. The period dependence of the results for Holocene fan deposits are similar to those for the overall Holocene (age-only) category.

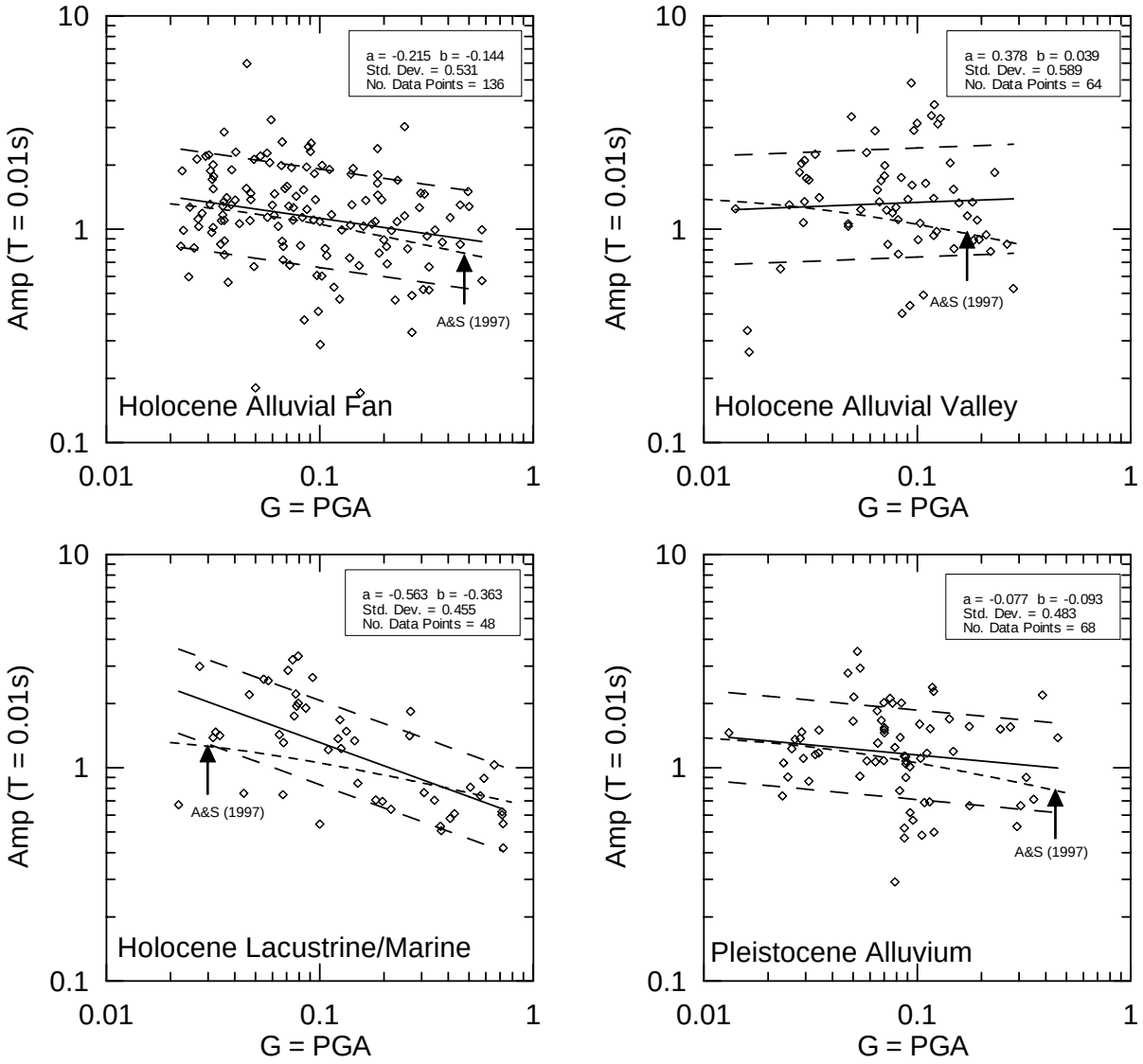

Figure 4(a): PGA amplification factors for age + depositional environment classification scheme along with A&S (1997) site factor

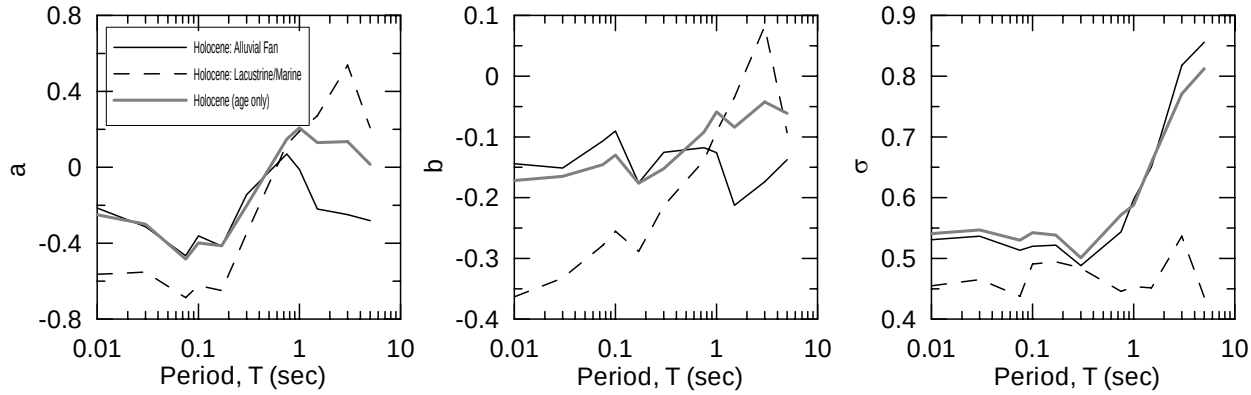

Figure 4(b): Regression parameters for age + depositional environment classification scheme

Figure 5 presents data on PGA amplification for Quaternary sediments sorted by material gradation along with the A&S site factors for soil sites. Data is most abundant for Holocene coarse-grained soils, which exhibit PGA amplification levels (Figure 5a) comparable to those for the overall Holocene (age-only) category. Data for Holocene fine-grained and mixed gradation sediments exhibited similar amplification levels, and so these categories were combined. The fine grained/mixed category exhibits relatively high levels of weak shaking PGA amplification and non-linearity. The period-dependence of the *a*, *b*, and σ parameters (Figure 5b) for coarse and fine/mixed materials deviate from the Holocene (age-only) results, with the period dependence of *a* and *b* being more pronounced for fine/mixed sediments than coarse sediments. Results for Pleistocene sediments follows similar trends to those for Holocene, but the deviations between fine/mixed and coarse are relatively small, and the results are less robust due to a paucity of data. These data do not appear to justify subdivision of the Pleistocene category.

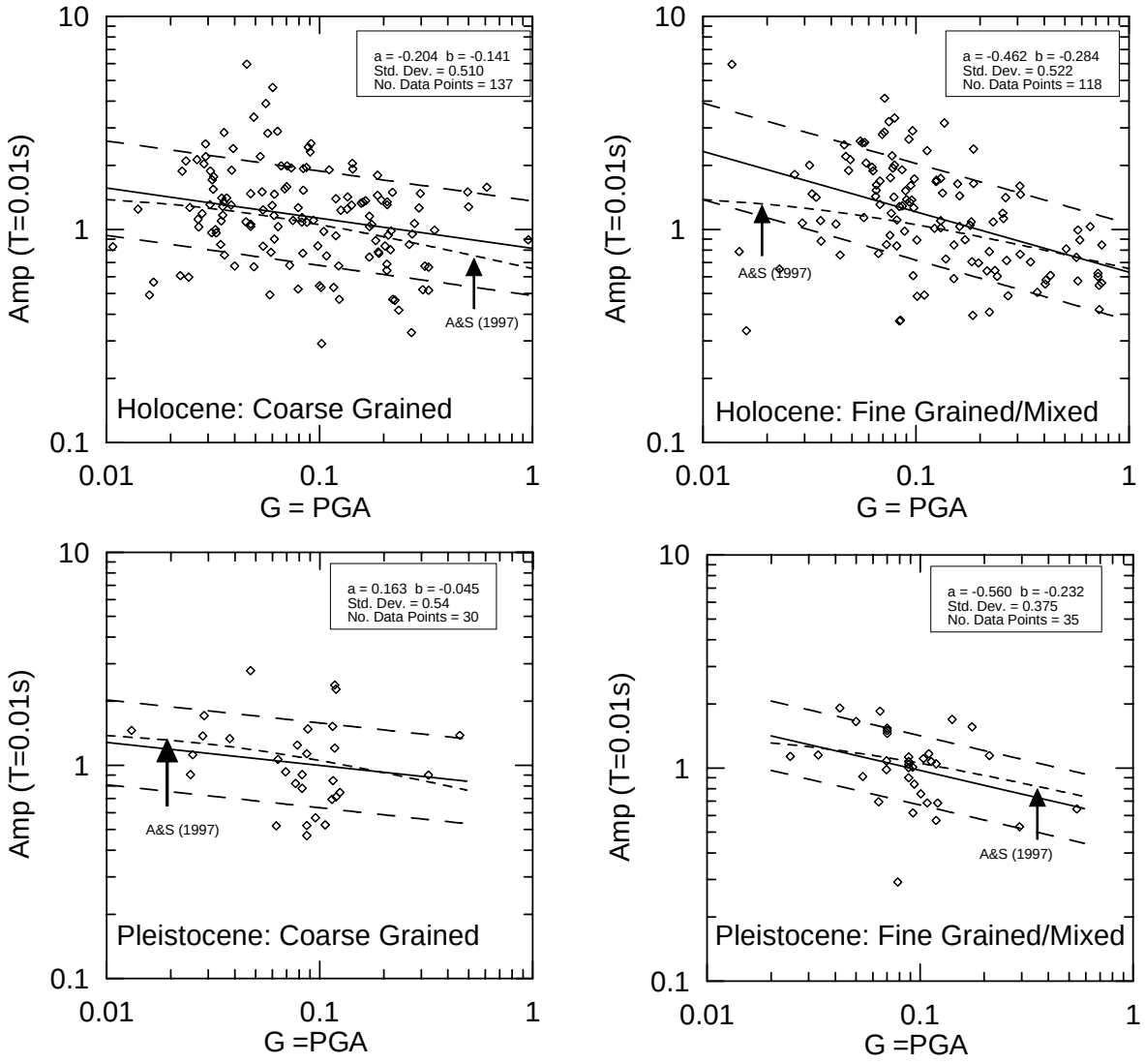

Figure 5(a): PGA amplification factors for age + material gradation classification scheme along with A&S (1997) site factor

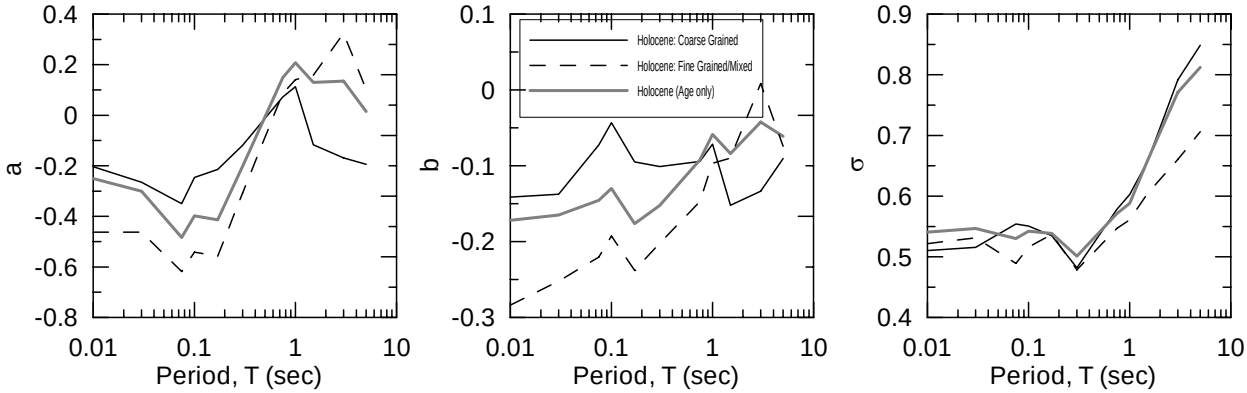

Figure 5(b): Regression parameters for age + material gradation classification scheme

An interesting feature of material gradation-based regression results is that material non-linearity is greater for fine sediments than for coarse sediments. This is contrary to what would generally be expected from standard geotechnical modulus reduction and damping curves (e.g., Vucetic and Dobry, 1991). This finding is not without precedent, however, as many of the sites classified as "coarse-grained" are in southern California, and other recent studies of such sites (i.e., Silva et al., 1998) have found from back-analysis of ground motion data that regional sediment response was more linear than predicted by standard modulus reduction and damping curves.

Results for Other Reference Motion Parameters

In the preceding analyses, the amplification factors compiled for the three geologic classification schemes were regressed against peak acceleration (i.e., G=PGA). Regressions were also performed against peak ground velocity (PGV) and spectral acceleration at the period of amplification (G=S_a). These different reference motion parameters did not significantly affect data dispersion. For example, Figure 6 shows regression coefficients for Pleistocene sediments as a function of G. Variations are apparent in the *a* and *b* parameters, but standard error is essentially unaffected. Results are similar for other geologic categories. Accordingly, any of the reference motion parameters could be used, and PGA is adopted due to its familiarity among practitioners.

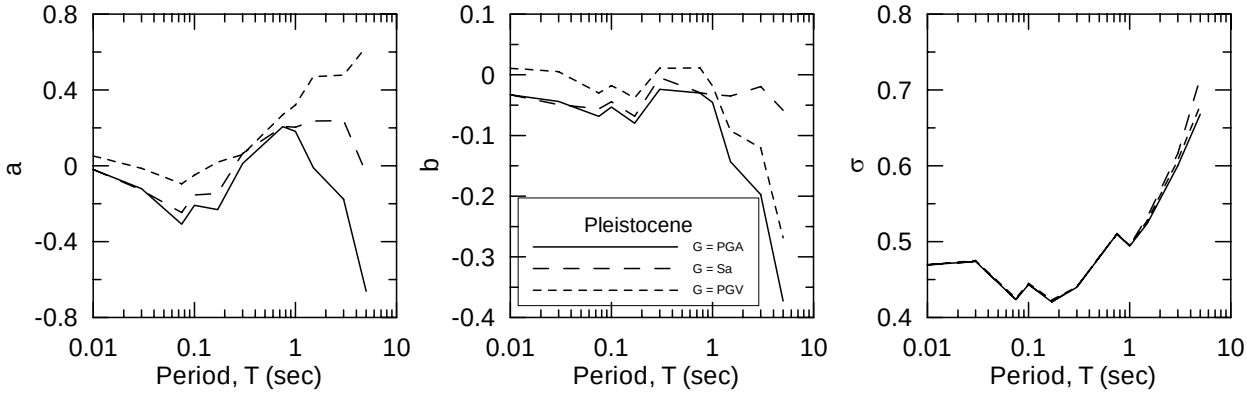

Figure 6: Sensitivity of regression parameters for Pleistocene sediments to reference motion parameter (G)

Identification of Optimal Geologic Classification Scheme

Taking *G*=PGA, inter-category median residuals (*R*) and standard errors (σ_R) were evaluated for each of the three geologic classification schemes as,

$$R = \frac{1}{M}\sum_{i=1}^{M} R_i \tag{6a}$$

$$\sigma_R = \sqrt{\frac{\sum_{i=1}^{M}\sum_{j=1}^{N_i}\left(R_{ij} - R_i\right)^2}{\left(\sum_{i=1}^{M} N_i\right) - 1}} \tag{6b}$$

where *M* = the number of categories in scheme *i*. The standard error results are plotted as a function of spectral period in Figure 7 (the median residuals are zero, and are not plotted). The inter-category standard error for the age + depositional environment scheme is lower than the other schemes, suggesting that this scheme best captures the observed ground motion variations.

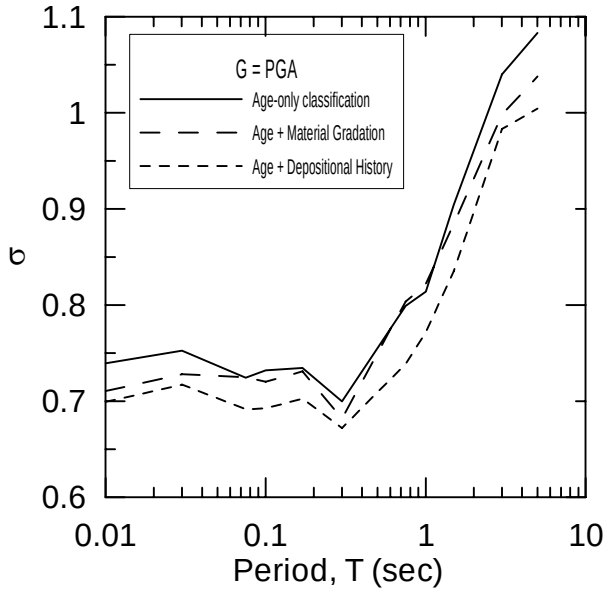

Figure 7: Inter-category standard error terms for three geologic classification schemes. The age + depositional environment scheme provides the minimal data dispersion at all periods.

Magnitude/Duration Effect

The regression equation used in the above analyses (Eq. 3a) is based on the assumption that amplification for a given geologic category is only a function of reference motion amplitude. Due to the finite time required for soil profiles to reach their steady-state resonant response, some dependence of amplification on the duration of strong shaking might be expected. Figure 8(a) presents PGA and *T*=3.0 s spectral acceleration amplification factors for Holocene

sediments (age-only scheme) sorted into bins with magnitude, $M_w < 7$ and $M_w \geq 7$. The amount and dispersion of amplification are seen to vary with magnitude. The large changes in standard error have been observed previously (e.g., Youngs et al., 1995), and are incorporated into several attenuation models (e.g., Abrahamson and Silva, 1997; Sadigh et al., 1997).

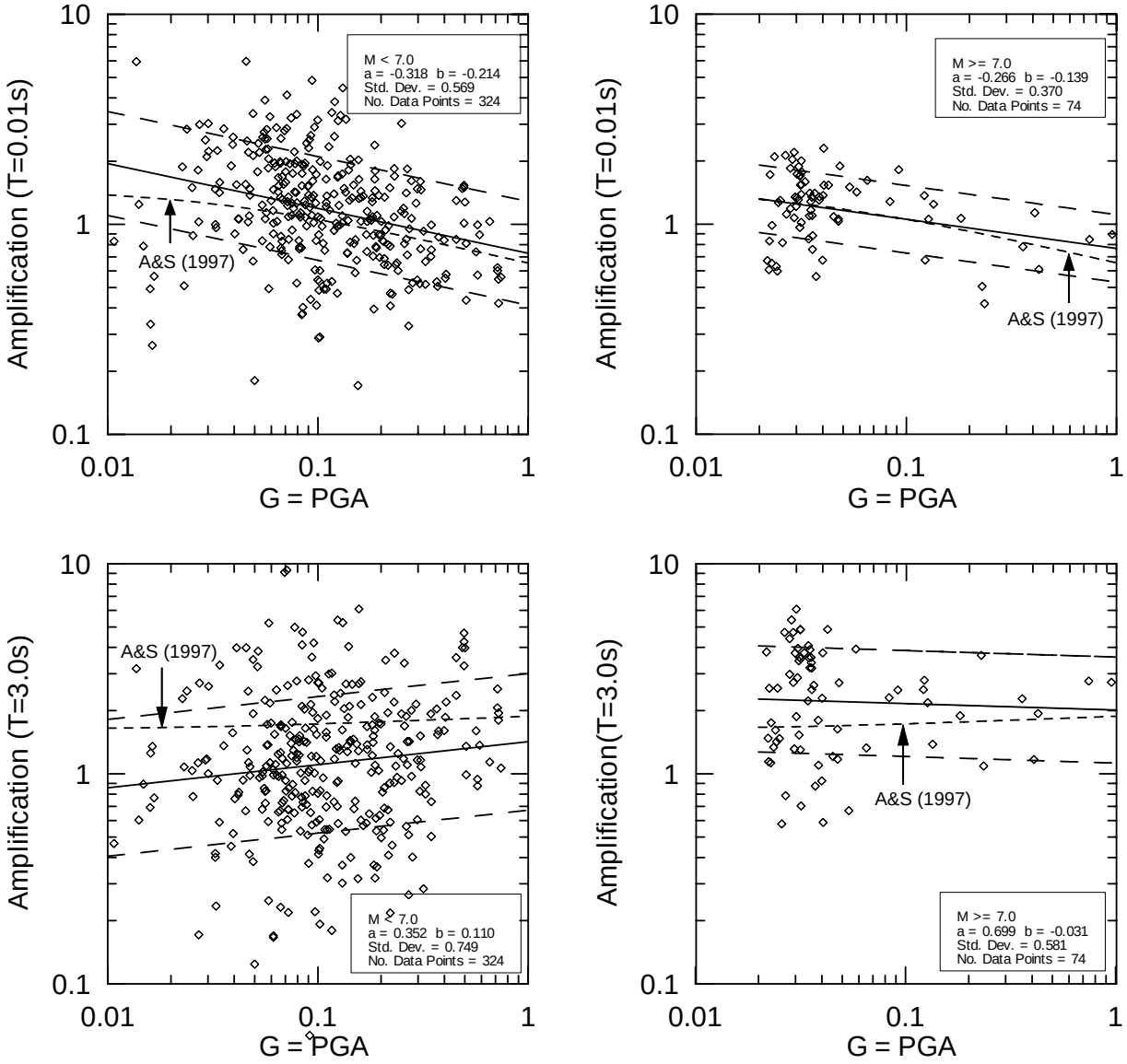

Figure 8(a): Amplification factors for Holocene sites sorted according to magnitude

To investigate the effect of duration (which correlates closely with magnitude) on ground response, amplification factors for the age + depositional environment scheme were regressed according to the following equation:

$$\ln(F_{ij}) = a + b\ln(G_{ij}) + d\ln(D_{5-75}) \qquad (7)$$

where $D_{5\text{-}75}$ is the duration (in s) defined as the elapsed time between 5% and 75% normalized Arias intensity, and d is a regression coefficient. $D_{5\text{-}75}$ is taken as the median duration for a rock site condition from the attenuation relationship by Abrahamson and Silva (1996). Note that in these preliminary analyses, $D_{5\text{-}75}$ estimates have not been corrected for rupture directivity effects nor for event terms. Median results of these preliminary regression analyses are presented in Figure 8(b) along with results of regressions without duration. Amplification for these sediments is seen to be strongly period dependant, an effect observed in other geologic categories as well. The standard error is reduced through the use of Eq. 7 by about 5-20% at long periods (relative to the regression using Eq. 3a).

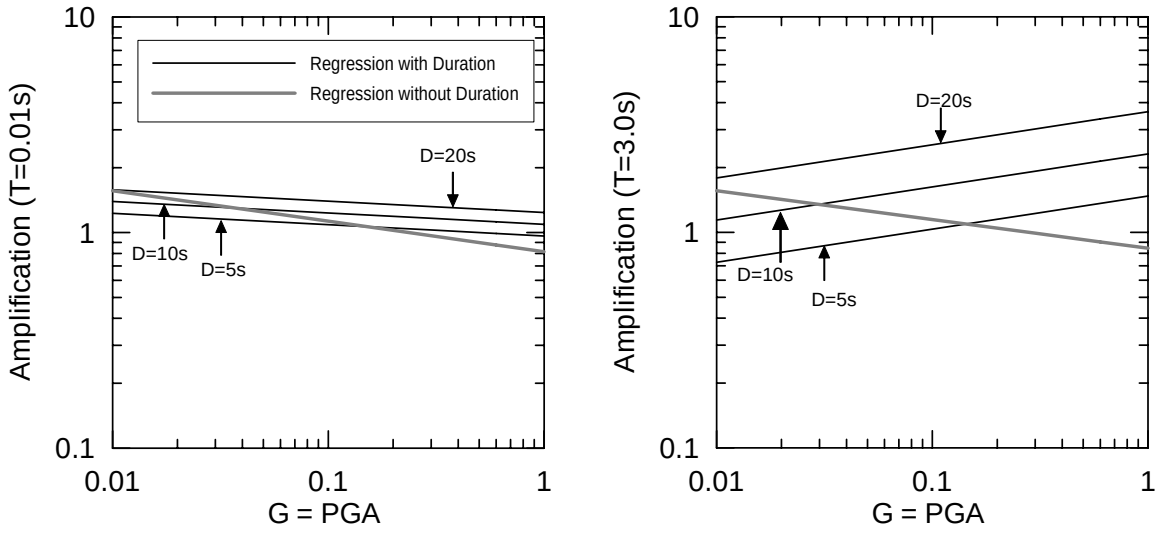

Figure 8(b): Effect of duration on median amplification of Holocene fan deposits

Comparison to Previous Findings

It is of interest to compare the results of this study to the findings of previous research that identified amplification factors using recordings from adjacent rock/soil stations. Figure 9 compares PGA amplification identified from soft soil sites in the San Francisco Bay Area and Mexico City by Idriss (1990) to regression results for the lacustrine/marine geologic category. The median regression relations indicate lower site factors than predicted by Idriss. There are two possible explanations for this. First, many sites in this category are not "soft soil," which would be expected to produce relatively large amplification levels. Second, and perhaps more importantly, Idriss' site factors are based on reference site recordings from relatively competent bedrock sites, whereas the amplification factors for this study are based on reference motions for soft rock site conditions. Soft rock ground motions have larger amplitudes than firm rock, therefore producing smaller geologic amplification factors.

Of considerable practical interest is a comparison of the regression results to UBC amplification factors. This comparison is made by evaluating F_{ij} (refer to Eq. 3a) across short- (0.1 - 0.5 s, defined as F_a) and mid-period bands (0.4 – 2.0 s, defined as F_v). Only the age + depositional environment classification scheme is considered. The results are presented in Figure

10(a) for F_a and Figure 10(b) for F_v. It should be noted that the F_a and F_v factors to which the regression analyses are compared are empirically based only up to PGA ≈ F_a ≈ 0.1g (from Borcherdt, 1994), and are based on analysis at stronger levels of shaking (Martin, 1994). The regression results are seen to provide amplification levels for soil sites (i.e., Holocene, Pleistocene age groups) that are smaller than the code provisions. As described above, this is attributed to the use of a soft rock reference site condition in the derivation of reference ground motions, as compared to the relatively firm rock conditions present in the empirical studies by Borcherdt (1994) and the analytical studies by Martin (1994).

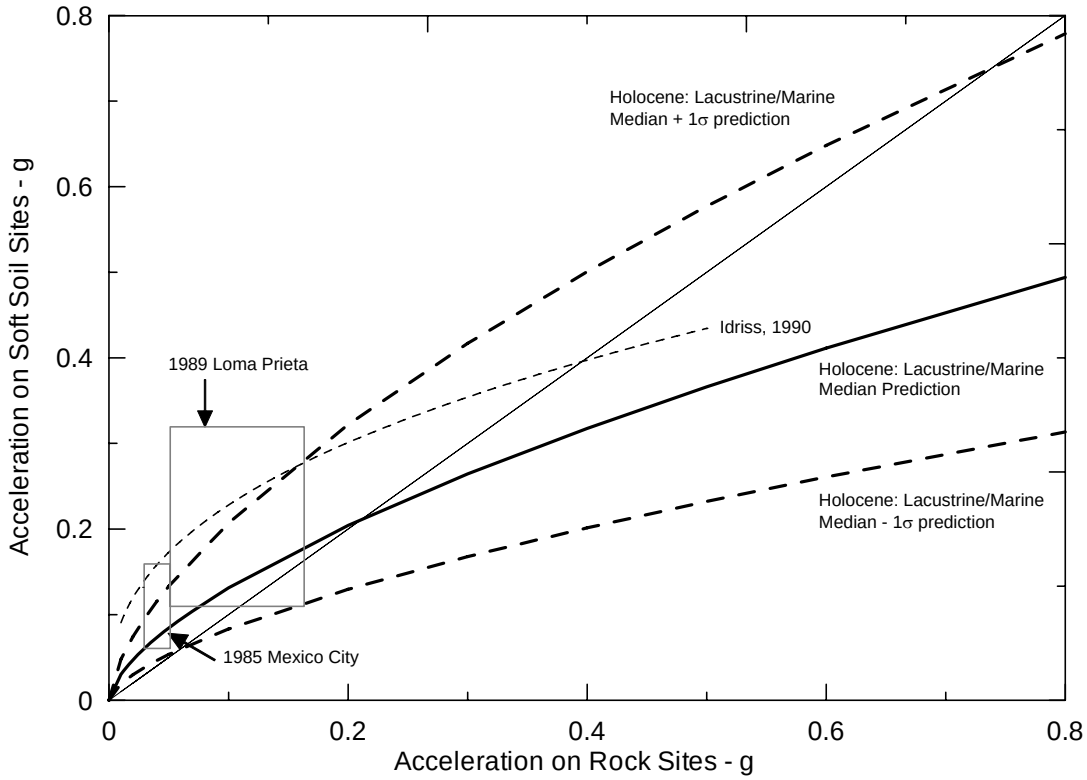

Figure 9: Comparison of regression results for Holocene lacustrine/marine soils to findings of Idriss (1990) for soft clay sites.

CONCLUSIONS

Many current strong motion attenuation relations (e.g., Abrahamson and Silva, 1997; Sadigh, 1997) sub-divide site conditions into two broad categories: rock and soil. This project has developed amplification factors that can be used to modify the predictions of soft rock relations on the basis of mapped surficial geology. Amplification is found to be strongly a function of the age and depositional environment of the surface deposits. Materials of Holocene age are found to have the highest levels of weak shaking amplification and soil non-linearity, particularly when deposited in lacustrine or marine environments. The non-linearity in such materials is typically sufficiently pronounced that high frequency spectral ordinates are de-amplified at strong levels of shaking (PGA >~ 0.2g). Relatively coarse materials such as Holocene fan and valley sediments experience less weak shaking amplification, but less non-

linearity as well. Ground motion amplification is found to be strongly period-dependant, with less non-linearity, and often more amplification, at longer spectral periods. Materials of Pleistocene, Tertiary, and Mesozoic age generally experience significantly less amplification than Holocene sediments. The available data was not sufficient to justify subdivisions within these geologic categories.

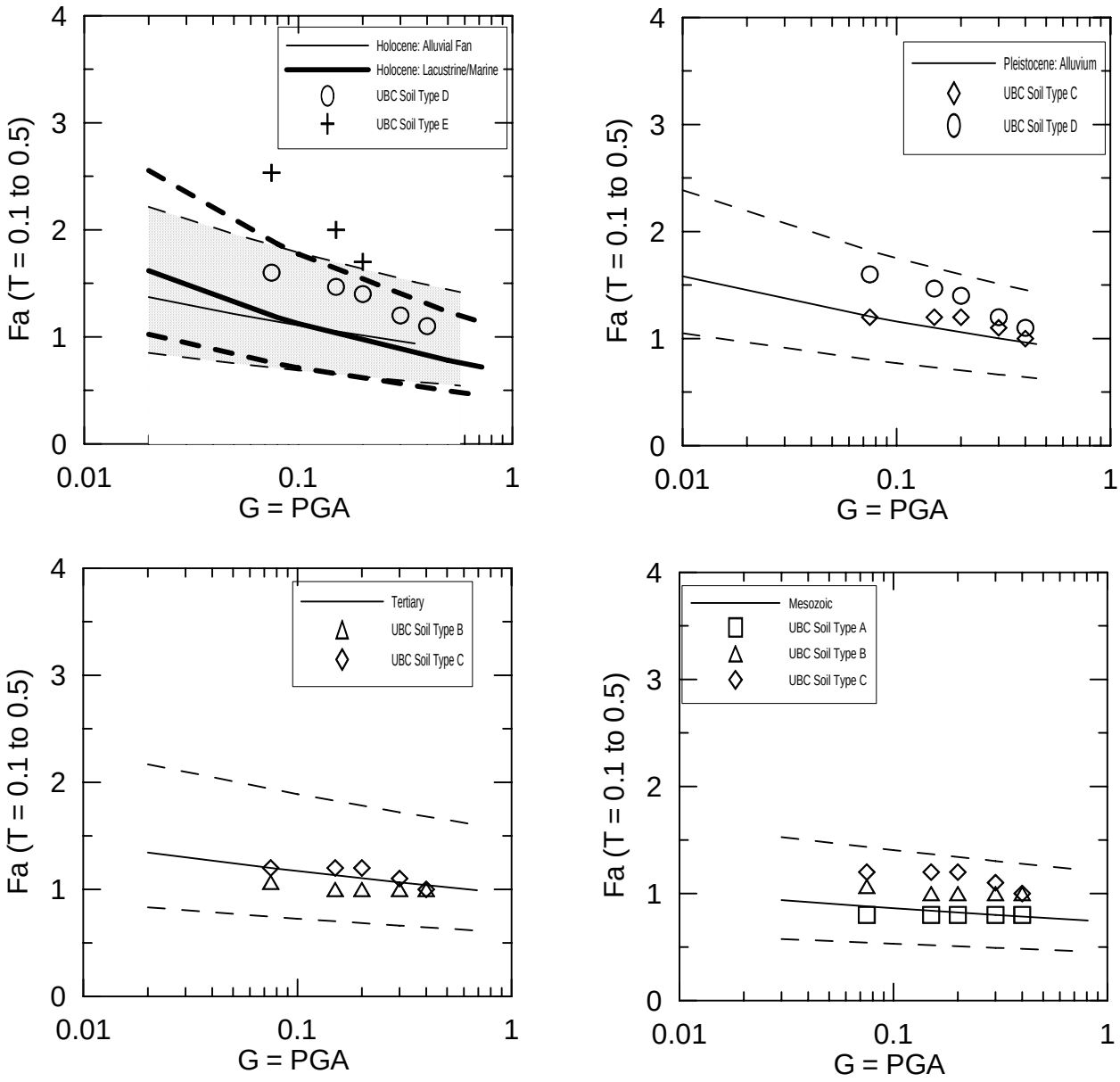

Figure 10(a): Comparison of F_a regression results with UBC provisions

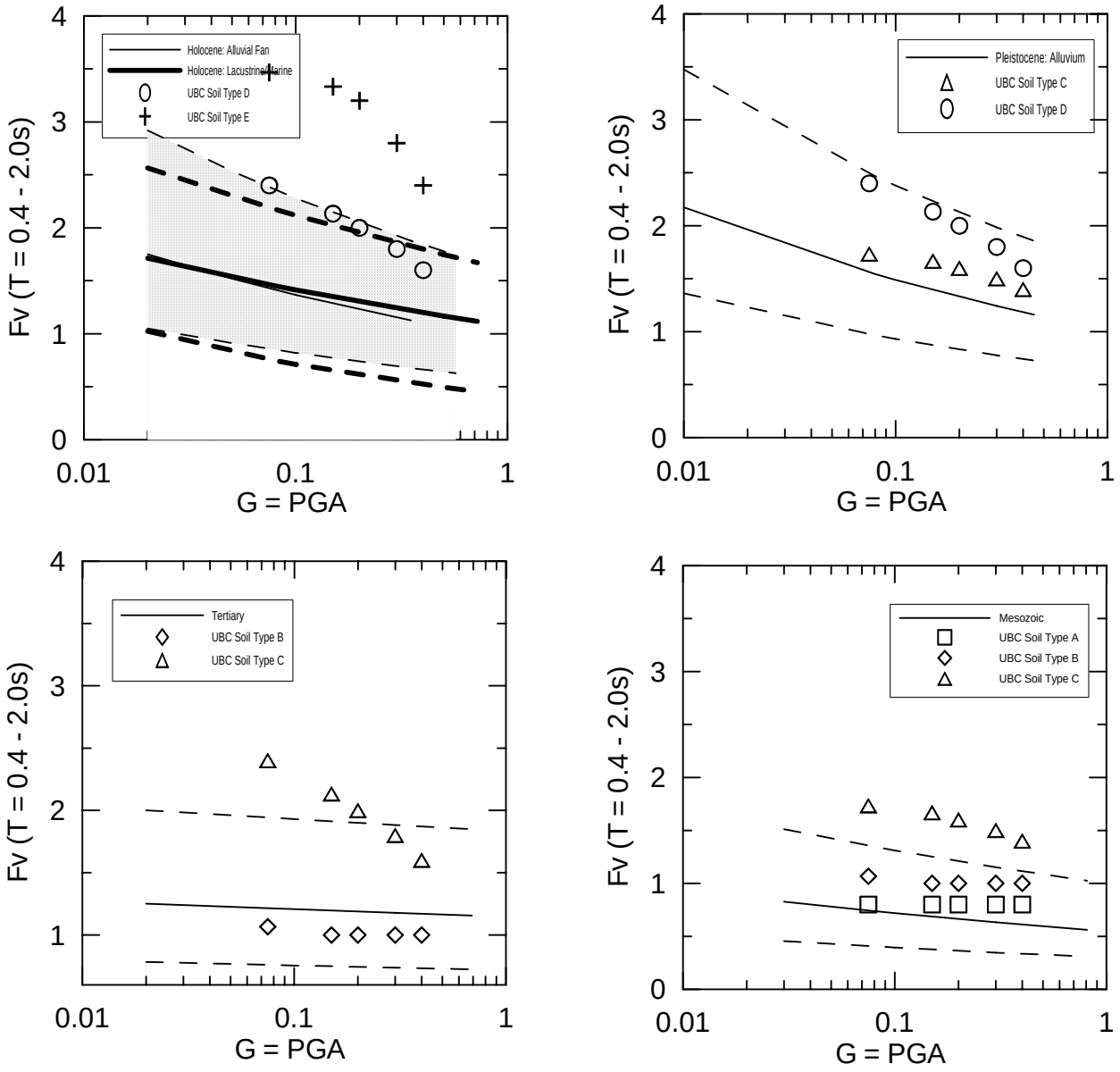

Figure 10(b): Comparison of F_v regression results with UBC provisions

Based on the preliminary analyses completed to date, it is recommended that geologic classification schemes for ground motion studies should include information on geologic age and depositional environment. The recommended regression equation is Eq. 3a, with the coefficients in Figure 5b. Further adjustments to this scheme are anticipated as the data from the 1999 earthquakes in Turkey and Taiwan becomes processed, and as the effects of duration are more formally integrated into the amplification model.

One important outcome of this study is insight gained into the critical influence of reference motion site condition on amplification factors. In concept, any reference site condition could be used to define amplification factors, provided that subsequent use of such factors is coupled with

design motions appropriate for the reference site condition. In California, the predominant condition of consolidated (non-soil) geologic materials can be described as "soft rock." Accordingly, attenuation models based on "rock" recordings in California are actually appropriate for a soft rock condition. For this reason, soft rock was selected as the reference site condition, and the amplification factors presented herein are appropriate for use with standard rock attenuation models. The use of amplification factors defined from relatively firm rock reference sites coupled with these same rock attenuation models may produce unnecessarily conservative design ground motions.

ACKNOWLEDGEMENTS

This study was supported principally by the California Department of Conservation, Division of Mines and Geology, Strong Motion Instrumentation Program, Contract 1098-712. Additional support was provided by the Pacific Earthquake Engineering Research Center under Contract Number 021544. This support is gratefully acknowledged. We would like to thank Moh Huang and Anthony Shakal of CSMIP, and the member of the CSMIP Advisory Committee, for their valuable advice and contributions of data. In particular, CSMIP staff provided accurate station locations that increased the quality of the geologic classifications. Charles Real of CDMG facilitated the acquisition of digital SCAMP maps for southern California. James Chen and M. B. Baturay of UCLA assisted with data synthesis and analysis.

REFERENCES

Abrahamson, N.A. and Silva, W.J. (1996). "Empirical ground motion models," Report prepared for Brookhaven National Laboratory, New York, NY, May, 144 p.

Abrahamson, N.A. and Silva, W.J. (1997). "Empirical response spectral attenuation relations for shallow crustal earthquakes," *Seism. Res. Letters*, 68(1), 94-127.

Abrahamson, N.A. and Youngs, R.R. (1992). "A stable algorithm for regression analyses using the random effect model," *Bull. Seism. Soc. Am.*, 82, 505-510.

Ang, A.H.-S. and Tang, W.H. (1975). *Probability Concepts in Engineering Planning and Design, Volume I – Basic Principles*, John Wiley & Sons, New York, NY.

Bazzuro, P. and Cornell, C.A. (1999). "Efficient PSHA for nonlinear soil sites with uncertain properties," Ph.D. dissertation, Stanford University (in progress).

Boatwright, J., Fletcher, J.B., and Fumal, T.E. (1991). "A general inversion scheme for source, site and propagation characteristics using multiply recorded sets of moderate-sized earthquakes," *Bull. Seism. Soc. Am.*, 81, 1754-1782.

Borcherdt, R.D. (1970). "Effect of local geology on ground motion near San Francisco Bay," *Bull. Seism. Soc. Am.*, 60, 29-61.

Borcherdt, R.D. (1994). "Estimates of site-dependent response spectra for design (methodology and justification)," *Earthquake Spectra*, EERI, 10(4), 617-653.

Borcherdt, R.D. and Glassmoyer, G. (1994). "Influences of local geology on strong and weak ground motions recorded in the San Francisco Bay region and their implications for site-specific building-code provisions," in *The Loma Prieta earthquake of October 17, 1989 – Strong Ground Motion*, R.D. Borcherdt (ed.), U.S. Geological Survey Prof. Paper 1551-A, p 77-108.

Borcherdt, R.D. (1996). "Preliminary amplification estimates inferred from strong ground motion recordings of the Northridge earthquake of January 17, 1994," *Proc. Int. Workshop on Site Response Subjected to Strong Earthquake Motions*, Yokosuka, Japan, Vol. 2, 21-46.

Building Seismic Safety Council, BSSC (1998). *NEHRP Recommended Provisions for Seismic Regulations for New Buildings and Other Structures*, Part 1 – Provisions and Part 2 – Commentary, Federal Emergency Management Agency, Washington D.C., February.

Campbell, K.W. (1997). "Empirical near-source attenuation relations for horizontal and vertical components of peak ground acceleration, peak ground velocity, and pseudo-absolute acceleration response spectra," *Seism. Res. Letters*, 68(1), 154-179.

Campbell, K.W. (2000). Erratum to Campbell, 1997, *Seism. Res. Letters*, 71(3), 352-354.

CDMG staff (2000). "Preliminary working digital geologic maps of portion of Los Angeles, Orange, and Ventura Counties, California, compiled for seismic hazard zoning," 1:24,000 scale.

Chang, S.W., Bray, J.D., and Seed, R.B. (1996). "Engineering implications of ground motions from the Northridge earthquake," *Bull. Seism. Soc. Am.*, 86(1B), S270-S288.

Dickenson, S.E. and Seed, R.B. (1996). "Nonlinear dynamic response of soft and deep cohesive soil deposits," *Proc. Int. Workshop on Site Response Subjected to Strong Earthquake Motions*, Yokosuka, Japan, Vol. 2, 67-81.

Field, E.H. and Jacob, K.H. (1995). "A comparison and test of various site-response estimation techniques, including three that are not reference-site dependent," *Bull. Seism. Soc. Am.*, 85, 1127-1143.

Field, E.H., Johnson, P.A., Beresnev, I.A., and Zeng, Y. (1997). "Nonlinear ground motion amplification by sediment during the 1994 Northridge earthquake," *Nature*, 390, 599-602.

Geomatrix Consultants (1993). "Compilation of geotechnical data for strong motion stations in the Western United States," Report to Lawrence Livermore National Lab., Project No. 2256.

Hartzell, S.A., Leeds, A., Frankel, A., and Michael, J. (1996). "Site response for urban Los Angeles using aftershocks of the Northridge earthquake," *Bull. Seism. Soc. Am.*, 86, S168-S192.

Hartzell, S.A., Cranswick, E., Frankel, A., Carver, D., and Meremonte, M. (1997). "Variability of site response in the Los Angeles urban area," *Bull. Seism. Soc. Am.*, 87, 1377-1400.

Idriss, I.M. (1990). "Response of soft soil sites during earthquakes," *Proc. H. Bolton Seed Memorial Symposium*, J. M. Duncan (editor), Vol. 2, 273-290.

Lermo, J. and Chavez-Garcia, F.J. (1993). "Site effect evaluation using spectral ratios with only one station," *Bull. Seism. Soc. Am.*, 83, 1574-1594.

Martin, G., ed. (1994). *Proc. NCEER, SEAOC, BSSC Workshop on Site Response during Earthquakes and Seismic Code Provisions*, Univ. Southern California, Los Angeles, CA, November.

Morton, D.M., Hauser, R.M., and Ruppert, K.R. (1999). "Preliminary Digital Geologic Map of the Santa Ana 30' x 60' Quadrangle, Southern California," *Open-File Report 99-172*, U.S. Geological Survey, Menlo Park, CA.

Rathje, E.M., Idriss, I.M., and Somerville, P. (2000). "Strong ground motion and site effects," *Earthquake Spectra*, Special Volume on 1999 Kocaeli, Turkey, earthquake, (in press).

Sadigh, K., Chang, C.-Y., Egan, J.A., Makdisi, F., and Youngs, R.R. (1997). "Attenuation relations for shallow crustal earthquakes based on California strong motion data," *Seism. Res. Letters*, 68(1), 180-189.

Seed, H.B. and Idriss, I.M. (1971). "Influence of soil conditions on building damage potential during earthquakes," *J. Struct. Engrg*., ASCE, 97(2), 639-663.

Seed, H.B. and Idriss, I.M. (1982). *Ground Motions and Soil Liquefaction During Earthquakes,* Mongraph, Earthquake Engrg. Res. Institute, Oakland, CA.

Seed, H.B., Romo, M.P., Sun, J.J., and Lysmer, J. (1987). "Relationships between soil conditions and earthquake ground motions in Mexico City in the earthquake of September 19, 1985," *Rpt. No. UCB/EERC-87/15*, Earthquake Engrg. Res. Ctr., Univ. of California, Berkeley.

Seed, H.B., Ugas, C., and Lysmer, J. (1974). "Site-dependent spectra for earthquake resistant design," *Rpt. No. UCB/EERC-74/12*, Earthquake Engrg. Res. Ctr., Univ. of California, Berkeley.

Seed, H.B., Whitman, R.V., Dezfulian, H., Dobry, R., and Idriss, I.M. (1972). "Soil conditions and building damage in 1967 Caracas earthquake," *J. Soil Mech. and Fndns. Div*., ASCE, 98(8), 787-806.

Seed, R.B., Dickenson, S.E., and Idriss, I.M. (1991). "Principal geotechnical aspects of the 1989 Loma Prieta earthquake," *Soils and Foundations*, 31(1), 1-26.

Silva, W.J., Costantino, C., and Li, S. (1998). "Quantification of nonlinear soil response for the Loma Prieta, Northridge, and Imperial Valley, California earthquakes," in *The effects of surface geology on seismic motion*, Balkema, Vol. 2, 1137-1143.

Sokolov, V.Y. (1997). "Empirical models for estimating Fourier-amplitude spectra of ground acceleration in the northern Caucasus (Racha seismogenic zone)," *Bull. Seism. Soc. Am.*, 87, 1401-1412.

Sokolov, V.Y., Loh, C.-H., and Wen, K.-L. (2000). "Empirical study of sediment-filled basin response: The case of Taipei City," *Earthquake Spectra*, 16(3), 681-707.

Somerville, P.G., Smith, N.F., Graves, R.W., and Abrahamson, N.A. (1997). "Modification of empirical strong ground motion attenuation relations to include the amplitude and duration effects of rupture directivity," *Seism. Res. Letters*, 68(1), 199-222.

Spudich, P., Hellweg, M. and Lee, W.H.K. (1996). "Directional topographic site response at Tarzana observed in aftershocks of the 1994 Northridge, California, Earthquake: Implications for mainshock motions," *Bull. Seism. Soc. Am.*, 86(1B), S139-S208.

Uniform Building Code, 1997 edition. *(1997). International Conference of Building Officials, Whittier, CA.*

Vucetic, M. and Dobry, R. (1991). "Effect of soil plasticity on cyclic response," *J. Geotech. Engrg.*, ASCE, 117(1), 89-107.

Youngs, R.R. (1993). "Soil amplification and vertical to horizontal ratios for analysis of strong motion data from active tectonic regions," Appendix 2C in *Guidelines for Determining Design Basis Ground Motions, Vol. 2*, Electrical Power Research Institute, Report No. TR-102293.

Youngs, R.R., Abrahamson, N.A., Makdisi, F., and Sadigh, K. (1995). "Magnitude dependent dispersion in peak ground acceleration," *Bull. Seism. Soc. Am.*, 85, 1161-1176.

RECENT DATA RECORDED FROM DOWNHOLE GEOTECHNICAL ARRAYS

Vladimir Graizer, Anthony Shakal

California Department of Conservation, Division of Mines and Geology
Strong Motion Instrumentation Program, Sacramento, California

and

Patrick Hipley

California Department of Transportation
Division of Structures, Sacramento, California

ABSTRACT

Data recorded by downhole arrays with sensors installed at different depths and geologic layers provide critical information for studies of local site amplification effects.

The soft-soil/rock array at Treasure Island near San Francisco was installed by the California Strong Motion Instrumentation Program in cooperation with other agencies. Analysis of the recorded low amplitude data shows that the average amplification factor from the bedrock to the surface of the soft soil reaches factor of 10 at periods of 1.2-1.3 seconds.

Geotechnical arrays at La Cienega in Los Angeles, Meloland in El Centro, in Eureka and the newly instrumented arrays near the Vincent Thomas Bridge in Long Beach represent deep soft alluvium sites. A comparison was made of the average site amplifications calculated for a number of M<5 events with the site amplification for the 7.1 M_w Hector Mine earthquake. The site amplification curves are similar at short periods, but at longer periods the amplification factor is significantly lower for the distant large-event records.

The Tarzana downhole is located on the top of a small hill, and represents a soft-rock site. The downhole data from small events recorded so far demonstrate a significantly higher amplification effect for the component perpendicular to the hill than for the component parallel to the hill.

Large (up to 10 cm) long-period (up to 8 seconds) displacements were recorded at the La Cienega, El Centro, Tarzana and Long Beach arrays during the Hector Mine earthquake at the distances of more than 200 km from the epicenter. In contrast to the small events, the data recorded during the Hector Mine earthquake show that for the displacements and velocity curves there is practically no near-surface site amplification.

Introduction

In an effort to study site amplification effects the California Strong Motion Instrumentation Program (CSMIP) began instrumenting boreholes with strong-motion accelerometers in 1989. As of August 2000 eleven geotechnical arrays are operational (listed in Table 1), and installation of eight new arrays is planned for 2000-2001. Most of the arrays were installed with the support and cooperation of the California Department of Transportation (Caltrans), but others were installed with the National Science Foundation (NSF), Electric Power Research Institute (EPRI) and the U. S. Geological Survey.

Table 1. CSMIP Instrumented Geotechnical Arrays

	Station No.	Station Name	Lat.	Long.	No. of Depths	No. of Sen-sors	Sensor Depths, m	Geology	Partner
1	36520	Parkfield - Turkey Flat #2	35.882	120.350	3	9	Surface, 11, 23	Alluvium	SMIP
2	36529	Parkfield - Turkey Flat #1	35.878	120.358	2	6	Surface 24	Rock	SMIP
3	58642	Treasure Island - Geotechnical Array	37.825	122.373	7	21	Surface 7, 16, 31, 44, 104,122	Fill, Alluvium, Rock	NSF
4	24703	Los Angeles - La Cienega Geotech Array	34.036	118.378	4	12	Surface 18, 100 252	Deep Soft Alluvium	Caltrans
5	58700	San Francisco - Golden Gate Bridge	37.818	122.477	1	3	152	Rock	Golden Gate Bridge District
6	89734	Eureka - Geotechnical Array	40.819	124.164	5	15	Surface 19, 33, 56, 136	Deep Soft Alluvium	Caltrans
7	24764	Tarzana - Cedar Hill B	34.160	118.534	2	6	Surface 60	Soft Rock	ROSRINE
8	14785	Los Angeles - Vincent Thomas Geotech Array East	33.750	118.270	4	12	Surface 18, 46 91	Deep Soft Alluvium	Caltrans
9	14786	Los Angeles - Vincent Thomas Geotech Array West (two close sites combined)	33.750	118.280	6	21	Surface 15, 30, 30, 91, 189	Deep Soft Alluvium	Caltrans
10	1794	El Centro - Meloland Geotechnical Array	32.773	115.447	4	12	Surface 30, 100, 195	Deep Alluvium	Caltrans
11	58798	Hayward - San Mateo Br Geotech Array	37.617	122.153	5	15	Surface 10, 23, 46, 91	Deep Alluvium	Caltrans

Treasure Island Geotechnical Array

The Treasure Island Array near San Francisco represents a soft-soil/rock geological profile. One of the goals of the array is to explain the amplification of rock motion by soil deposits observed during the M_L 7.0 Loma Prieta earthquake.

Treasure Island is a 400-acre manmade island created in the 1930's by hydraulic filling. The island was constructed over a natural sand spit and Bay Mud, and is located in the San Francisco Bay north of the Franciscan outcrops on Yerba Buena Island. Figure 1 shows the depth profile of the instrumentation. The P and S-wave velocity (after Gibbs and others, 1992) are also shown. At the array site there is approximately 12 m of hydraulic fill and sand overlying about 15 m of medium-stiff Holocene Bay Mud (soft silt and clay sediments) over dense sand and stiff Pleistocene Bay Mud (Old Bay Clay). Generally, the clay stiffness increases with depth. Franciscan sandstone and shale are encountered at 91 m beneath the site. The hydraulic fill consists of silty fine sands with clayey zones. The fill is in a relatively loose condition due to the construction method. After the Loma Prieta earthquake sand boils on Treasure Island indicated liquefaction within 100 m of the array site (Shakal and others, 1989; Darragh and Shakal, 1991). Array site characterization studies are described in greater detail in Darragh and others (1993), and de Alba and others (1994).

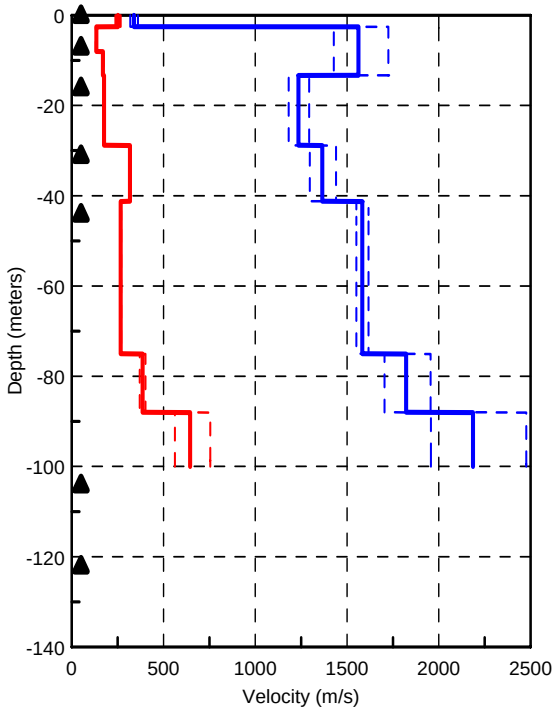

Figure 1. P- and S-wave velocities, and sensor location depths (triangles) at Treasure Island.

The array includes seven triaxial accelerometers that have been installed at the surface and in six boreholes (Fig. 1). Borehole accelerometers are located in the artificial fill at 7 m; near the top of the Young Bay Mud at 16 m; near the top of a dense gray sand at 33 m; near the top of the Old Bay Mud at 44 m; and below the bedrock surface at 104 m and

122 m (instruments added at this depth in 1996). The accelerometers are secured in the borehole using the CSMIP orientation and locking system (Shakal and Petersen, 1992).

Low amplitude data from 7 earthquakes with magnitudes up to 5.4 (Table 2) have been recorded by the Treasure Island Array (Graizer and others, 1999). Maximum ground acceleration recorded at the site was 2% g.

Table 2. Earthquakes recorded by the Treasure Island Geotechnical Array

No.	Date yr/mo/dy	Time (UTC) Hour:min:sec	M_L	Lat	Long	Depth (km)	Epic dist. (km)	Azim	PGA (g)
1	93/01/16	06:29:35.0	4.8	37.018	121.463	7.9	120.4	318	.015
2	94/06/26	08:42:50.3	4.0	37.916	122.286	6.6	12.6	217	.020
3	96/05/21	20:50:20.2	4.5	37.359	121.723	8.1	77.3	312	.009
4	98/08/12	14:10:25.1	5.4	36.753	121.462	9.2	143.8	326	.005
5	98/12/04	12:16:07.8	4.1	37.920	122.287	6.9	13.0	169	.014
6	99/08/18	01:06:18.9	5.0	37.907	122.687	6.7	29.0	108	.017
7	00/09/03	08:36:30.0	5.2	38.377	122.414	9.4	61.4	183	.009

Comparison of strong-motion data recorded in the deepest holes demonstrates that records obtained in the bedrock at the depths of 104 m and 122 m are very similar to each other in amplitude and shape, as shown in the sample record set in Figure 2. The motion is significantly amplified by the relatively soft surface layers.

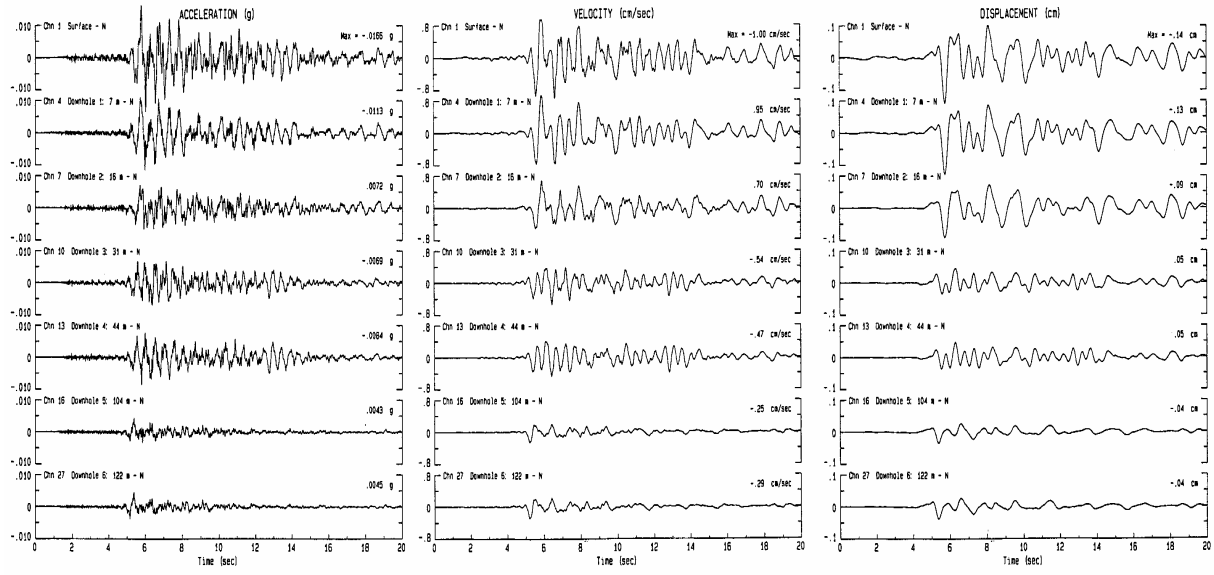

Figure 2. Acceleration, velocity and displacement recorded during the M5.0 earthquake of Aug.18, 1999 at Treasure Island, at the surface and depths of 7, 16, 31, 44, 104 and 122m.

Comparison of the response spectra (with 5% damping) for the surface and downhole records was made. Spectral ratios show that the average amplification from the bedrock to the surface of the soft soil reaches a factor of 6 at a period of 0.55 seconds, and a factor of 10 at periods of 1.2-1.3 seconds (Fig. 3).

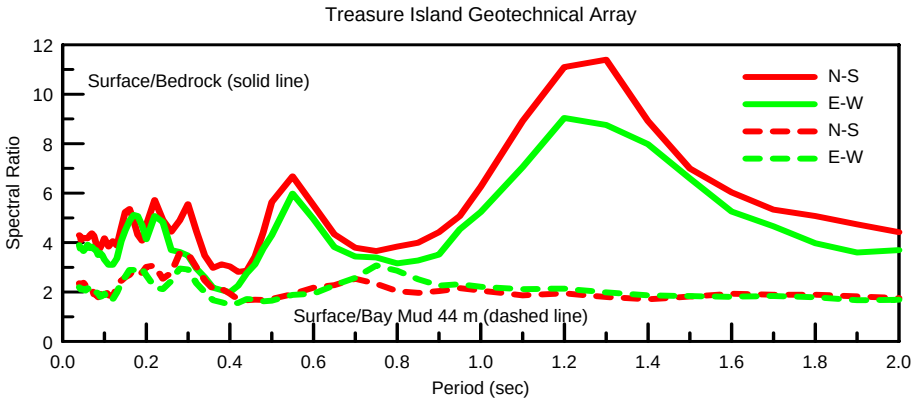

Figure 3. Average spectral site amplification calculated for 5 earthquakes with 4.0≤M≤5.4.

These data demonstrate strong site amplification effect (up to 10 times) from the bedrock to the surface of the soft soil at Treasure Island for low-amplitude motion.

La Cienega Downhole Array

To study the site response effect of a deep soil geologic structure an array was installed with support of Caltrans near the Santa Monica freeway (I-10) at La Cienega, which collapsed during the Northridge earthquake. Topographic maps from 1902 and 1926 (R. Sydnor, personal communication) show small lakes and marshy ground on the surface near the site of the collapsed Santa Monica freeway (La Cienega means "the swamp" in Spanish).

The geology of the two shallow holes was logged during drilling by Robert Sydnor. The profile consists of recent fluvial deposits of about 30 m in thickness over marine deposits (sands, silts, clays and gravels). P-wave and S-wave velocity surveys performed by Caltrans (suspension logging method) and the U. S. Geological Survey (averaging along the geologic layers) are shown in Figure 4. S-wave velocities are about 140 m/sec near the surface and increase to about 600 m/sec at the depth of 100 m. Using the site classification proposed by Boore et al. (1993) the La Cienega Geotechnical Array is a deep soft soil site (site class D).

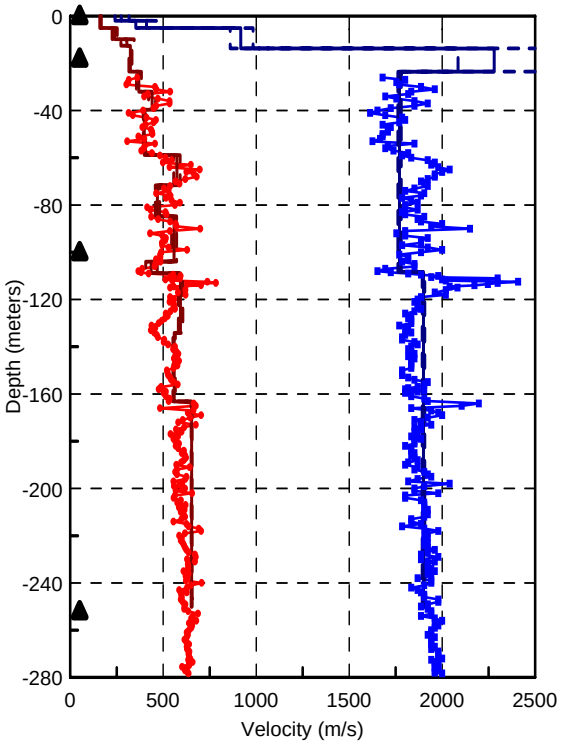

Figure 4. P- and S-wave velocities, and sensor location depths (triangles) at La Cienega array.

Table 3. Earthquakes recorded at La Cienega Geotechnical Array

No.	Date yr/mo/dy	Time (UTC) Hour:min:sec	M_L	Lat	Long	Depth (km)	Epic dist. (km)	Azim	PGA (g)
1	95/06/95	08:40:28.9	5.0	34.390	118.670	13.3	47.6	145	.011
2	97/03/18	15:24:47.7	5.1	34.970	116.820	1.8	176.7	235	.004
3	97/04/04	09:26:24.5	3.3	33.980	118.350	4.2	6.7	337	.078
4	97/04/04	09:35:09.5	2.4	33.990	118.360	4.5	6.4	342	.010
5	97/04/05	14:33:25.3	2.5	33.990	118.360	4.1	6.4	342	.022
6	97/04/26	10:37:30.7	5.1	34.370	118.670	16.5	45.8	144	.015
7	97/04/27	11:09:28.4	4.9	34.380	118.650	15.2	45.7	147	.007
8	98/01/12	06:36:24.9	3.4	34.190	118.470	11.3	19.1	154	.009
9	98/04/15	20:13:21.6	3.2	34.100	118.260	9.2	13.0	237	.014
10	98/05/05	18:14:08.6	1.9	34.050	118.390	9.2	1.9	144	.012
11	99/06/17	01:11:50.1	3.0	34.010	118.220	8.5	15.2	275	.012
12	99/06/29	12:55:00.8	3.8	34.010	118.220	8.0	15.2	275	.042
13	99/10/16	09:46:44.1	7.1	34.594	116.271	6.0	203.6	253	.035
14	99/10/16	09:59:35.1	5.8	34.682	116.285	5.8	205.0	250	.007
15	99/11/30	18:27:02.1	3.3	34.121	118.417	2.8	10.1	159	.017
16	99/11/30	18:46:27.1	3.1	34.125	118.416	2.8	10.5	160	.011

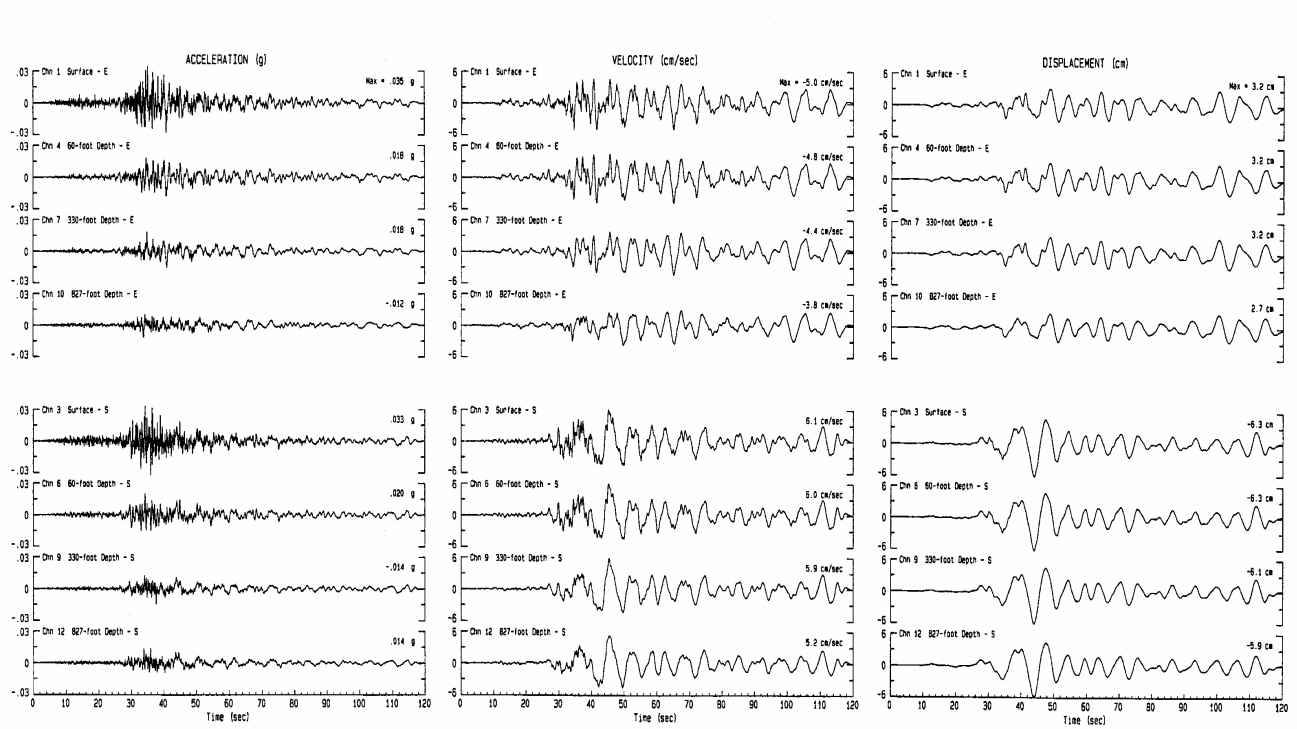

Figure 5. Acceleration, velocity and displacement recorded at the La Cienega array during the M7.1 Hector Mine earthquake, at the surface and depths of 18, 100, and 252 m. The maximum displacement is about 6 cm, at all depths.

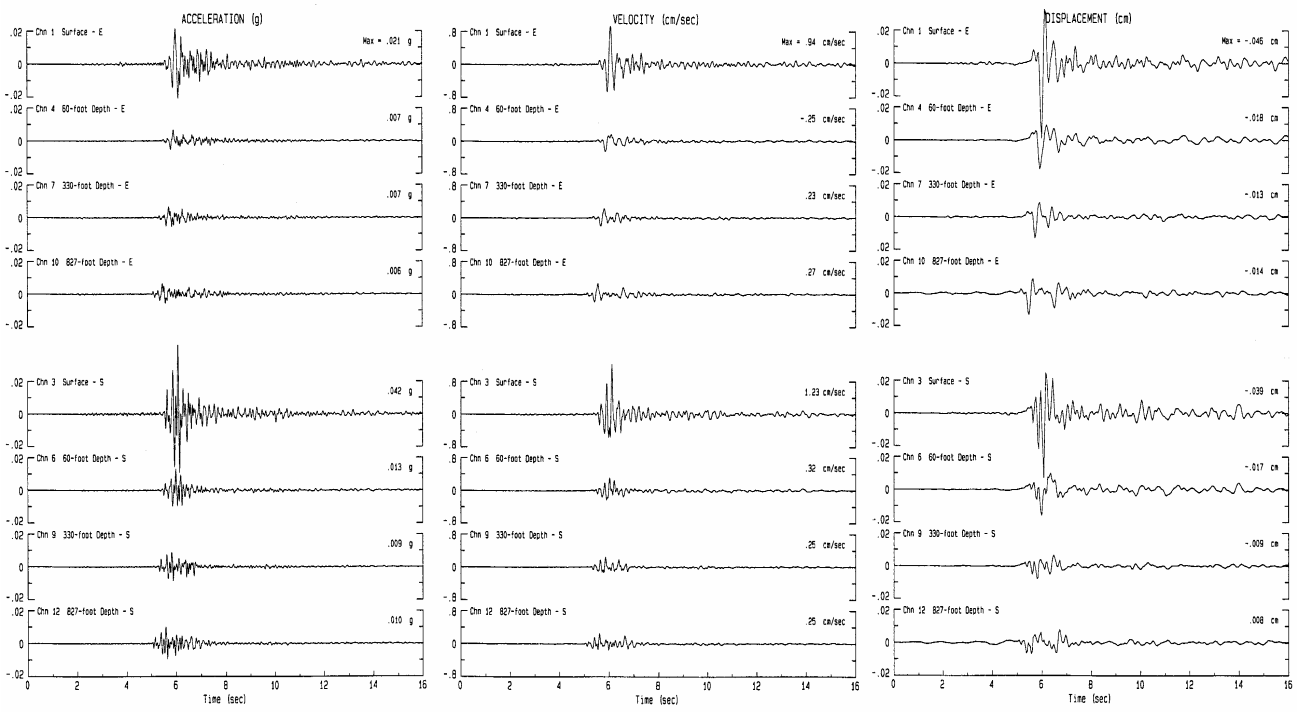

Figure 6. Contrasting example of acceleration, velocity and displacement recorded at the La Cienega array during the local M3.8 June 29, 1999 earthquake, at the surface and depths of 18, 100, and 252 m.

Sixteen earthquakes with magnitudes 1.9<M<7.1 have been already recorded at this site, at the surface and at depths of 18 and 100 m (Table 3). The last four events, including the M7.1 Hector Mine and its M5.8 aftershock, were also recorded at the recently instrumented deepest hole (252 m). Maximum ground acceleration recorded at the site was 8% g.

Acceleration, velocity and displacement recorded at the La Cienega array at the surface and 3 depths during the M7.1 Hector Mine earthquake are shown in Figure 5. Acceleration (short period motion) at the surface is amplified 2.5-3 times relative to the motion at depth. Long-period (up to 8 seconds) displacements with amplitudes more than 6 cm were recorded at this array during the Hector Mine earthquake, at a distance of more than 200 km. The difference between displacements recorded at all four depths during this earthquake is less than 10%. Both the velocity and displacement show practically no amplification from the depth to the surface for the distant large earthquake.

In contrast, ground motion during a M3.8 earthquake at the La Cienega array is shown in Figure 6. This is typical of small local events - acceleration, velocity and displacement are all amplified 3-4 times at the surface relative to the motion at depth.

The average site amplification (spectral ratio) at La Cienega calculated from thirteen events with 1.9<M<5.1 was compared with the site amplification from the 7.1 M_w Hector Mine earthquake (Fig.7). The site amplification curves are similar at short periods. But at longer periods (1.2<T<2.0 sec), the site amplification factor is significantly lower for the distant, larger event (Graizer and others, 2000). Periods are limited to 2 seconds because of the filter's bandwidth used to process low magnitude earthquake data, for which noise is dominant at longer periods.

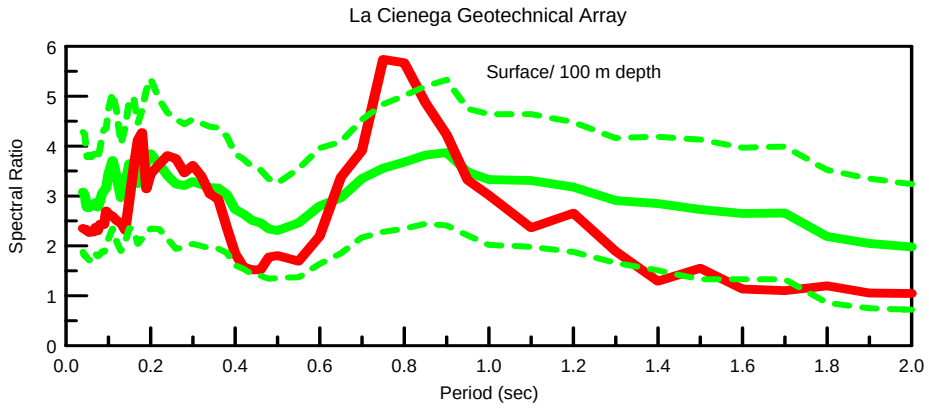

Figure 7. Comparison of site amplification (surface/100 m depth) during the Hector Mine event (dark solid line) and the average amplification for thirteen M<5.1 events (light solid line) ±one standard deviation (dashed lines).

El Centro Downhole Array

A downhole array was instrumented recently at Meloland Overpass near El Centro (surface and 2 depths). Similarly to La Cienega, it also represents a deep soft alluvium profile, with shear wave velocities increasing from approximately 150 m/sec near the surface to 450 m/sec at the depth of 100 m (silt, sand, clay) (Norris, 1988). P-wave and S-wave velocity surveys of the recently drilled downhole were performed by Caltrans.

Five earthquakes recorded by the array are listed in Table 4. Maximum ground acceleration recorded at the site was 4% g.

Table 4. Earthquakes recorded at El Centro Geotechnical Array

No.	Date yr/mo/dy	Time (UTC) Hour:min:sec	M_L	Lat	Long	Depth (km)	Epic dist. (km)	Azim	PGA (g)
1	99/07/24	02:01:26.0	3.9	32.770	115.560	15.4	10.6	88	.015
2	99/10/16	09:46:44.1	7.1	34.594	116.271	6.0	216.0	159	.016
3	00/04/09	10:48:09.7	4.3	32.692	115.392	10.0	10.4	330	.043
4	00/06/14	19:00:20.0	4.2	32.896	115.502	5.1	14.6	159	.015
5	00/06/14	21:49:18.0	4.5	32.884	115.505	4.9	13.5	156	.009

Acceleration, velocity and displacement recorded at the El Centro array at the surface and 2 depths during the M7.1 Hector Mine earthquake are shown in Figure 8. Acceleration (short period motion) at the surface is amplified approximately 2 times relatively to the motion at the depth. Long-period (up to 8 seconds) displacements with amplitudes up to 7 cm were recorded at this array during the Hector Mine earthquake at the distances of 216 km from the epicenter. The difference between displacements recorded during this earthquake at all four depths is less than 10%. There is almost no near-surface amplification for the displacement and velocity (Fig. 8).

Ground motion at the El Centro array during a M4.2 earthquake is shown in Figure 9. Typical of the small local earthquakes recorded, accelerations, velocities and displacements are all amplified approximately 3-4 times at the surface relative to the 100 m depth.

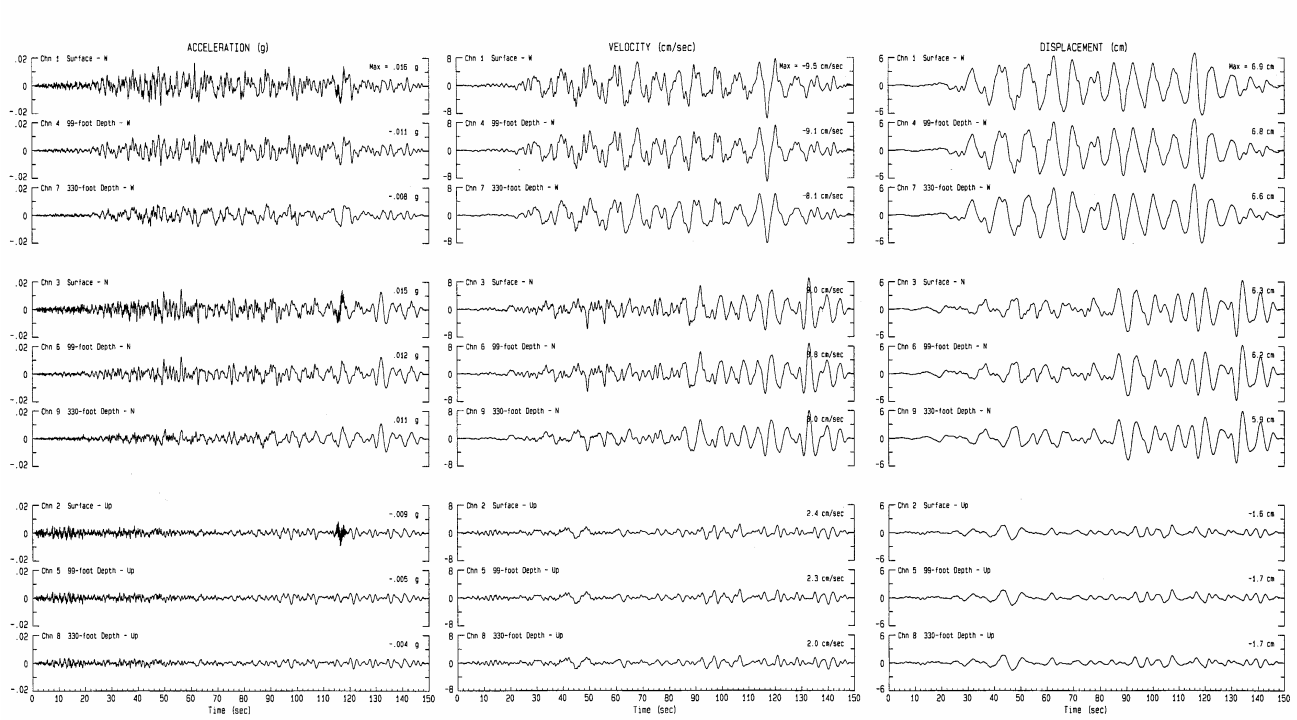

Figure 8. Acceleration, velocity and displacement recorded at El Centro array during the M7.1 Hector Mine earthquake, at the surface and depths of 30, and 100 m. The maximum displacement is about 7 cm, at all depths.

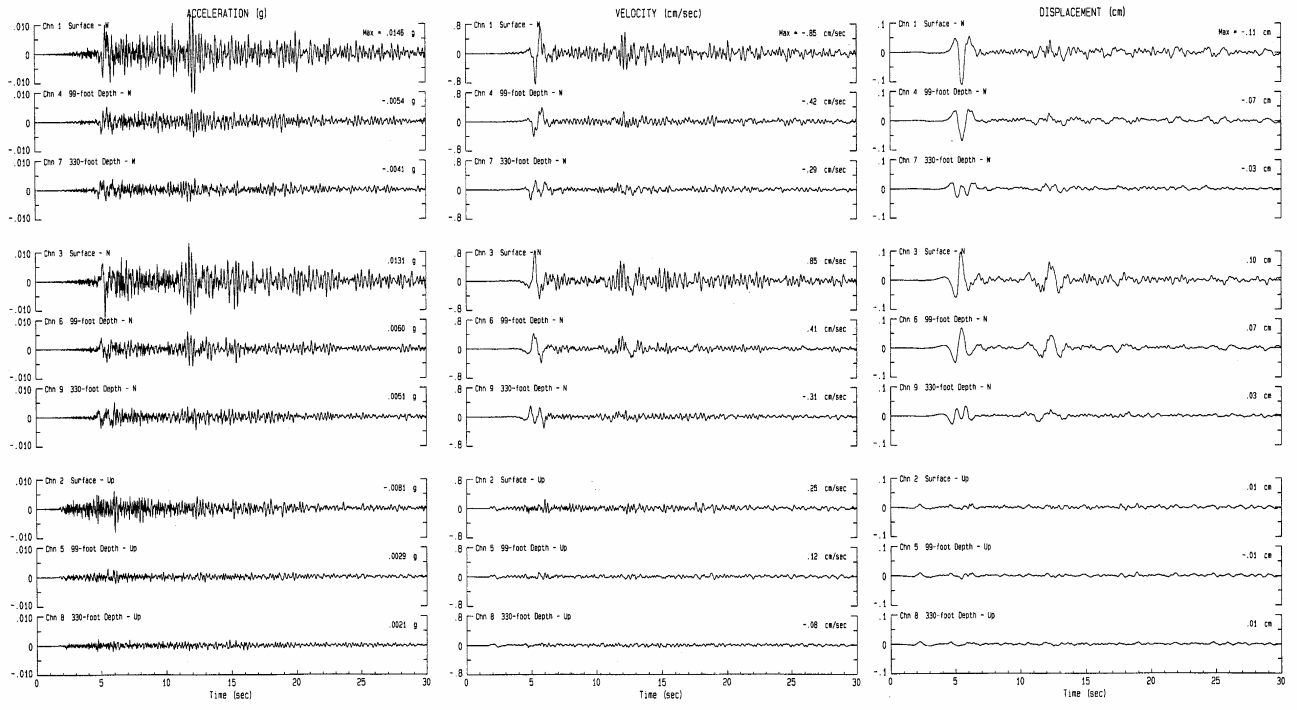

Figure 9. Contrasting example of acceleration, velocity and displacement recorded at El Centro array during the local M4.2 June 14, 2000 earthquake, at the surface and depths of 30, and 100 m.

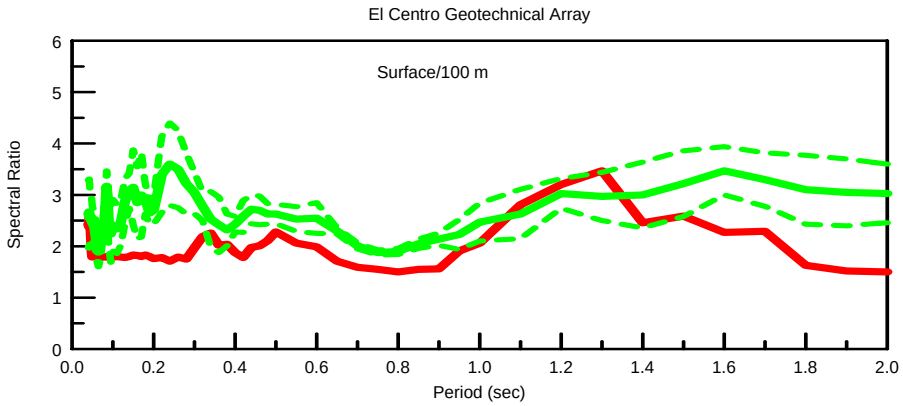

Figure 10. Comparison of site amplification during the Hector Mine event (dark solid line) and the average amplification for four M<5.0 events (light solid line) ±one standard deviation (dashed lines).

The average site amplifications (spectral ratios) at El Centro calculated from four events with M<5 were compared with the site amplification from the 7.1 M_w Hector Mine earthquake (Fig.10). Similar to the La Cienega data, site amplification curves at longer periods (1.4<T<2.0 sec), are lower for the distant, larger events.

The Hector Mine earthquake was also recorded at another deep soft alluvium site near the Vincent Thomas Bridge near Long Beach at a distance of 200 km from the epicenter. Long-period (up to 8 seconds) displacements with amplitudes up to 10 cm were recorded at this site. Similarly to the La Cienega and El Centro arrays, there is almost no difference among displacements recorded at all depths.

Tarzana Downhole

Ground motion amplification has been observed at Tarzana in many earthquakes and for both strong and weak motions. Both the Whittier Narrows and Northridge mainshocks produced larger than expected motions at Tarzana (Shakal et al., 1988). In contrast with the Northridge amplification, some events (Landers, Big Bear and Sierra Madre mainshocks, Whittier Narrows aftershock and some Northridge aftershocks) did not produce significant site amplifications.

The Tarzana site is located on a gentle 20 m high hill, about 500 m in length by 130 m in width with a strike near $N78^0E$. The Tarzana site has been drilled and logged to a depth of 100 m by Agbabian Associates under contract with CSMIP. Low shear-wave velocities (about 200 m/sec) were found in the top 4 m in colluvial soil (soft, silty diatomaceous clay). Decomposed shale is found from 4 to 12 m. Highly to slightly weathered shale of the Modelo formation was found from the 12 to 100 m. Gypsum crystals were observed in the drill cuttings near 6 m. Velocities generally increased gradually to near 750 m/sec near 80 m depth, except in several zones of hard shale and at the water table (Darragh and others, 1997). The hill was found to be well drained with a water table at a depth of 17 m. The results of P-wave and S-wave velocity surveys performed by the U. S. Geological Survey and Agbabian Associates are shown in Fig. 11.

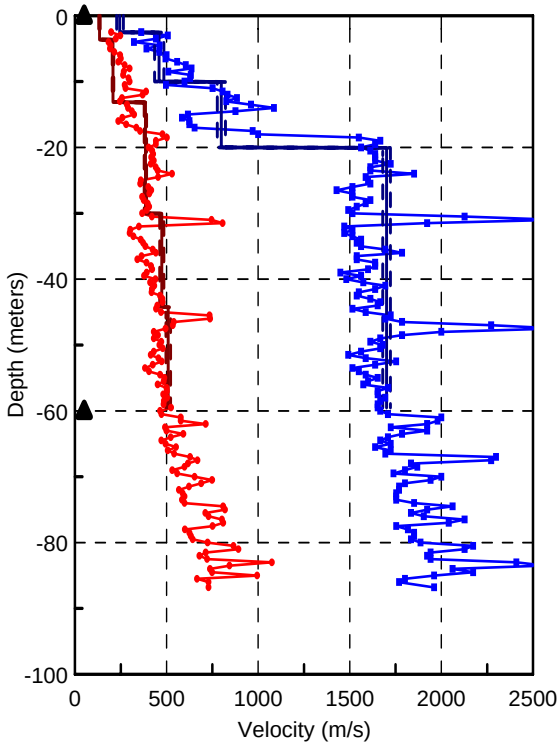

Figure 11. P- and S-wave velocities, and sensor location depths (triangles) at Tarzana downhole.

The Tarzana site was instrumented with support of the ROSRINE project. Eleven earthquakes recorded by the array are listed in Table 5. Maximum ground acceleration recorded by the array was 6% g.

Table 5. Earthquakes recorded at Tarzana Array

No.	Date yr/mo/dy	Time (UTC) Hour:min:sec	M_L	Lat	Long	Depth (km)	Epic dist. (km)	Azim	PGA (g)
1	98/01/04	09:11:45.1	3.3	34.200	118.640	3.5	10.7	114	.009
2	98/01/05	18:14:06.5	4.3	33.950	117.710	11.5	79.6	287	.004
3	98/01/12	06:36:24.9	3.4	34.190	118.470	11.3	6.8	241	.030
4	98/01/15	22:54:08.1	3.0	34.260	118.430	10.6	14.7	221	.006
5	98/03/11	12:18:51.8	4.5	34.020	117.230	14.9	121.3	278	.006
6	98/05/01	21:02:37.8	3.8	34.350	118.670	14.2	24.5	149	.015
7	98/06/03	05:22:50.6	3.0	34.120	118.480	7.7	6.7	312	.026
8	98/09/24	11:41:42.7	2.6	34.110	118.590	6.0	7.6	43	.007
9	98/11/11	05:40:28.9	2.5	34.160	118.500	11.3	3.1	270	.011
10	99/04/11	09:09:19.0	3.6	34.350	118.580	2.3	21.5	169	.007
11	99/10/16	09:46:44.1	7.1	34.594	116.271	6.0	213.6	258	.055

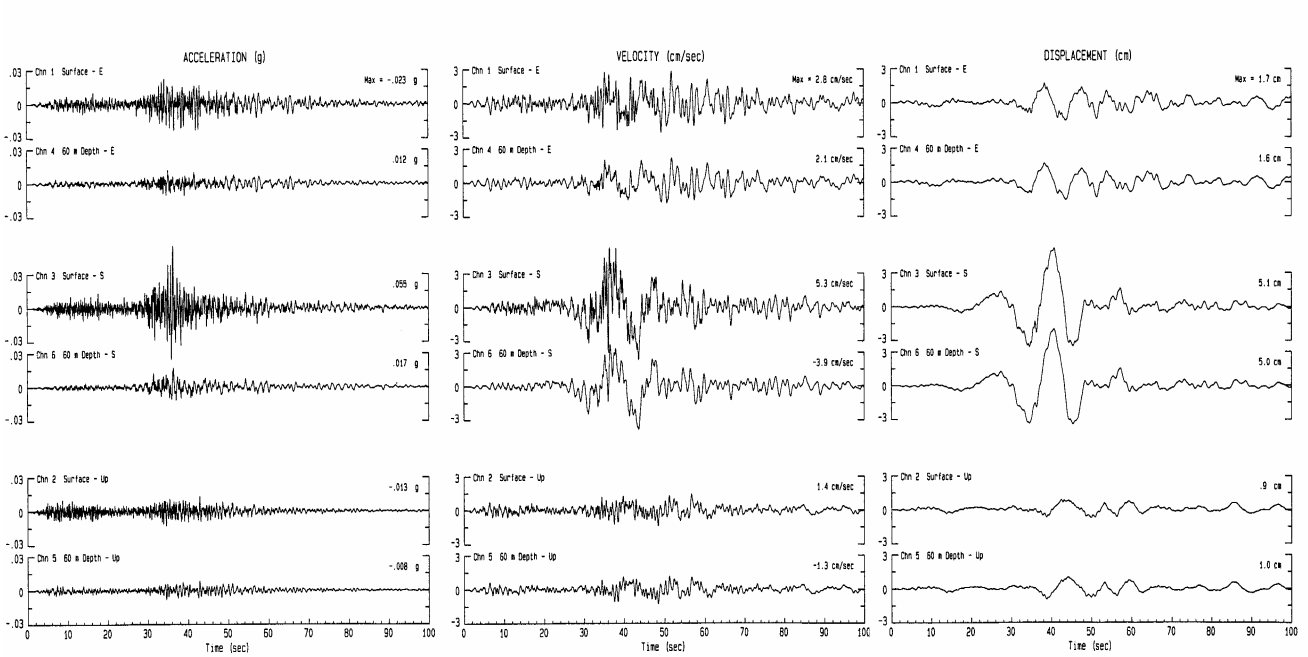

Figure 12. Acceleration, velocity and displacement recorded at Tarzana array during the M7.1 Hector Mine earthquake, at the surface and depth of 60 m. The maximum displacement is about 5 cm.

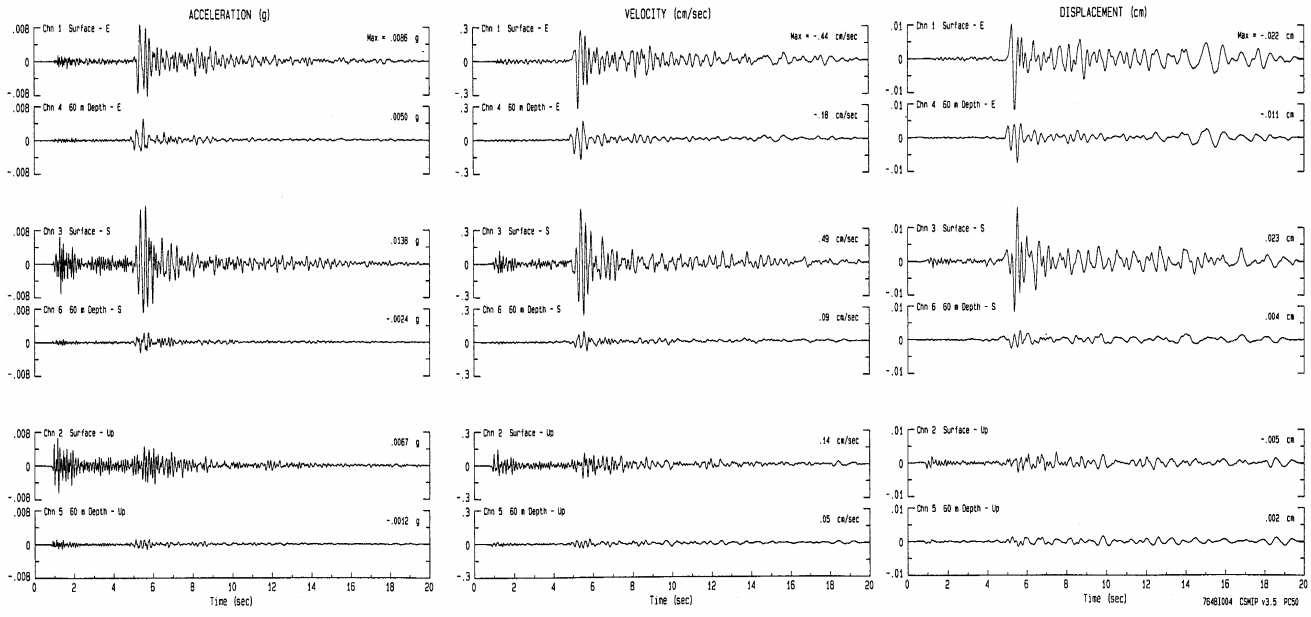

Figure 13. Acceleration, velocity and displacement recorded at Tarzana array during the M3.8 May 1, 1998 earthquake, at the surface and depth of 60 m.

Acceleration, velocity and displacement recorded at Tarzana array at the surface and 60 m depth during the M7.1 Hector Mine earthquake and a M3.8 earthquake are shown in

Figures 12 and 13. For the Hector Mine earthquake, acceleration (short period motion) at the surface is amplified 2-3 times relative to the motion at depth, and there is almost no near-surface amplification for the displacement and velocity (Fig. 12). In contrast, for small earthquakes, accelerations, velocities and displacements are all amplified up to 6 times at the surface relative to the 60 m depth (Fig. 13).

Comparison of the average site amplification for the ten 2.5<M<4.5 earthquakes with the amplification during the M7.1 Hector Mine earthquake is shown in Fig. 14. Similarly to the La Cienega and El Centro data, site amplification curves at longer periods (1.0<T<2.0 sec), are lower for the distant, larger events.

The site amplification effect is much higher for the component perpendicular to the hill compared to the parallel component with maximums at periods of 0.2 and 0.5 seconds (5 and 2 Hz). Note that N-S component is almost perpendicular, and the E-W component is almost parallel to the hill. The source of the site amplification that produces large motions at Tarzana is still under investigation. The three-dimensional topographic effect (Spudich et al. (1996) and Bouchon and Barker (1996)) only partially explains the site amplification on the top of the hill.

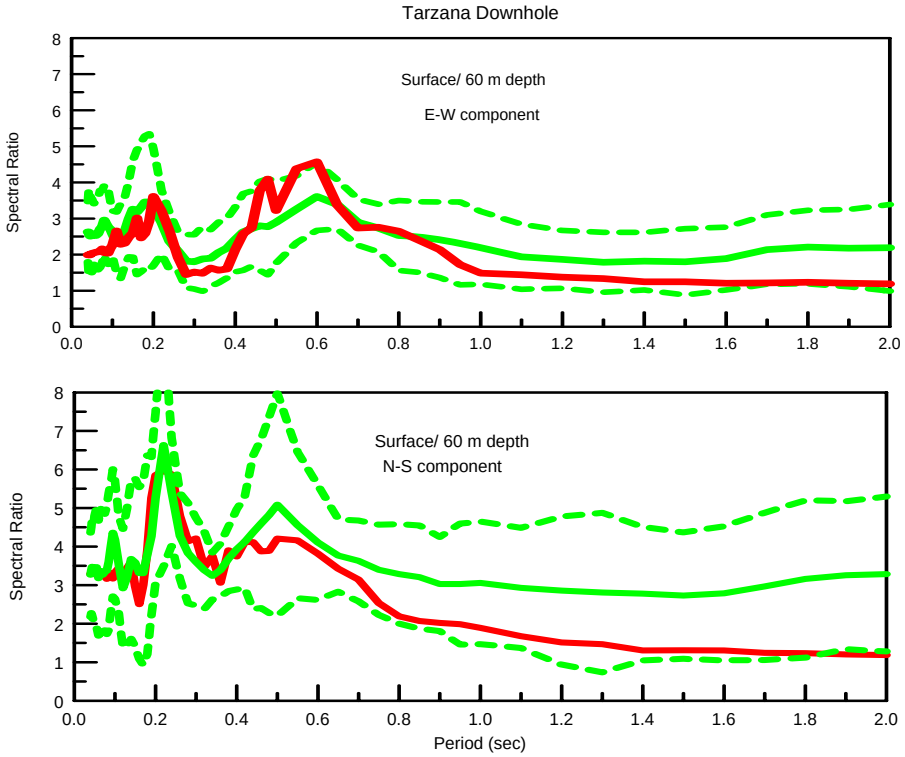

Figure 14. Comparison of site amplification during the Hector Mine event (dark solid line) and the average amplification for M<5.0 events (light solid line) ±one standard deviation (dashed lines).

Conclusions

Data recorded at downhole arrays so far represent low amplitude motions, not exceeding a few percent g (Tables 2-4). This allows relatively representative studies of linear response of the soil profiles.

The 7.1 M_W Hector Mine earthquake of October 16, 1999 and other low amplitude data from a number of events with M<5.0 were recorded by the following geotechnical arrays in Southern California instrumented by CSMIP: La Cienega in Los Angeles, Tarzana, Vincent Thomas Bridge (East and West ends) near Long Beach, and Meloland in El Centro. The geotechnical arrays at La Cienega, Meloland, and the newly instrumented arrays near the Vincent Thomas Bridge represent deep soft alluvium sites. Tarzana represents a soft-rock site, and it was instrumented with support of the ROSRINE project.

Long-period (up to 8 seconds) large amplitude (up to 10 cm) displacements were recorded at the La Cienega, El Centro, Tarzana and Long Beach arrays during the Hector Mine earthquake at epicentral distances of 200 - 220 km.

Comparison of site amplification effects during the M7.1 Hector Mine earthquake with that of closer small events with M<5.0 was made. Site amplification curves are similar at short periods, but are lower at longer periods for the distant, larger events. In contrast to the small local events, data recorded at the four arrays during the Hector Mine earthquake show that for the displacements and velocity curves there is practically no near-surface site amplification.

A possible explanation of these differences which is being investigated, is that in the case of local earthquakes body waves and waves reflected from upper layer boundaries may be predominant. In the case of distant events like the Hector Mine earthquake, surface and basin waves may be predominant. Those waves are of much longer periods. In contrast to a large earthquake, very few basin waves may be generated in the Los Angeles basin for local events with M<5.0.

Further downhole studies are necessary to investigate site amplification effects during different levels of shaking and types of earthquakes. This will allow the generation of empirical site amplification relationship taking into account nonlinear effects, and the effect of different types and periods of waves.

Processed data recorded at the geotechnical arrays are available at the CSMIP website: ftp://ftp.consrv.ca.gov/pub/dmg/csmip/GeotechnicalArrayData

Acknowledgements

The records presented in this report were made possible through the efforts of CSMIP technicians who installed and maintained these stations. We also thank Robert Darragh and Robert Sydnor for their contribution at the early stage of La Cienega and Tarzana studies.

We thank California Department of Transportation, National Science Foundation and ROSRINE (Resolution of Site Response Issues from the Northridge Earthquake) project for their support of downhole instrumentation projects.

References

Boore, D. M., W. B. Joyner and T. E. Fumal (1993). Estimation of response spectra and peak accelerations from western North American earthquakes: An interim report, U. S. Geological Survey, Open-File Report, 93-509.

Bouchon, M., and J. S. Barker (1996). "Seismic Response of a hill: The example of Tarzana, California." *Bull. Seism. Soc. Am.*, V. 86, No. 1A, p. 66-72.

Darragh, R., and A. Shakal (1991) "The site response of two rock and soil station pairs to strong and weak ground motion." *Bull. Seism. Soc. Am.*, V. 81, p.1885-1899.

Darragh, R., M. Huang and A. Shakal (1993) "Processed CSMIP strong-motion data from the Treasure Island geotechnical array from the Gilroy area earthquake of January 16, 1993." Calif. Div. Mines and Geology, OSMS 93-09, 37 pp.

Darragh, R., V. Graizer and A. Shakal (1997). Site Characterization and Site Response Effects at CSMIP Stations: Tarzana and La Cienega Near the Santa Monica Freeway (I-10). Calif. Div. Mines and Geology, OSMS 96-07, 262 pp.

Darragh, R., V. Graizer and A. Shakal (1998). "Tarzana, California: Site Response and Characterization." Proceedings of the NEHRP Conference and Workshop on Research on the Northridge, California Earthquake of January 17, 1994. Vol. II, Earth Science, p. 323-330.

de Alba, P., J. Benoit, D. G. Pass, J. L. Carter, T. L. Youd and A. F. Shakal (1994). "Deep instrumentation array at Treasure Island Naval Station." U. S. Geol. Surv. Prof. Pap. 1551-A, p.155-168.

Gibbs, J. F., T. E. Fumal, D. M. Boore and W. B. Joyner (1992) "Seismic velocities and geologic logs from borehole measurements at seven strong-motion stations that recorded the Loma Prieta earthquake." U. S. Geol. Surv. Open-File Report 92-287.

Graizer V. M., Shakal, A. F. and C. J. Roblee (1999). "Geotechnical arrays instrumented by the California Strong Motion Instrumentation Program (CSMIP)." (Abstract). *Seismological Research Letters*, V. 70, No. 2, p.225.

Graizer V. M., Cao T., Shakal, A. F. and P. Hipley (2000). "Comparison of the site amplification effects from the M7.1 Hector Mine earthquake with that of small events recorded at downhole arrays." (Abstract). *Seismological Research Letters*, V. 71, No. 2, p.244.

Norris, G. M. (1988) "Liquefaction at the Meloland Overcrossing During the Imperial Valley Earthquake of 1979." *Bull. Assoc. Engineering Geologists.* V. XXV, No.2, p. 235-247.

Shakal, A., Huang, M. Reichle, C. Ventura, T. Cao, R. Sherburne, M. Savage, R. Darragh, and C. Petersen (1989). CSMIP strong-motion records from the Santa Cruz Mountains (Loma Prieta), California earthquake of 17 October 1989, Calif. Div. of Mines and Geology, OSMS 89-06, 196 pp.

Shakal, A. F. and C. P. Petersen (1992). "Downhole strong-motion accelerometry: Objectives and techniques." (Abstract). *Seismological Research Letters*, V. 63, No. 1, p.30.

Shakal, A. F., M. J. Huang and R. B. Darragh (1996). "Interpretation of significant ground-response and structure strong motions recorded during the 1994 Northridge earthquake." *Bull. Seism. Soc. Am.*, V. 86, No. 1B, p. S231 - S246.

Spudich, P., M. Hellweg, and W. H. K. Lee (1996). "Directional topographic site response at Tarzana observed in aftershocks of the 1994 Northridge, California, earthquake: Implications for mainshock motions." *Bull. Seism. Soc. Am.*, V. 86, No. 1B, p. S193 - S208.

VALIDATION OF EVALUATION METHODS AND ACCEPTANCE CRITERIA IN EVOLVING PERFORMANCE-BASED SEISMIC CODES

Sashi K. Kunnath, Quan Nghiem, Alfred John Jr. and Sherif El-Tawil

Department of Civil and Environmental Engineering
University of Central Florida, Orlando

ABSTRACT

A critical evaluation of the four analytical methods recommended in FEMA-273 for the estimation of seismic demands is carried out using measured response characteristics of four instrumented steel buildings. Prior to conducting the FEMA-273 analyses, computer models of each structural system were calibrated to the observed response. Two of the buildings which experienced little or no damage were modeled as fully three-dimensional systems while the remaining two buildings which suffered moderate damage in recent seismic events were further tuned to simplified two-dimensional models to permit detailed inelastic evaluations. Dozens of linear and nonlinear computer analyses under both static and seismic loads were carried out on each building, however, only a few typical results are presented in this paper. Results of the evaluations provide insight into both modeling issues and the validity of the four analytical procedures outlined in the FEMA-273 document. It is found that calibrating structural models to observed response is sensitive to mass and stiffness modeling assumptions. Linear and nonlinear static procedures do not adequately predict inter-story drift estimates, a critical parameter in seismic evaluation and design.

INTRODUCTION

The design philosophy advocated in FEMA-273 (1997) is roughly composed into three steps: definition of a performance objective which incorporates a seismic hazard level, estimation of seismic demands in the system and its components, and verification of acceptance criteria which determines if the design objective has been met. Of these, the second step can be considered the most vital since an accurate estimate of expected performance is essential to assessing the suitability of the final design. Two types of analysis methods, which can be broadly classified as linear and nonlinear procedures, are outlined in the FEMA document. This implies that an engineer can make reliable estimates of deformation demands using either one of these analysis methods. The estimation of seismic demands using linear or nonlinear *static* procedures are inevitably going to be favored by practicing engineers over nonlinear time-history methods because of the complexity and uncertainty involved in material modeling and identification of appropriate ground motion characteristics for fully nonlinear dynamic procedures. The four FEMA analytical approaches evaluated in this study are:

Linear Static and Dynamic Procedures (LSP and LDP): This procedure is recommended for regular buildings with heights not exceeding 100 ft. Additionally, the demand to capacity ratio for any element in the structure should typically not exceed 2.0. Certain exceptions to the rule are outlines in Section 2.91 of FEMA-273.

Nonlinear Static and Dynamic Procedures (NSP and NDP): Nonlinear procedures are generally applicable for all buildings with the exception that NSP is limited to buildings where high mode effects are small. Again, FEMA-273 has specific guidelines using response spectrum methods to determine the limits of NSP. It is also suggested that two lateral load patterns be considered in the analysis: an inverted triangular pattern (referred to as NSP-1 in this paper) based on Equation (3-7) in FEMA-273, and a uniform distribution (referred to as NSP-2).

One of the primary aims of this project is to evaluate the four analytical methods. The ability of each analytical procedure to predict inter-story drift demands will be examined. In the case of damaged buildings, the ability of the nonlinear static method to identify critical connection fracture locations in the structure will be verified. A secondary objective of the project deals with system identification and issues related to calibrating building models to observed response.

Four steel buildings, all instrumented by the California Strong Motion Instrumentation Program (CSMIP), were considered in this evaluation exercise. The recorded data was made available by CSMIP and details of the instrumented information are available in numerous publications (Darragh et al., 1995; Shakal et al, 1995 etc.). Building data, the system identification tasks leading to the calibration of the building models followed by the FEMA-273 evaluations of the buildings are summarized in this paper.

It is essential to point out that each building was analyzed using different building models and numerous loading scenarios. In all, over a hundred simulations were carried out including linear and nonlinear evaluations of static and seismic loading. The results presented in this paper cover only a typical subset of evaluations.

SIX-STORY COMMERCIAL BUILDING, BURBANK

This is the first of four buildings evaluated in this study. Recorded response data on this building is available for three earthquakes: the 1987 Whittier Narrows earthquake, the 1991 Sierra Madre earthquake and the 1994 Northridge earthquake. Studies on this building comprised of system identification studies to calibrate the building model and FEMA-273 evaluation using the four different analytical approaches.

Building Details

This building is a 6-story steel structure designed in 1976 as per the 1973 UBC requirements. The primary lateral load resisting system is a moment frame around the perimeter of the building. The structural system is essentially symmetrical. Moment continuity of each of the perimeter frames is interrupted at the ends where a simple shear connection is used to connect to the weak column axis. The plan view of the building and the elevation of a typical frame is shown in Figure 1. The interior frames were designed as gravity frames and consist of simple shear connections only. Exterior columns are supported on piles while the interior columns are supported on spread footings. The building was instrumented with a total of 13 strong motion sensors at the ground, 2nd, 3rd and roof levels, as displayed in Figure 2. Instrumentation at the third floor level was not fully functional during the Northridge earthquake and was not available for this study.

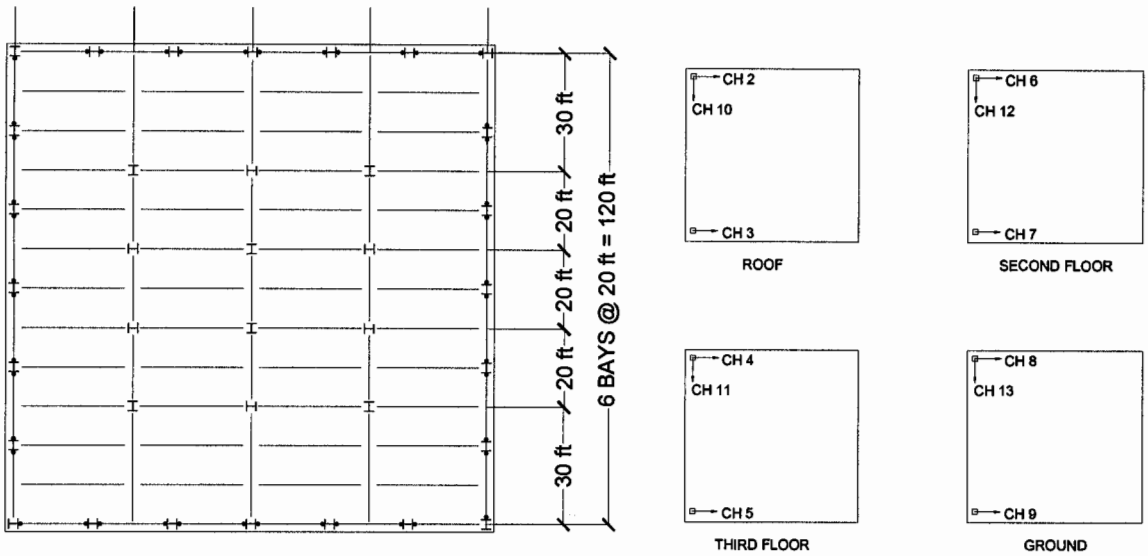

Figure 1. Plan View of Building and Location of Instrumentation

The building performed well in all three earthquakes with no visible signs of damage. Recorded data indicates an essentially elastic response. In constructing the building model, the base was assumed to be fixed (all columns are supported by base plates anchored on foundation beams which in turn are supported on a pair of 32 feet 30-inch diameter concrete piles). Section properties were computed for A-36 steel with an assumed yield stress of 44 ksi as established from coupon tests conducted on the steel used in the building (Anderson and Bertero, 1991). The total building weight (excluding live loads) was estimated to be approximately 7600 kips.

Calibration of Observed Response

A three-dimensional computer model of the building was created using SAP2000 (Computers and Structures, 2000). The model included both the lateral load resisting perimeter frames and the interior gravity frames. An isometric view of the SAP2000 model is displayed in Figure 2 along with an elevation of a typical frame showing member sizes and dimensions. Several modeling assumptions were tested: 1) beam models with and without full composite action; 2) increased damping in higher modes; 3) effect of panel zone yielding.

An earlier study by Shen and Astaneh (1990) on the same building indicated that proper modeling of the floor diaphragm was crucial in reproducing observed response. It is important to point out that their evaluation was based on the building response to the 1987 Whittier earthquake which was smaller in magnitude than the Northridge event. Given the low magnitude response, it is likely that both composite floor action and the participation of non-structural elements were significant. To gain a better understanding of the system characteristics during the three different earthquakes, a spectral analysis of the roof vs. ground accelerations was carried out. Figure 3 shows the transfer function of the roof accelerations for the three recorded ground motions.

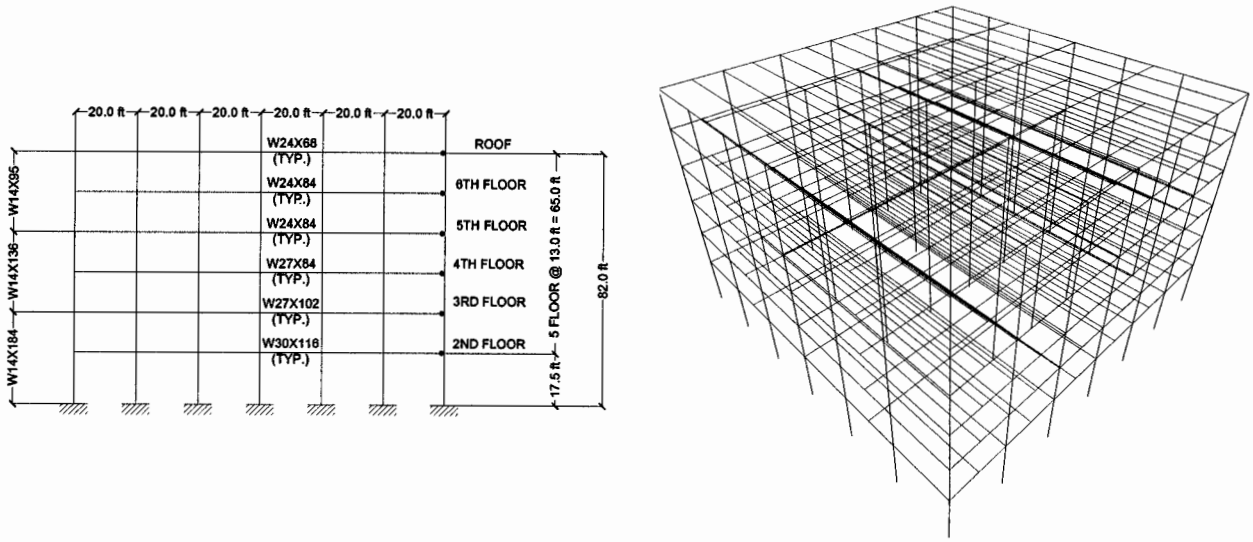

Figure 2. Elevation of Typical Perimeter Frame and SAP2000 Model of Building

It is evident from Figure 3 that the system response is a function of both the ground motion spectral characteristics and the ground motion intensity. The predominant frequency for the relatively low magnitude events (Whittier and Sierra Madre) is 0.78 Hz (1.28 sec) and for Northridge is 0.71 Hz (1.41 sec).

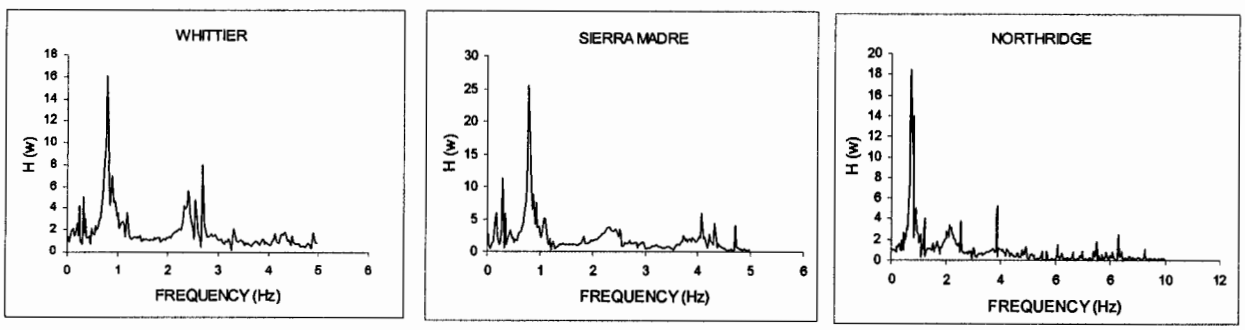

Figure 3. Transfer Function of Observed Roof Acceleration During Whittier, Sierra Madre and Northridge Earthquakes

Several aspects of modeling the 6-story Burbank building were explored. Three separate models were developed as part of the calibration exercises: (i) a fully three-dimensional model including internal gravity frames; (ii) a 3D model considering the exterior frames only; and (iii) a 2D model of a typical exterior frame. Results of separate 3D lateral analysis indicated that the perimeter frames carry about 85% of the lateral load. Consequently, 2D models in which only 42.5% of the mass was considered produced the best correlations with observed response. In all cases, it was established that the bare frame stiffness was inadequate to represent the true structure stiffness. Considering full composite action of the floor slabs provided the additional 10% structural stiffness needed to calibrate the observed response. Figure 4 shows the correlation between computed and recorded response during the Northridge earthquake.

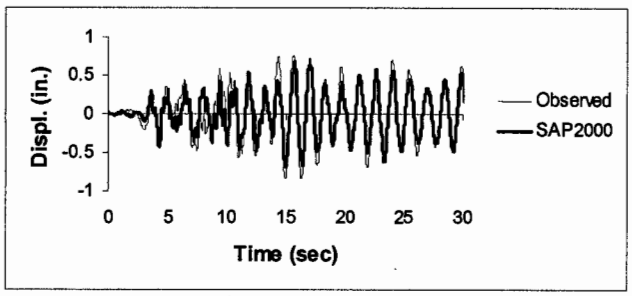

(a) N-S response (2nd level)

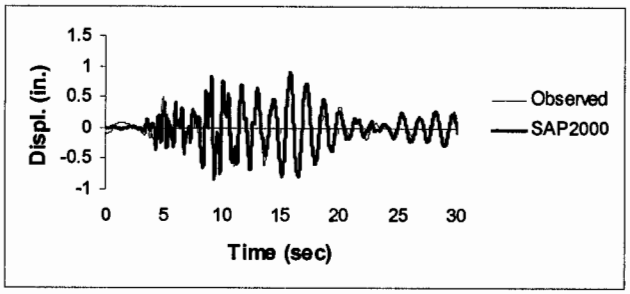

(b) E-W response (2nd level)

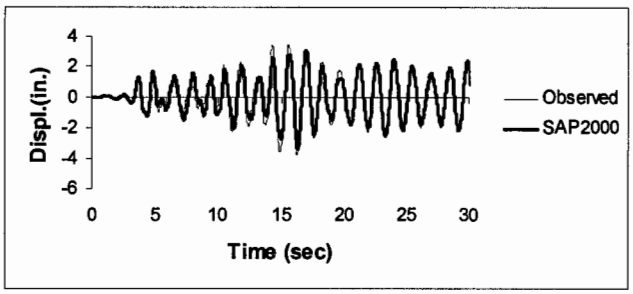

(c) N-S response (roof level)

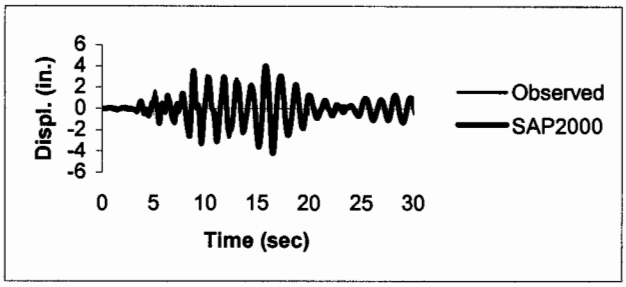

(d) E-W response (roof level)

Figure 4. Calibrated Response of 6-Story Building to the Northridge Earthquake

A constant viscous damping of 3% in the first mode and 10% in the remaining modes was used in the analysis. The increased damping value used in higher modes was necessary to match the observed acceleration response and did not influence the displacement response. The computed acceleration response histories for the 2nd level and the roof are shown in Figure 5.

A systematic evaluation of the section properties of the building revealed the potential for weak panel zones. Given the fact that the structure experienced a slight period shift from 1.33 seconds during the early phase of the earthquake to 1.43 seconds, it was considered worthwhile to investigate potential panel zone yielding. A 2D model of the structure was, therefore, developed and calibrated. The results did show some panel zone yielding but the resulting period shift was not evident. Panel zone plastic rotations were less than 0.5% which would be categorized as being within FEMA-273 IO (Immediate Occupancy) limits.

Evaluation of FEMA-273 Analytical Procedures

The final set of evaluation tasks consisted of performing a FEMA-273 based evaluation of the building. To investigate the validity of static procedures to estimate seismic demands, the building was subjected to lateral loads of the form of Equation (3-7) in FEMA-273. The magnitude of the loads was adjusted uniformly so as to obtain the same maximum roof displacement observed in the Northridge earthquake. The resulting displacement and drift profiles are shown in Figure 6.

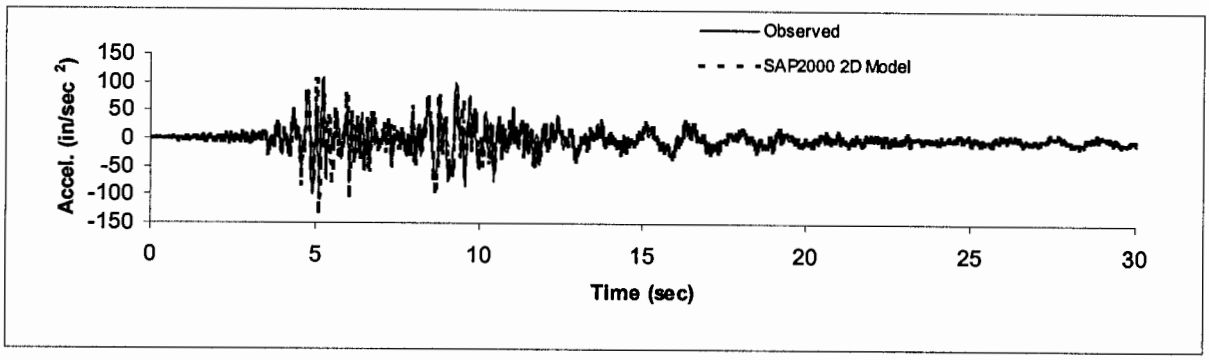

(a) Second Floor Level

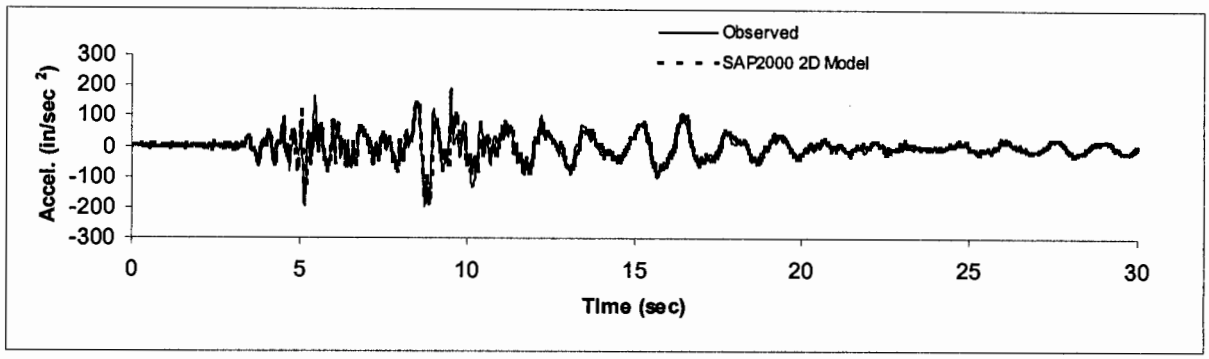

(b) Roof Level

Figure 5. Correlation of Analytically Computed Acceleration Response with Recorded Data in EW Direction During Northridge Earthquake

Next, the building was subjected to lateral loads corresponding to BSE-1 and BSE-2 events as specified in FEMA-273. The Basic Safety Objective (BSO) as defined in FEMA-273 requires Life-Safety (LS) performance for BSE-1 and Collapse Prevention (CP) for BSE-2. In addition to LSP and NSP, a linear dynamic procedure (LDP) using a response spectrum analysis was also carried out. The spectra for both hazard levels were generated using procedures described in the FEMA guidelines. Some of the relevant results of the evaluation are summarized in Figures 7 and 8. A discussion of these results is presented in the next section.

Summary

It was concluded that modeling the structural system using bare section properties did not represent the actual structural stiffness. The contribution of non-structural elements, semi-rigid connections, etc. could be considered in an equivalent sense by incorporating full composite action of the floor slabs. The peak drift profile is not adequately estimated by linear or nonlinear static procedures. Estimates of deformation demands using linear static methods are more conservative than linear dynamic methods based on a response spectrum analysis. FEMA-273 based evaluations suggest that the building will pass BSO requirements with the exception of the nonlinear static procedure which indicates CP requirements being violated at the lowest level.

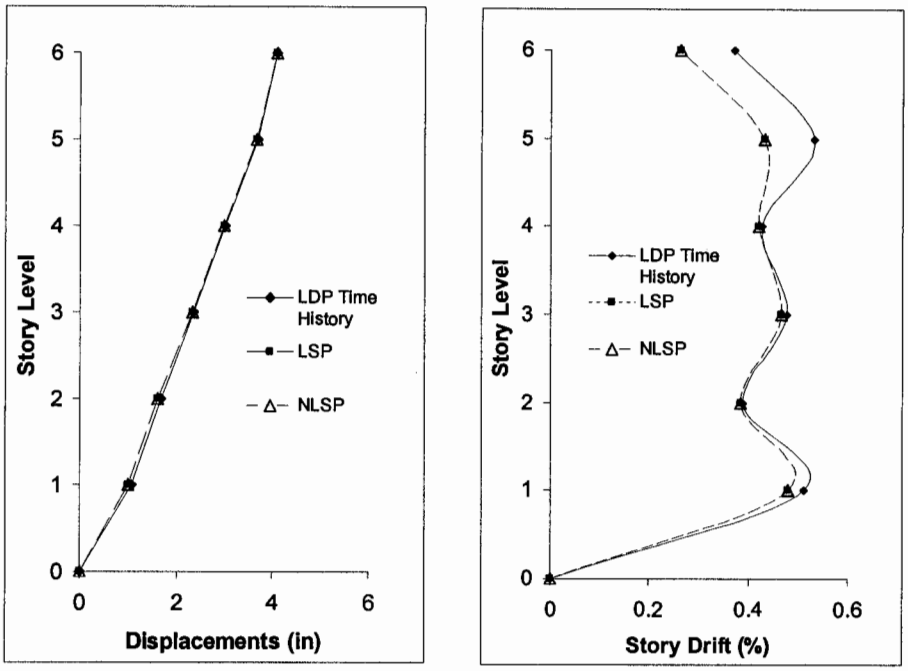

Figure 6. Peak Displacement and Drift Profile Estimates Using Various Analysis Methods (EW Direction Response During Northridge)

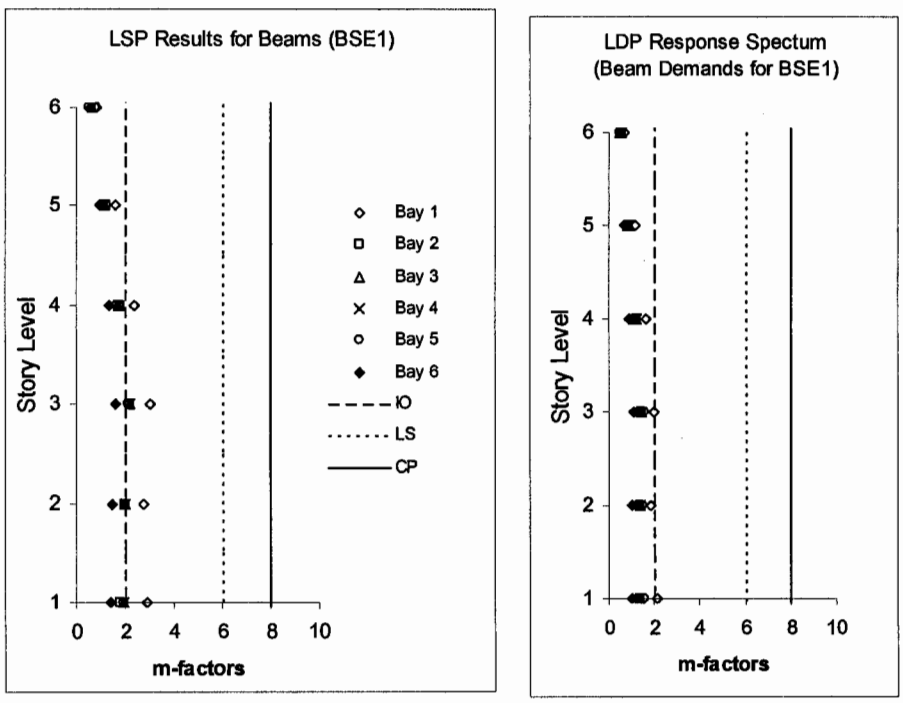

Figure 7. Comparison of Beam Deformation Demands with FEMA-273 Acceptance Criteria for Linear Procedures

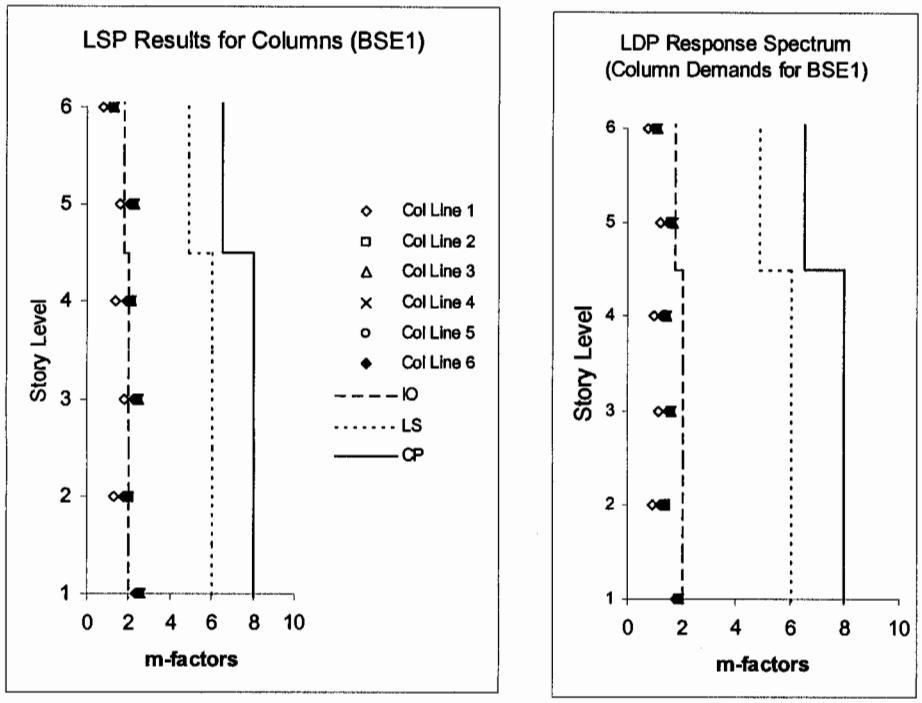

Figure 7 (continued). Comparison of Column Deformation Demands with FEMA-273 Acceptance Criteria for Linear Procedures

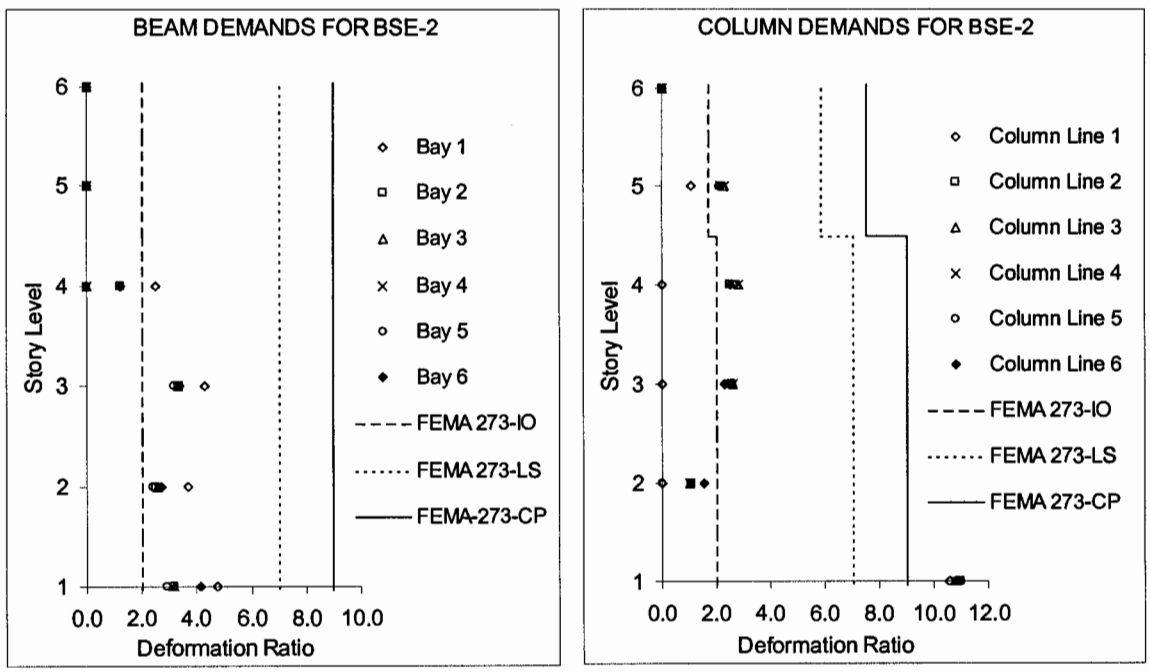

Figure 8. Comparison of Deformation Demands vs. FEMA-273 Acceptance Criteria for Nonlinear Static Procedure (NSP)

NINETEEN STORY OFFICE BUILDING, LOS ANGELES

The second building to be evaluated is a high-rise office building with nineteen stories above ground and four parking levels below ground. Instrumented data for this building are available since the 1971 San Fernando earthquake. While there were only three sensors present during the 1971 earthquake, as many as fifteen sensors during the Northridge earthquake. No structural damage has been reported in any earthquake, however, non-structural damage and resulting losses have not been insignificant. The evaluation reported in this study is limited to the response of the building to the Northridge event.

Building Details

The true geographical North-South direction does not coincide with the orientation of either of the building directions. The long direction of the building (referred to as the EW direction in this study) is oriented at S44°W. The lateral load resisting system consists of four ductile steel moment frames in the EW direction and five X-braced steel frames in the NS axis (short building direction). A typical plan of the building and the location of the strong motion sensors are indicated in Figure 9. The main structural system rests on steel I-beam piles up to a depth of 72.3 feet. The piles are capped in groups and connected by 24 inch square reinforced concrete tie beams.

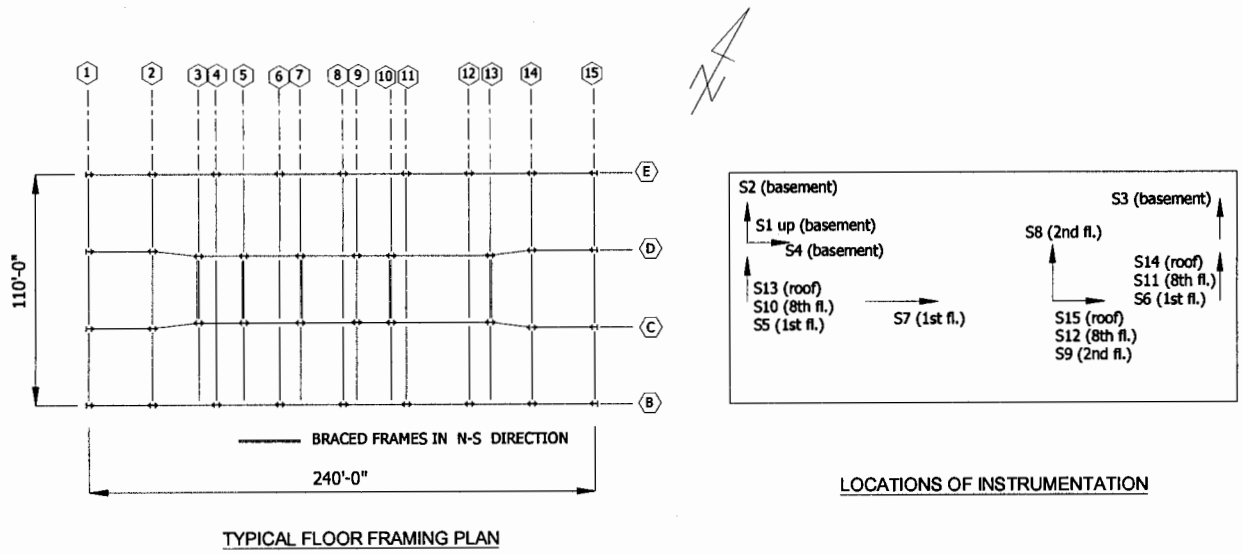

Figure 9. Typical Plan View and Instrumentation of 19-Story Building

Calibration of Observed Response

A three-dimensional model of the entire building was developed using SAP2000. In all, 58 separate column types and 23 different beam types were used to model the building. Though this appears reasonable for a building of this size, the difficulty with modeling and processing the results stems from the fact that different beam sizes are used in each bay at a given level. The building weight, including estimates of non-structural elements such as partition walls and the

mechanical equipment in the roof, was estimated to be 58,341 kips. A constant viscous damping factor of 3% of critical was used in all modes. Note that the building has an intermediate level between the ground and first floor and this level has been modeled as the first level, hence results are shown for 20 levels. A wire-frame model of the building as used in the SAP2000 evaluation is shown in Figure 10.

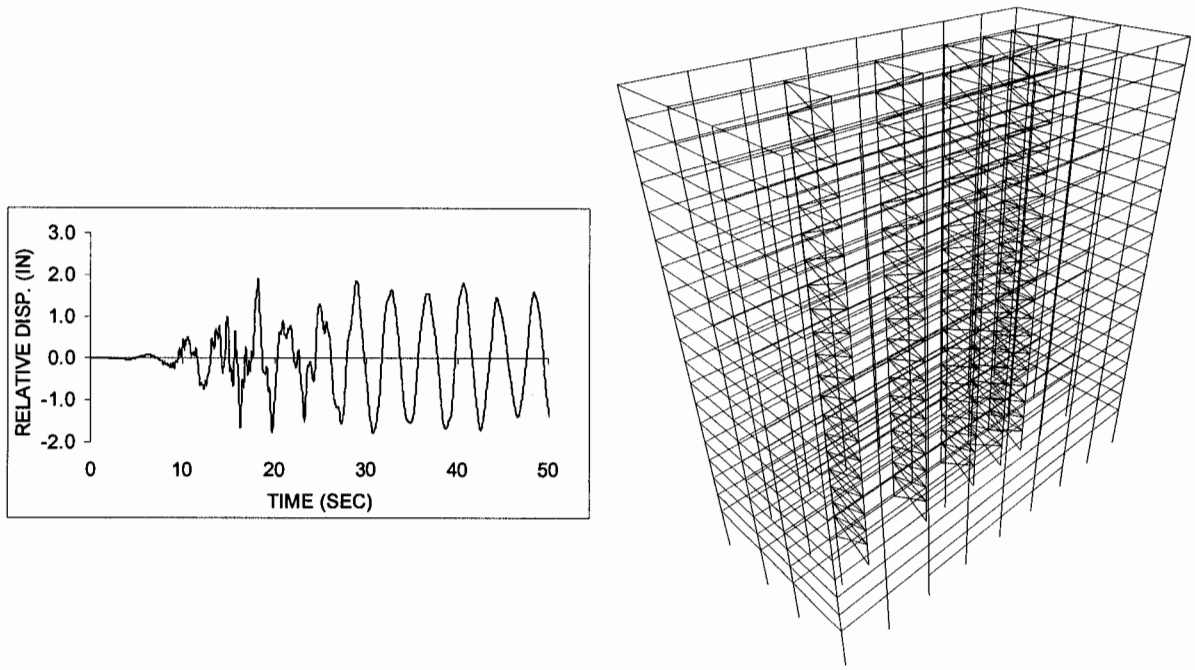

Figure 10. SAP200 Model of 19-Story Building and Relative Displacement Between Channel 13 and Channel 14 at Roof Level

An eigenvalue analysis of the structure indicated a dominant torsional mode of vibration at a period of 4.27 seconds. A plot of the relative displacement between channels 13 and 14 (see Figure 9) which are located at either end of the building shows a differential displacement of almost 2.0 inches (approximately 15% of the total displacement) supports this finding. The first lateral mode of vibration is in the long (EW) direction of the building at a period of 3.8 seconds and the next lateral mode in the NS direction has a period of 3.12 seconds.

The building model was subjected to the recorded Northridge accelerations in both building directions, independently and simultaneously. A rigid diaphragm assumption was used in the analysis. Results of the analyses indicate that the structural system remained elastic throughout the duration. A more accurate match of the recorded response was obtained with both lateral components of the earthquake applied simultaneously. The resulting time histories of the displacements at various levels are shown in Figure 11. Additionally, it was observed that the torsional mode of vibration was not excited in the analysis and the relative displacement recorded in the actual building (Figure 10) was not captured in the SAP2000 run. It may be concluded that some diaphragm flexibility may have contributed to the relative movement.

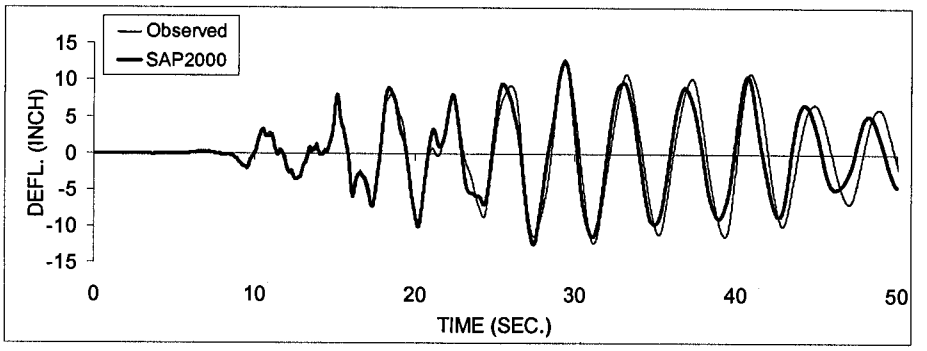

(a) Roof Displacement History

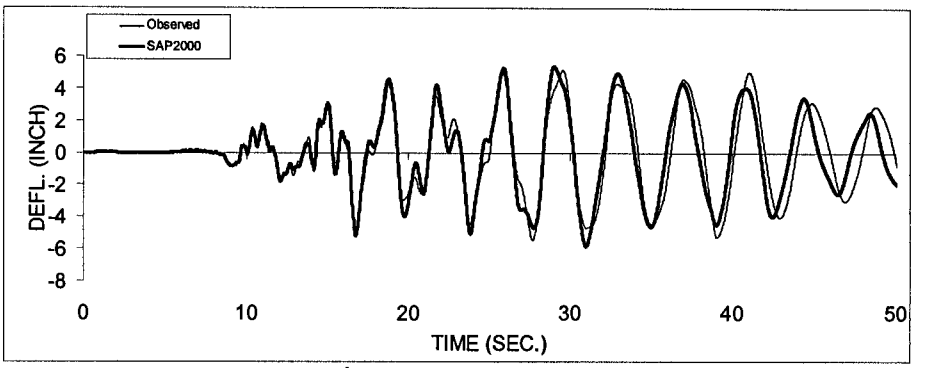

(b) 8th Floor Displacement History

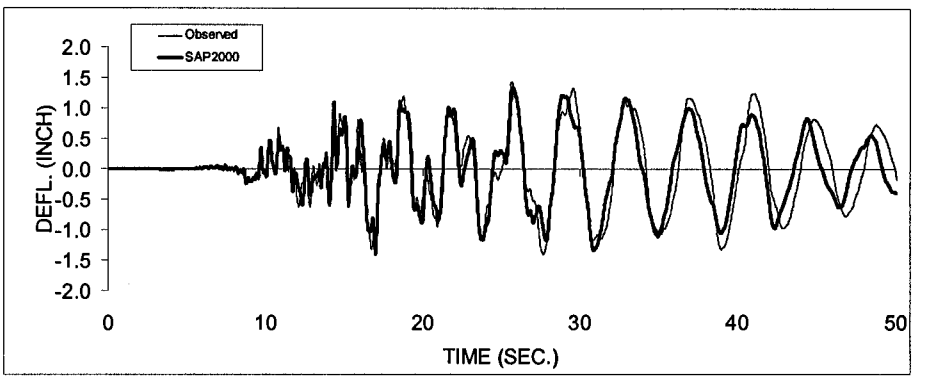

(c) 2nd Floor Displacement History

Figure 11. Validation of Building Model with Recorded Response

Evaluation of FEMA-273 Analytical Procedures

The calibrated building model was then evaluated using the different analytical approaches recommended in FEMA-273 for both BSE-1 and BSE-2 loading. Separate evaluations were carried out in each building direction. Since the building is composed of four moment frames in the long direction and five braced frames in the short direction and the elements in a given bay for each frame varies, the task of carrying out a detailed FEMA-273 evaluation was tedious. Due to space limitations, only essential results for one critical frame in the weak direction of the building is presented here.

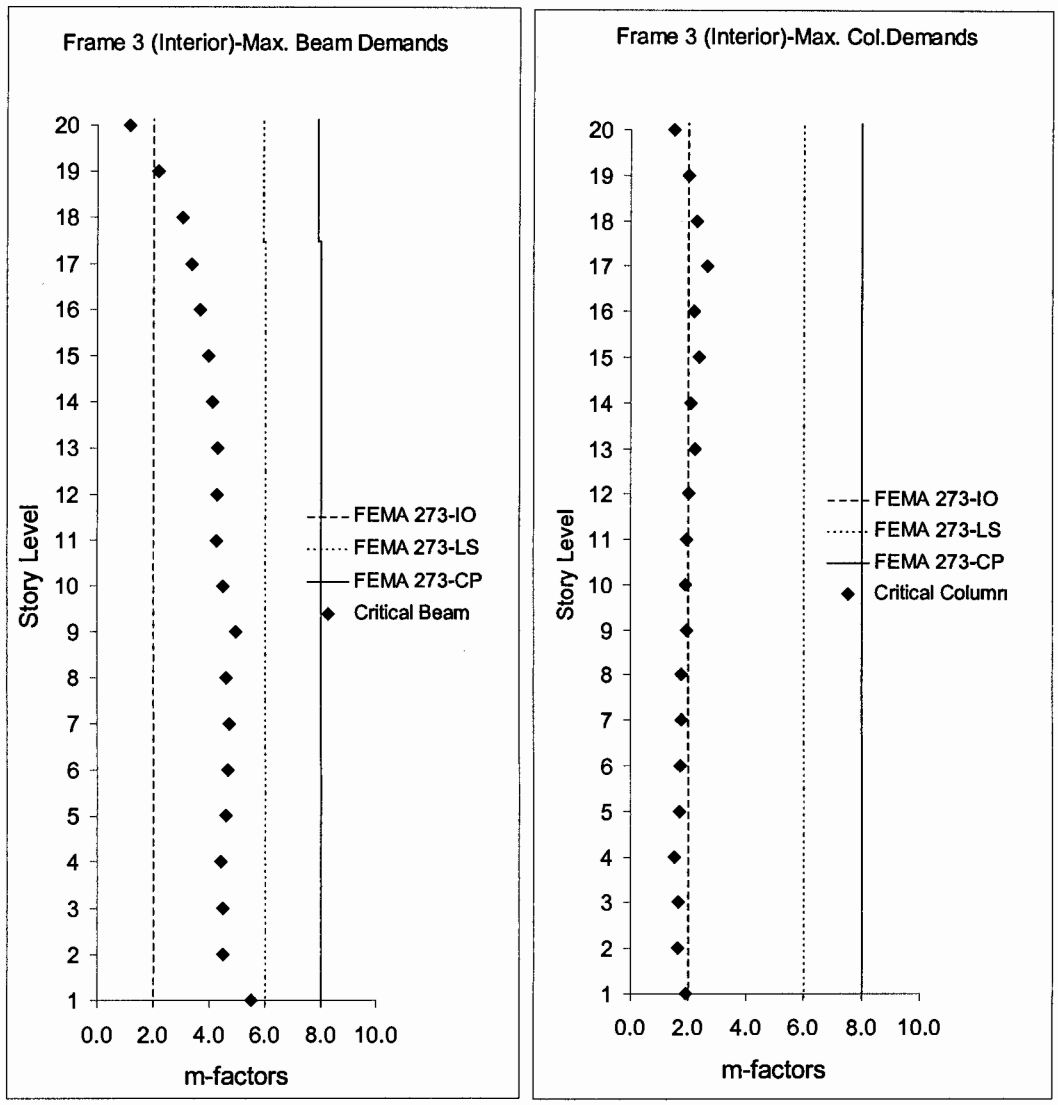

Figure 12. Comparison of Critical Component Demands using LSP with FEMA-273 Criteria for BSE-2 Loading

Figure 12 shows the demand to capacity ratios for one critical frame in the long building direction using LSP (linear static procedure). The applied lateral loads were based on BSE-2 loading. Also shown in the figure are the acceptance criteria based on the m-factor for the most critical component at each story level. In general, similar m-values were obtained for all components in a story except the interior frames in the EW direction which were composed of different sections in each bay. Figure 13 shows a similar set of results using the linear dynamic procedure (LDP). The dynamic analysis was carried out using a response spectrum approach using the FEMA-273 spectra for BSE-2 loading. Finally, results of the evaluation using an inverted triangular loading and NSP (nonlinear static procedure) are displayed in Figure 14. The target displacement, in this case, was estimated using BSE-1 loading.

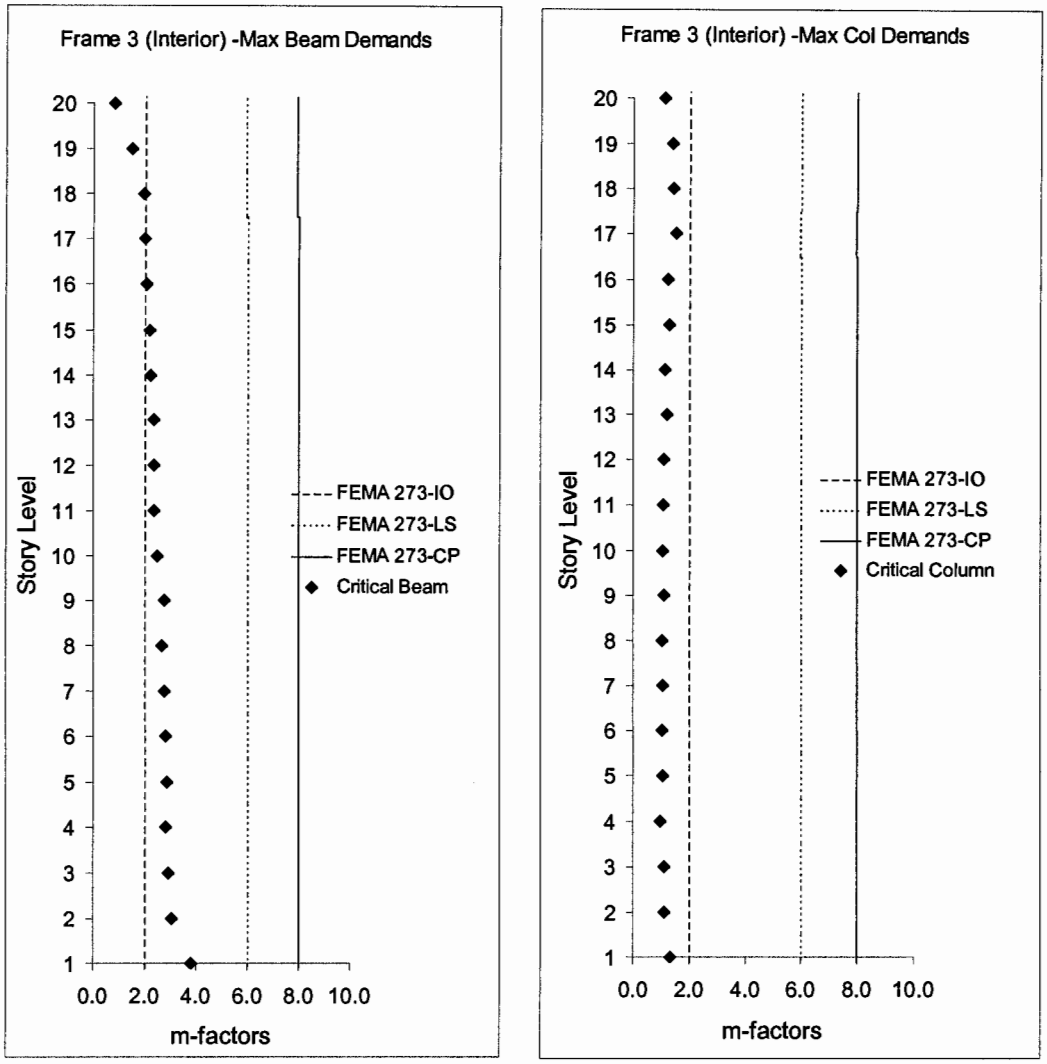

Figure 13. Comparison of Critical Component Demands using LDP with FEMA-273 Criteria for BSE-2 Loading

Summary

System identification studies revealed moderate torsional response in the building. Since most of the frames in this building was designed to resist lateral loads, the influence of the gravity frames was minimal. Good correlation was obtained with recorded response using bare section properties for all elements. Response results with base accelerations applied in both directions produced improved correlation than if the base motions were applied independently. As in the case of the previous building, damping did not influence displacement response but increased damping in higher modes improved the computed acceleration response. The FEMA-273 evaluations demonstrated once again that LSP demands are more conservative that LDP demands if a response spectrum analysis is used. Demands from NSP did not correlate well with the results from linear procedures.

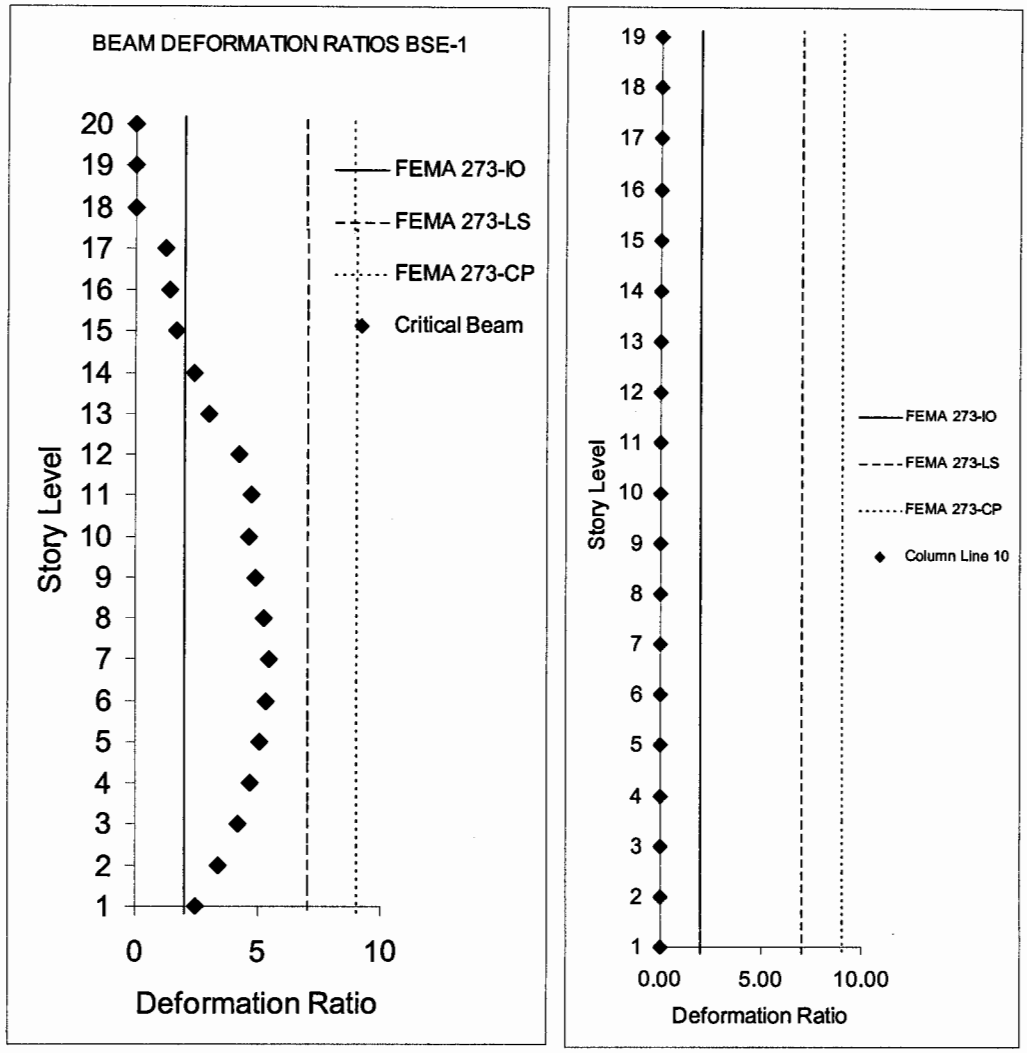

Figure 14. Comparison of Critical Component Demands using NSP with FEMA-273 Criteria for BSE-2 Loading

It is appropriate to point out that the pushover analysis of this building using SAP2000 was almost prohibitive. In addition to the excessive computational time (estimated at over 20 hours on a 400 MHz Pentium II Processor with 96mB RAM) for a single run in one direction, the enormous amount of output generated was extremely difficult to process. The feasibility of conducting routine iterative pushover analyses of tall buildings with a large number of degrees-of-freedom may be called into question, particularly in structural design offices.

Further, the results of the pushover analysis indicates that the deformation demands in the columns are significantly smaller than that predicted by linear approaches. In fact, no column yielding was reported. Of the three approaches, LSP demands clearly resulted in the most conservative estimates.

THIRTEEN STORY COMMERCIAL BUILDING, SOUTH SAN FERNANDO VALLEY

The Northridge earthquake caused widespread damage to numerous steel buildings, particularly local failures in beam-to-column welded connections. The third building considered in this study was among the many steel moment frame structures that experienced weld fracture at beam-to-column connections. This 13-story building is located in South San Fernando valley about 5 km southwest of the Northridge epicenter. This building is actually composed of one basement floor and 13 floors above ground. It was built in 1975 on a design based on the 1973 UBC code. This building has been the subject of a previous investigation (Uang et al., 1995).

Building Details

The floor plan of the perimeter frames and a typical elevation of one of these frames are shown in Figure 15. The overall building dimensions are 160 x 160 feet. Member sizes are also shown in the figure. It should be noted that the corner columns are composed of box columns. All structural steel was specified to be A36 steel, however, an expected yield strength of 45 ksi was used in the FEMA-273 evaluations. The floor plan increases at the second floor to form a plaza level which terminates on three sides into the hillside thereby making this level almost fixed against translation. There are concrete walls in the basement perimeter which also add to the stiffness of the basement level. The foundation consists of piles, pilecaps and grade beams.

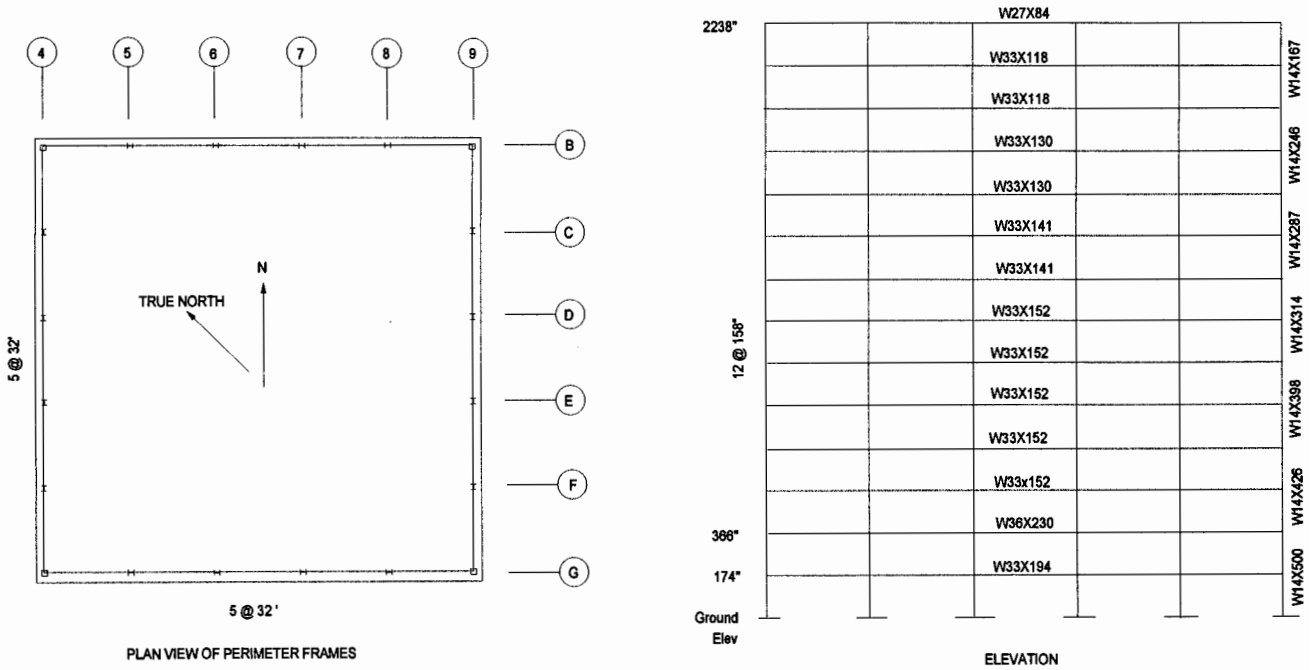

Figure 15. Plan and Elevation of Perimeter Frames of Blue-Cross Building

The typical floor system consists of about 2.5 inches of concrete fill over 3-inch 20-gage steel decking. The roof system is lighter with 2.25 inches of vermiculite fill on 3-inch 20-gage steel decking. 3 ksi concrete was specified for all deck fill. Exterior walls are composed of 6-inch 22

gage steel studs with 0.25 inch opaque glass and 2-inch precast panels. A total uniform load of 102.5 psf was used to calculate the building mass properties and axial load on columns. Strong motion data is available for 7 sensors: three each in the North-South and East-West directions, respectively, and one in the vertical direction. The instrumentation was located in the basement and on the sixth and twelfth floors. Recorded accelerations at the basement indicate that the building experienced a PGA of 0.41g in the NS direction and 0.32g in the EW direction.

Approximately 12% of the connections on the west perimeter of the North-South frame fractured during the earthquake. Connection fractures on the remaining three sides were less than half this number. The stronger component of the Northridge earthquake was oriented in this direction. Damage consisted of: (i) full or partial cross-flange cracks in the columns; (ii) flange cracking away from the heat-affected zone; (iii) fracture through the weld metal across partial or full width of the beam; (iv) weld fractures at beam-column interface; and (v) crack at the root of the weld (as identified by ultrasonic testing). Additional details related to observed damage are reported in Uang et al. (1995).

Calibration of Observed Response

A three-dimensional model of the building was developed using SAP2000. Both the exterior moment frames and the interior gravity frames were included in the model. Bare section properties without consideration for composite floor action were used to model the members. The building was subjected to both recorded components of the earthquake at the basement level. Results of the simulation in both directions are shown in Figure 16.

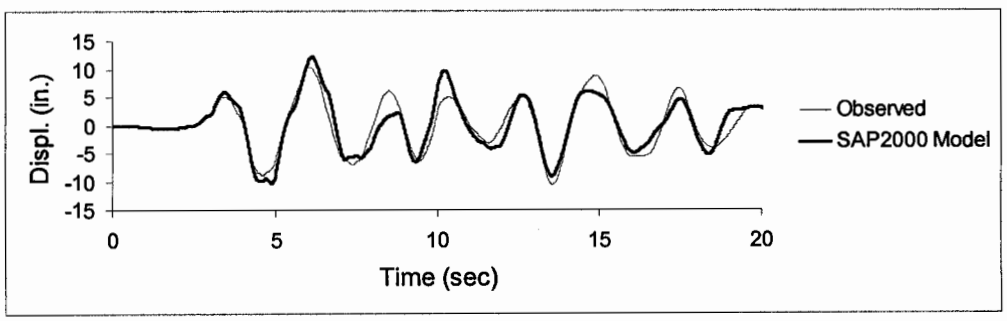

(a) East-West Direction

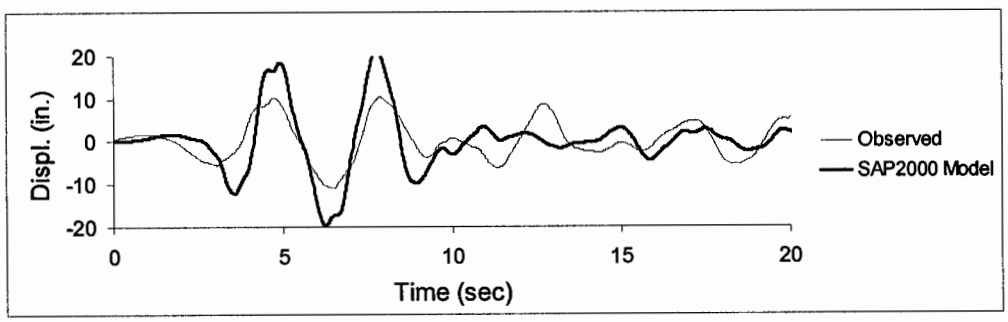

(b) North-South Direction

Figure 16. Simulation of Observed Roof Response During Northridge

As observed in Figure 16, the correlation in the NS direction is poor. This is to be expected since the building suffered numerous weld fractures in this direction. Hence, a detailed inelastic analysis was carried out on a two-dimensional frame using an advanced hysteresis model to represent the behavior of the fracturing weld connection. Figure 17 shows the weld-fracture model used in the simulation. This model is incorporated in the IDASS computer program (Kunnath, 1995). The weld-fracture model was first calibrated using available experimental data from tests conducted at the University of Berkeley (Popov et al., 1996). It was assumed that the welds fractured at approximately 70% of the specified yield strength (31.5 ksi). Results of the simulation in the NS direction using this model is shown in Figure 18. Some improvement in the simulation is observed though all features of the response could not be calibrated.

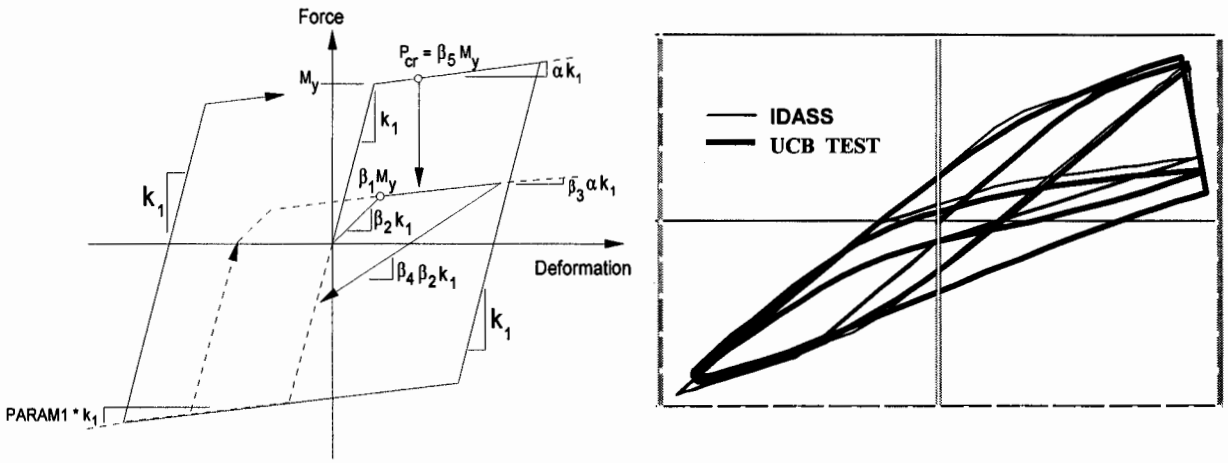

Figure 17. Calibration of Weld Fracture Model with Test Data

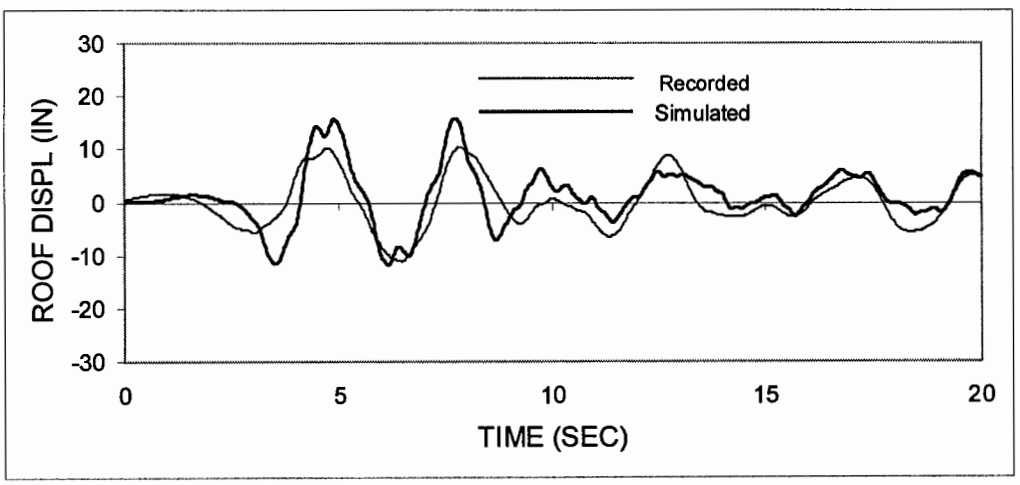

Figure 18. Simulation of Observed Roof Response Using Weld Fracture Model

Evaluation of FEMA-273 Analytical Procedures

FEMA-273 based evaluations of the building were carried out on a two-dimensional model of the building with the assumption that there was no potential for weld fracture. Results are presented only for the linear and nonlinear static procedures. Figure 19 shows the m-factors for both beam and columns as a function of the story level for BSE-2 loading. Exterior columns are distinguished from interior columns because the peak axial stresses occur in the exterior columns and typically govern the acceptance criteria for the building. Figure 20 displays the results of the nonlinear static analysis wherein an inverted triangular loading pattern was used. Post yield stiffness of both beams and columns was assumed to be 2% of the initial elastic stiffness. All plots also include the FEMA acceptance criteria for immediate occupancy, life safety and collapse prevention.

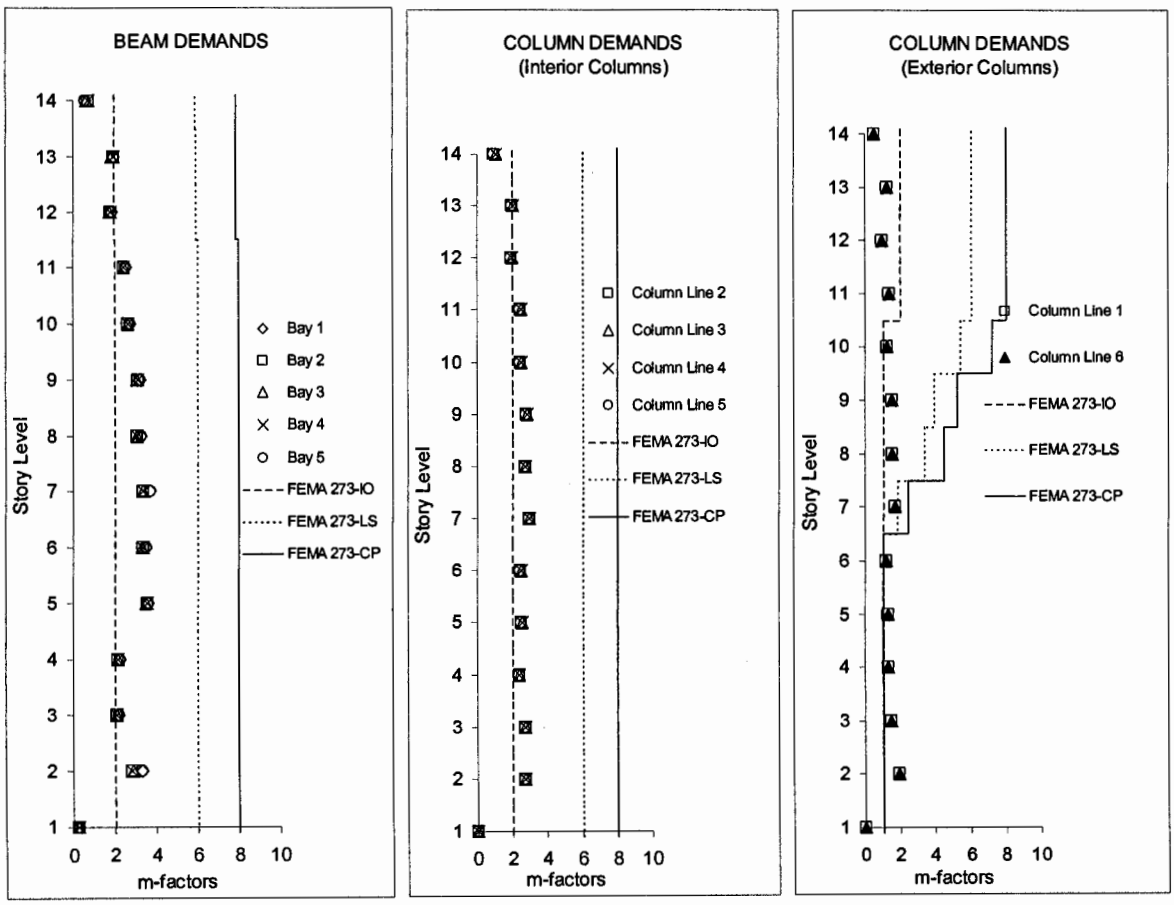

Figure 19. Comparison of Critical Component Demands using LSP with FEMA-273 Criteria for BSE-2 Loading

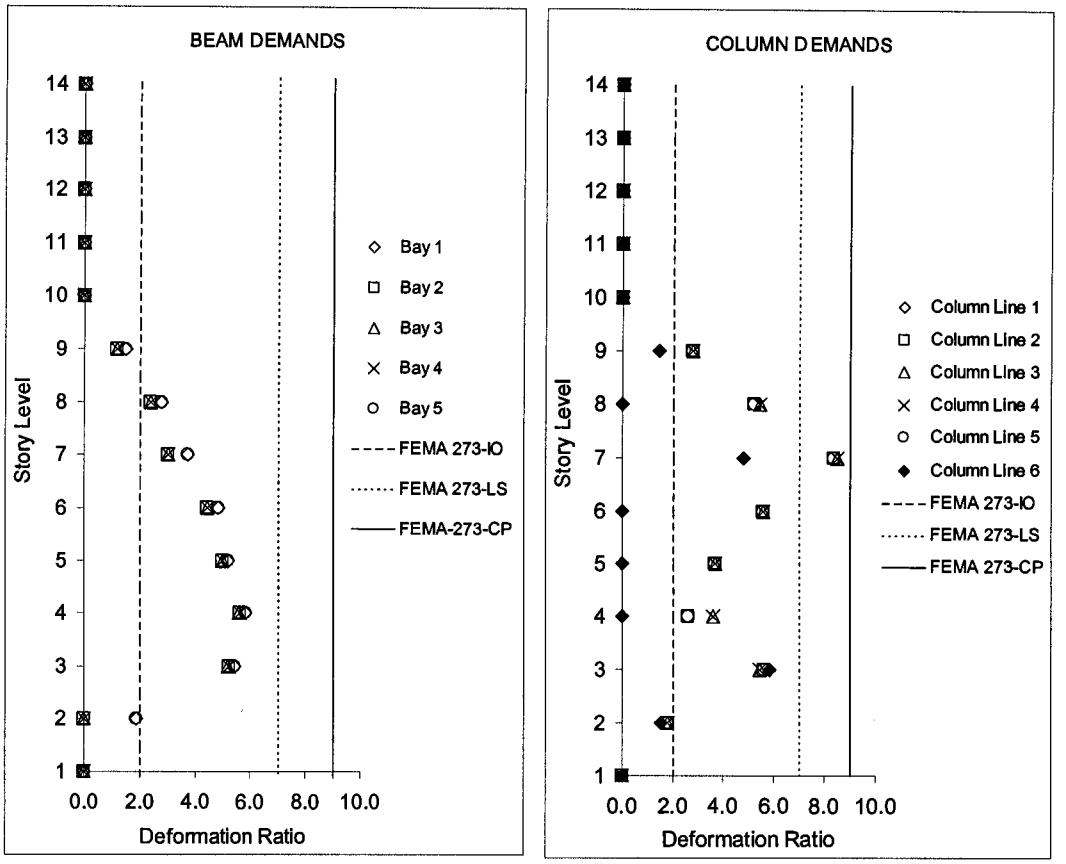

Figure 20. Comparison of Critical Component Demands using NSP with FEMA-273 Criteria for BSE-2 Loading

Figure 21 displays the FEMA evaluation of the welded connections. The criteria for potential connection failure is a function of the panel zone strength and the depth of the beam. Results are shown for three cases: LSP and NSP based on BSE-2 loading and NDP using the actual recorded time history. The observed connection fractures in the two perimeter frames in the NS direction is also shown for comparison. It is to be noted that the perimeter framing system is essentially symmetric, hence computer based simulations will result in identical damage scenarios in both the EW and NS directions. However, observed damage in the frames in the EW direction were substantially less. This is indicative of the fact that weld fractures possibly occurred at stresses below the yield stress of the material.

Summary

Calibration of the three-dimensional model was achieved in the East-West direction using bare section properties without composite floor action. The response in the North-South direction was overestimated since the SAP2000 run was based on linear elastic behavior. Post-earthquake investigation of the building revealed numerous weld fractures in the NS direction which explains the lack of correlation in this direction. An enhanced weld fracture model was used to

improve the simulation in the NS direction. FEMA-273 based analyses were carried out on the structure assuming no weld fractures. Results of the evaluation reconfirm previous evaluations that LDP based on a response spectrum approach is less conservative than LSP. In fact, results of LSP produce the most conservative demand estimates. There was no correlation in critical demand regions (story levels) between linear and nonlinear methods: NSP predicted maximum beam demands in the lower half of the building while LSP and LDP indicates critical demands in the middle third of the building.

Finally, the potential for connection failure was investigated using FEMA-273 criteria. Both LSP and NSP for BSE-2 loading indicated that CP criteria was not satisfied at several levels across the mid-height of the building.

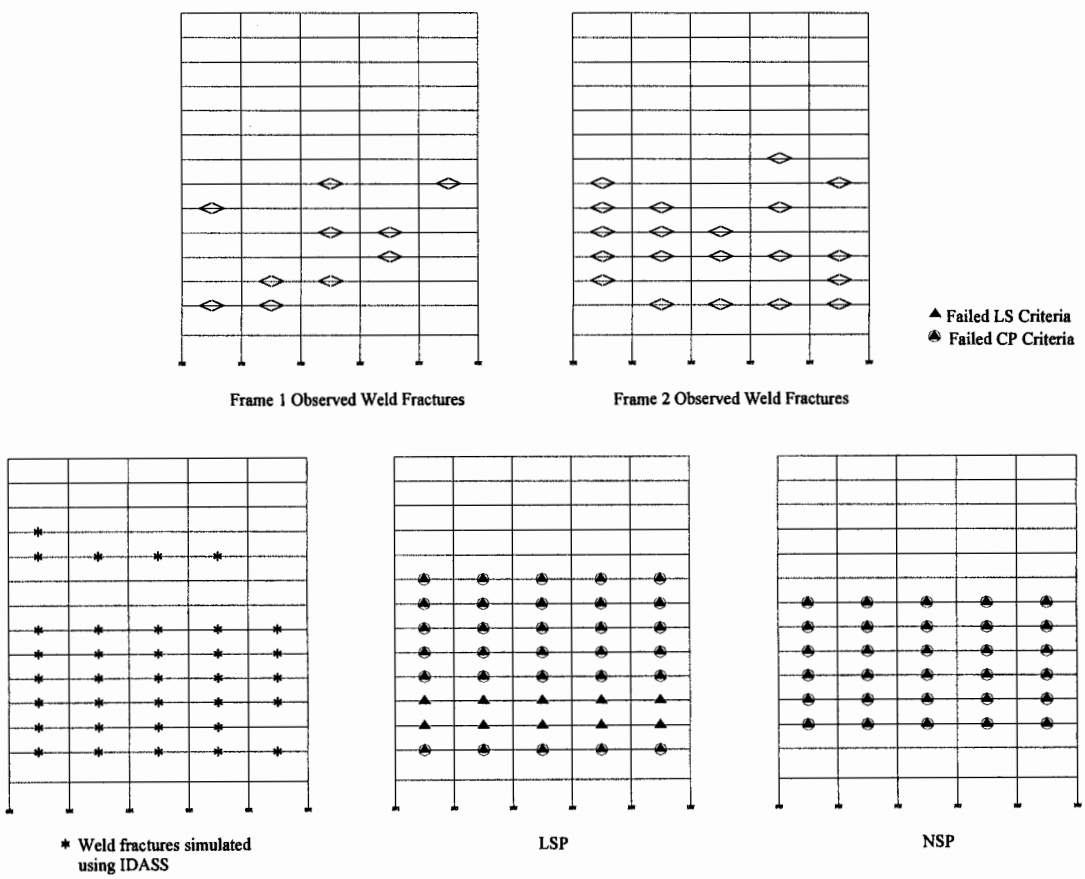

Figure 21. Observed vs. Predicted Connection Fractures Using Various Analysis Methods

TWO-STORY CITY HALL, BIG BEAR LAKE

The fourth and final building evaluated in this project is the two-story Big Bear civic center and city hall. There are no recording instruments in the building but free field records very close to the site indicate a peak ground acceleration of 0.48g in the east-west direction and 0.54g in the north-south direction during the Big Bear earthquake of 1992. No damage to the structure was reported based on visual external examination of the building. A detailed investigation of the building was not carried out until after Northridge. After weld fracture problems were identified following the Northridge event, a closer inspection of the 2-story civic center revealed severe cracking in several welded connections. A complete retrofit of the building has since been carried out. This building is included in the study since it represents a typical yet complex system with steel and timber members.

Building Details

Lateral resistance in the Big Bear building is provided by a set of moment frames. The main lateral force resisting system of the structure is not well defined. The building was completed in 1987 and was designed based on 1985 UBC provisions. The floor system consists of wood floor joists with plywood cover. The dead load of the floor was estimated at 35 psf. The total building weight was calculated to be approximately 450 kips including structural steel and plywood walls. Additional lateral stiffness is provided by plywood walls that infill the moment frames. Structural drawings show that the plywood diaphragms, reinforced with 2"x6" studs at 24 inch on center, are connected to the steel framing system through bolts at the upper and lower beams thereby participating in the initial response and contributing to the overall structural stiffness. No connections are provided between the wall diaphragm and the columns.

Simulation of Building Response

Several computer models of the building were investigated: a reduced 3D model in which only the main framing systems in each direction were included; a complete 3D model with all moment frames; a 3D model with diagonal braces to simulate the stiffness of the plywood wall panels; and two dimensional models in each direction of the building. The final model selected for preliminary evaluation was the full three-dimensional model of the building. The model was subjected to the free-field accelerations that were recorded near the site. The SAP2000 model of the building is shown in Figure 22. Note that the structure contains a few isolated single bay moment frames. Since these frames contribute to the overall stiffness of the building, they were included in the analysis. Most of these isolated frames are connected to the rest of the building through wooden beams and diaphragms or steel beams with simple shear connections. A rigid diaphragm assumption was used to tie all frames together.

The results of the seismic analysis of the building model subjected to bi-directional components of the free-field motion indicated several regions of high stress. Demand to capacity ratios for a typical frame in each building direction is shown in Figure 23. The peak ratios based on a yield stress of 36 ksi is 1.71for columns and 1.26 for beams. These ratios may be not appear to be critical considering factors such as material over-strength and redundancy. However, as

identified in the analysis of the 13-story frame, it is possible that brittle fracture was initiated before yielding of the connections.

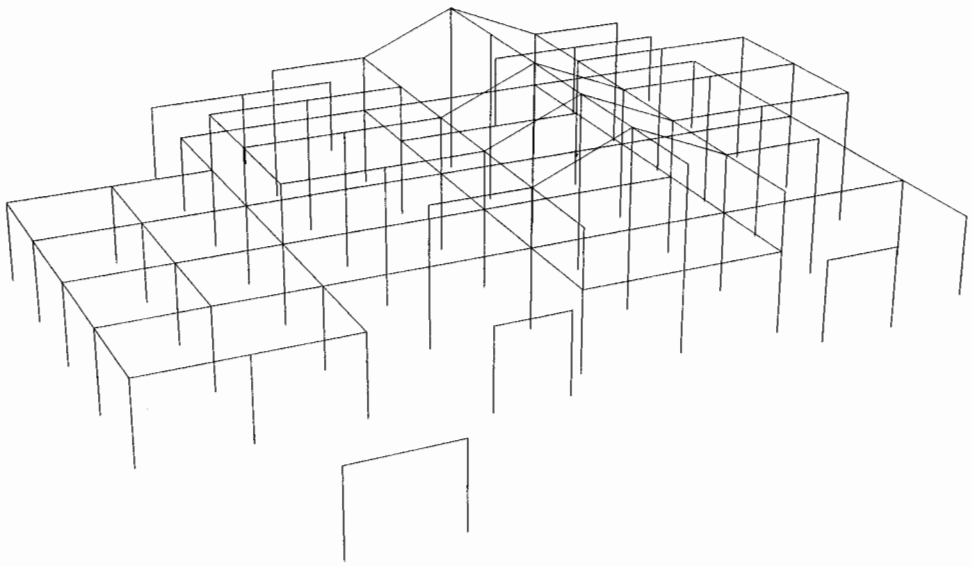

Figure 22. SAP2000 Model of 2-Story Big Bear Civic Center

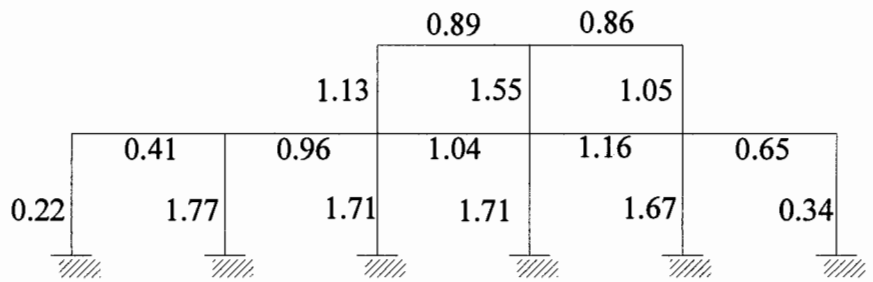

(a) Typical NS Frame

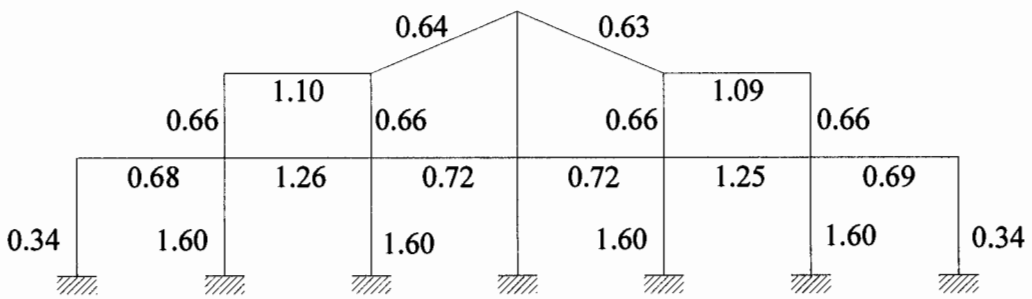

(b) Typical EW Frame

Figure 23. Demand to Capacity Ratios in Critical Frames of Big Bear Civic Center Subjected to Recorded Free Field Motions at Nearby Site

An additional factor not considered in the evaluation that may have played a significant role in the seismic forces experienced by the structure is the presence of plywood diaphragm walls. In order to consider the effects of the wood diaphragms, a separate set of analyses was carried out to identify the increase in stiffness due to the presence of these elements. Test data obtained from the city of Los Angeles (Nghiem, 2000) based on experiments conducted at the University of California, Irvine, was used to calibrate the approximate stiffness of a steel moment frame with plywood diaphragm walls. Figure 24 shows the conceptual process of calibrating the brace elements used to represent the walls. The equivalent shear stiffness of the frame with the brace element was simulated to represent the steel frame with the actual plywood wall. Membrane elements were used to model the plywood panel.

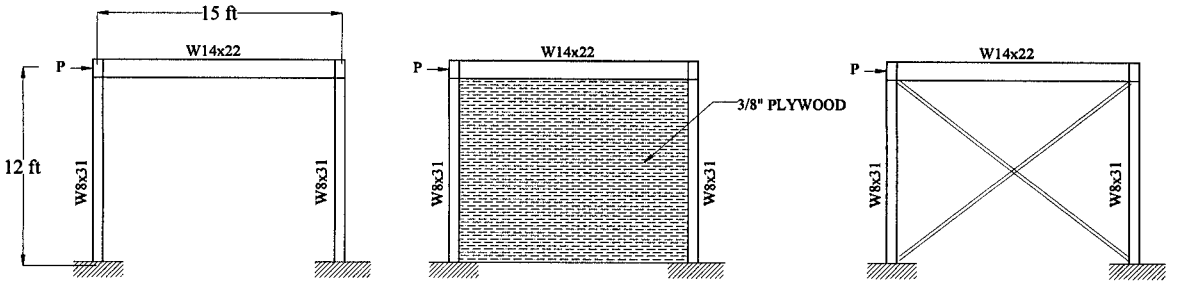

Figure 24. Modeling the Effect of Wood Diaphragm Walls

The calibrated brace element was then used in a new analysis of the building. It was observed that the model with the brace elements resulted in a 50% increase in shear in the EW direction and more than 30% increase in the NS direction. However, the DCR values in the beams and columns were reduced since it was not possible to limit the brace forces. In an actual event, the wall panels will most likely separate from the frame and the forces will be carried by the main framing system. Hence, the results of the evaluation with the equivalent braces in the inelastic range is not valid. The objective of analyzing the building with the wall panels was to ascertain the initial stiffness of the system and the resulting increase in shear forces.

Finally, the 3D SAP2000 model shown in Figure 22 was analyzed for FEMA-273 loading. Both BSE-1 and BSE-2 hazard levels were considered. Analyses were carried out using LSP and NSP. Beam and column demands for BSE-2 loading are shown in Figure 25. Additional investigation of connection behavior at these loading levels indicate no likelihood of connection fracture. While a few connections did not pass Immediate Occupancy criteria, all connections passed both LS and CP criteria for both loading levels. The demands resulting from the Big Bear earthquake were more severe than those determined from FEMA-273 loading.

Figure 26 shows the regions that were upgraded following the Northridge earthquake. A number of these locations coincide with the regions of maximum stress identified in Figure 23. The NS frame shown in Figure 23 lies along line 3 and the EW frame lies along B. The stress ratios along frame line B were generally higher than those along frame line D. Correlations between stress ratios and potential damage may not be consistent if welds fractured prior to yielding.

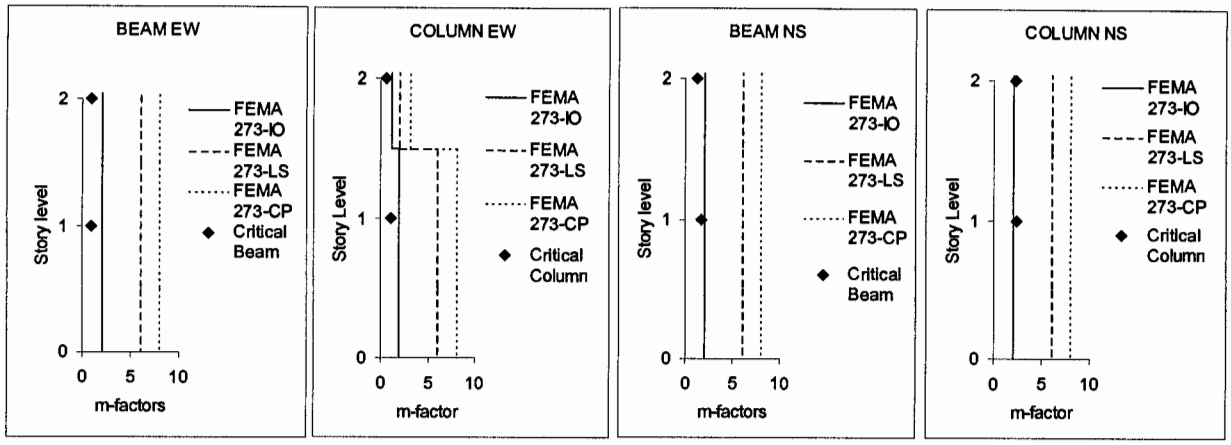

Figure 25. Comparison of Demand Estimates Using LSP with FEMA-273 Acceptance Criteria for BSE-2 Loading

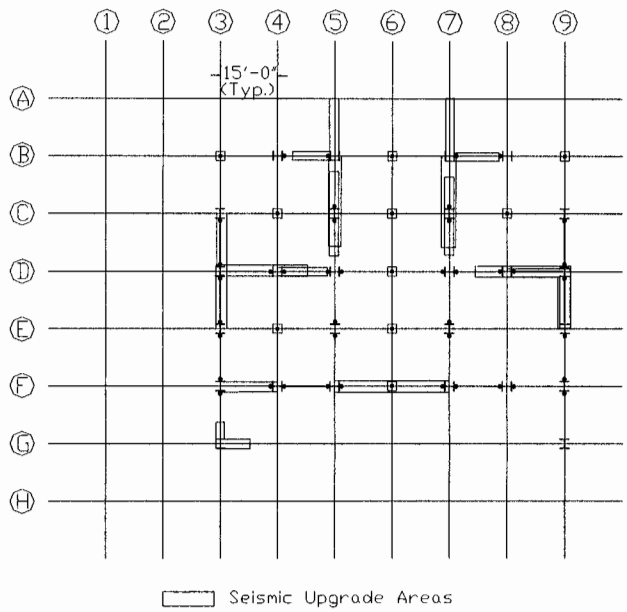

Figure 26. Plan View of Building Showing Locations of Connection Damage

Summary

Results of the evaluation of the 2-story Big Bear building were less conclusive given the complexity of the structural system. The influence of the wood wall panels in inducing more severe seismic demands in the initial phase of the response was demonstrated by utilizing equivalent diagonal brace elements. The actual response of the system in the presence of the walls could not be ascertained given the limitations of the computational tools available. The FEMA-273 criteria for connection failures appears to be inadequate for beams with limited

depth. The current criteria based on beam depth was incapable of predicting any of the observed weld fractures. Additional studies of the building are still underway.

ACKNOWLEDGEMENTS

The authors wish to thank the staff of the California Strong Motion Instrumentation Program (CSMIP), particularly Anthony Shakal and Moh Huang for their assistance and support during the project. The suggestions and helpful comments of Chris Poland and Charles Kircher during the Project Advisory committee meetings are also greatly appreciated. Balram Gupta and Saiful Islam of Saiful/Bouquet Consulting Engineers provided invaluable technical support during the course of the project.

The contents of this paper were developed under Contract No. 1098-713 from the California Department of Conservation, Division of Mines and Geology, Strong Motion Instrumentation Program. However, these contents do not necessarily represent the policy of that agency noe endorsed by the State Government.

REFERENCES

Anderson, J.C. and Bertero, V.V. (1997). "Implications of the Landers and Big Bear Earthquakes on Earthquake Resistant Design of Structures." Report UCB/EERC-97/08, University of California, Berkeley.

Computers and Structures, Inc. (1998). "SAP2000 Analysis Reference." CSI, Berkeley, CA.

Darragh, R. et al. (1994). "Los Angeles Code-Instrumented Building Records from the Northridge, California Earthquake of 17 January, 1994: Processed Release 1 and 2" California Department of Conservation, Sacramento, CA.

FEMA 273 (1997). "NEHRP Guidelines for Seismic Rehabilitation of Buildings." Building Safety Seismic Council, Washington, D.C.

Kunnath, S.K. (1995). Enhancements to Program IDARC: Modeling Inelastic Behavior of Welded Connections in Steel Moment Resisting Frames, Technical Report NIST GCR 95-673, National Institute of Standards and Technology, US Department of Commerce.

Nghiem, Doc (2000). Private Communication.

Popov, E.P., Blondet, M. Stepanov, L. and Stojadinovic, B. (1996). "Full-Scale Beam-Column Connection Tests." Technical Report SAC 96-01, Applied Technology Council, Redwood City, CA.

Shakal, A. et al. (1994). "CSMIP Strong-Motion Records from the Northridge, California Earthquake of 17 January, 1994." California Department of Conservation, Division of Mines and Geology, Sacramento, CA.

Shen, J-H. and Astaneh, A. (1990). "Seismic Response Evaluation of an Instrumented Six-Story Steel Building." Report UCB/EERC-90/20, University of California, Berkeley.

Uang, C.M., Yu, Q.S., Sadre, A., Bonowitz, D. and Youssef, N. (1995). "Performance of a 13-Story Steel Moment-resisting Frame Damaged in the 1994 Northridge Earthquake." Report SSRP-95/04, University of California, San Diego.

Seismic Performance Evaluations of Transportation Structures

Joseph Penzien and Wen S. Tseng

International Civil Engineering Consultants, Inc., Berkeley, California, USA

ABSTRACT

This paper discusses the steps that are necessary in assessing the seismic performance of existing and new transportation structures, including (1) characterizing expected ground motions, (2) setting performance criteria, (3) modelling and dynamic analysis, and (4) interpreting predicted dynamic response behavior. To establish a basis for assessing the performance of older existing bridges, the history of loading criteria over the past 50 years, as specified in the U.S. AASHO/AASHTO national bridge code, is reviewed.

INTRODUCTION

The importance of designing bridges to withstand the vibratory response produced during earthquakes was first revealed by the 1971 San Fernando, California earthquake during which many bridge structures collapsed. Similar bridge failures occurred during the 1989 Loma Prieta and 1994 Northridge, California earthquakes and the 1995 Kobe, Japan earthquake. As a result of these experiences, much has been done recently to improve provisions in seismic design codes, develop more effective detail designs, and advance modelling and analysis procedures for assessing seismic performance.

Unfortunately, many of the older existing bridges in the United States and other countries, which are located in regions of moderate to high seismic intensity, have serious deficiencies which threaten life safety during future earthquakes. Because of this threat, aggressive actions are being taken in California, New York, and elsewhere to retrofit such bridges to bring their expected performances during future earthquakes to acceptable levels. For new bridges, a rapid change is taking place toward "performance-based" design, which focuses on ensuring satisfactory performance under expected levels of seismic excitation.

SEISMIC LOADING CRITERIA

Revolutionary changes have taken place over the past 50 years in earthquake engineering as applied to transportation structures. This becomes apparent when one reviews the changes in seismic loading criteria specified by the American Association of State Highway Officials (AASHO) in its Standard Specifications for Highway Bridges, First (1931) through Eleventh (1973) Editions, and by the American Association of State Highway and Transportation Officials (AASHTO) in its 1973 Interim Specifications for Highway Bridges and the subsequent Standard Specifications for Highway Bridges, Twelfth (1975) through Sixteenth (1996) Editions, and in AASHTO's LRFD Bridge Design Specifications, First (1994) and Second (1999) Editions. All of the above-mentioned specifications apply to Ordinary Bridges having span lengths under 500 feet.

AASHO STANDARD SPECIFICATIONS, 1949-1975

Standard Specifications, 1949-1961

The first reference to considering earthquake effects on bridges came in the Fifth (1949) Edition of the Standard Specifications which stated that earthquake stresses should be considered; however, no guidelines for doing so were given. This same reference was stated again in the Sixth (1953) and Seventh (1957) Editions.

Standard Specifications, 1961-1975

The Eighth (1961) Edition of Standard Specifications was the first to specify an earthquake loading for design (EQ), namely

$$EQ = CD \tag{1}$$

which was to be applied statically in any horizontal direction as part of a Group VII load combination given by

$$\text{Group VII} = D + E + B + SF + EQ \tag{2}$$

in which D, E, B, and SF denote dead load, earth pressure, buoyancy, and stream flow, respectively. The numerical values of C were specified to be 0.02 for structures supported on spread footings where the soil bearing capacity was rated to be greater than 4t/ft^2 (383 kPa), 0.04 for structures supported on spread footings where the soil bearing capacity was rated to be less than 4 t/ft^2 (383 kPa), and 0.06 for structures founded on piles. The Group VII load combination was to be used in the working-stress design (WSD) with a 33-1/3 percentage increase in allowable stress because of the presence of the earthquake loading EQ. No seismic zone factors were provided in the specifications.

The above seismic loading provisions of the Eighth (1961) Edition of Standard Specifications were repeated, without modification, in the Ninth (1965), Tenth (1969), and Eleventh (1973) Editions. It should be noted that these seismic loading provisions were based mainly on the lateral force requirements for buildings developed prior to 1961 by the Structural Engineers Association of California (SEAOC).

AASHTO STANDARD SPECIFICATIONS, 1975-1992

As a result of the 1971 San Fernando, California earthquake during which many highway bridges were severely damaged, some of which even collapsed, the California Department of Transportation (Caltrans) issued new seismic design criteria for bridges in 1973, which formed the basis of the 1975 AASHTO Interim Specifications for Highway Bridges. The equivalent static lateral force loading specified in this document for bridges having supporting members of approximately equal stiffness was of the form

$$EQ = CFW \tag{3}$$

which was to be applied in any horizontal direction as part of the same Group VII load combination given by Eq. (2) in a working stress design with a 33 percent increase in allowable stress. In this equation, W represents dead load, F is a framing factor assigned the values 1.0 for single columns and 0.8 for continuous frames, and C is a combined response coefficient as expressed by

$$C = ARS/Z \tag{4}$$

in which A denotes maximum expected peak ground acceleration (PGA) as shown in a seismic risk map of the United States, R is a normalized (PGA = 1g) acceleration response spectral value for a rock site, S is a soil amplification factor, and Z is a force reduction factor depending upon structural-component type which accounts for the allowance of inelastic deformations. The numerical values specified for A were 0.09g, 0.22g, and 0.50g in seismic zones numbered I, II, and III, respectively. Numerical values for R, S, and Z were not provided in the 1975 Interim Specifications; rather, four plots of C as functions of period T were given for discrete values of A. Each of these plots represents a different depth range of alluvium to rock-like material, namely 0-10', 11-80', 81-150', or >150' (1' = 30.48 cm). Period T was to be evaluated using the single-degree-of-freedom (SDOF) relation

$$T = 0.32\sqrt{\frac{W}{P}} \tag{5}$$

in which P equals the total uniform static loading required to cause a 1-inch (2.54 cm) horizontal deflection of the whole structure at the center of gravity of the deck.

For complex or irregular structures, the 1975 Interim Specifications required use of the modal response-spectrum analysis method to generate design loads; and, in special cases of such structures having fundamental periods longer than 3 seconds, it required that they be designed using "current seismicity, soil response, and dynamic analysis techniques."

The same seismic loading criteria in the 1975 Interim Specifications were repeated in the Twelfth (1977), Thirteenth (1983), and Fourteenth (1989) Editions of AASHTO's Standard Specifications; however in these editions, the designer was given, for the first time, the choice of working-stress design (WSD) or load-factor design (LFD). When using the WSD, the same Group VII load combination given by Eq. (2) was specified to be used along with a 33 percent increase in allowable stress; however, when using the LFD, the Group VII load combination was changed to the form

$$\text{GroupVII} = \gamma\left[\beta_D D + \beta_E E + B + SF + EQ\right] \tag{6}$$

in which load factor γ was assigned the value 1.3, β_D was assigned the values 0.75, 1.0, and 1.0 when checking columns for minimum axial load and maximum moment or eccentricity, for maximum axial load and minimum moment, and for flexure and tension members, respectively, and β_E was assigned the value 1.3 for lateral earth pressure and 0.5 for checking positive moments in rigid frames.

AASHTO STANDARD SPECIFICATIONS, 1992-1999

After the 1989 Loma Prieta, California earthquake, the Applied Technology Council (ATC) issued its ATC-6 Seismic Design Guidelines for Bridges under the sponsorship of the Federal Highway Administration, Department of Transportation in 1981. These guidelines were reviewed and revised slightly by the National Center for Earthquake Engineering Research (NCEER) under sponsorship of the National Cooperative Highway Research Program (NCHRP) Project 20-7/45 to form the basis of AASHTO's Fifteenth (1992) and Sixteenth (1996) Editions of the Standard Specifications. In these editions, each bridge structure must first be classified as either "Essential" or "Other" in accordance with given definitions and then be assigned to one of four Seismic Performance Categories (SPC) A, B, C, or D as defined in Table 1 below

Table 1 - Seismic Performance Categories

Acceleration Coefficient	Bridge Classification	
	Essential	Other
$A \leq 0.09$	A	A
$0.009 \leq A \leq 0.19$	B	B
$0.019 \leq A \leq 0.29$	C	C
$0.29 \leq A$	D	C

in which the acceleration coefficient, A, for a given bridge site is taken from contour maps provided.

No dynamic analysis is required in these editions for bridges having single spans, regardless of the value of the site acceleration coefficient A, and for all bridges in SPC A. All other bridges, regular or irregular, having two or more spans must be analyzed by at least one of two dynamic analysis procedures, namely, the single-mode spectral method (SMSM) or the multi-mode spectral method (MMSM). The SMSM is specified as minimum for regular bridges in SPC B, C, and D; while the MMSM is specified as minimum for irregular bridges in these same categories. An "irregular" bridge is defined as one having abrupt or unusual changes in mass, stiffness, and/or geometry from abutment to abutment; a "regular" bridge is one not meeting the definition of an "irregular" bridge.

The seismic input in any horizontal direction to be used in each of these minimum dynamic analysis procedures is specified in terms of an elastic seismic response coefficient, C_{sm}, as expressed by

$$C_{sm} = \frac{1.2AS}{T_m^{2/3}} \tag{7}$$

in which T_m is the period of vibration of the m^{th} mode, S is a site coefficient having the values 1.0, 1.2, 1.5, and 2.0, respectively, for soil profile Types S_1, S_2, S_3, and S_4 ranging from hard (S_1) to very soft (S_4), and A is an acceleration coefficient taken from the contour

map prepared by the U.S. Geological Survey for the 1988 Edition of NEHRP "Recommended Provisions for the Development of Seismic Regulations for New Buildings". The values of *A* in this map represent peak ground accelerations having a mean return period of 475 years.

Since each analysis procedure generates internal force components in members caused by only a single horizontal component (x or y) of seismic input, the procedure selected must be repeated using the same response-spectrum seismic input applied in each of the two orthogonal horizontal directions. The corresponding pairs of internal force components $(Q_x \text{ and } Q_y)$ produced by both inputs must then be combined, using the "30-percent" rule, into two combined forms, $Q_x + 0.3\,Q_y$ and $Q_y + 0.3\,Q_x$, with the larger of these two used for design. It is more rational, however, to use the "40-percent" rule when the two orthogonal horizontal inputs are of the same intensity as specified in the AASHTO Standard Specifications. The square-root-of-the-sum-of-squares (SRSS) method, which is the basis for both the "30-percent" and "40-percent" rules, can be used directly to combine pairs of force components regardless of whether or not the inputs are of the same intensity.

Since inelastic deformations are allowed in ductile bridge elements, the combined elastic force components are then divided by appropriate response modification factors, *R*, as specified in Table 2 below to obtain modified earthquake response values, *EQM*.

Table 2 - Response Modification Factors (*R*)

Substructure	*R*	Connections	*R*
Wall-Type Pier	2	Superstructure to Abutment	0.8
Reinforced Concrete Pile Bents a. Vertical piles only b. One or more battered piles	 3 2	Expansion joints within a span of the superstructure	0.8
Single Columns	3	Columns, piers, or pile bents to cap beam or superstructure	1.0
Steel or Composite Steel & Concrete Pile Bents a. Vertical piles only b. One or more battered piles	 5 3	Columns or piers to foundations	1.0
Multiple-Column Bent	5		

These modified values, *EQM*, replace the values *EQ* in Eq. (2) for use in WSD of structures in Categories, B, C, and D, allowing a 50 percent increase in allowable stresses for structural steel and a 33-1/3 percent increase for reinforced concrete.

AASHTO LRFD SPECIFICATIONS, FIRST (1994) AND SECOND (1999) EDITIONS

The working-stress design (WSD) philosophy, which requires that calculated design stresses not exceed specified levels, underwent adjustment in the 1970's through the introduction of load factors reflecting the variable predictabilities of different load types, a philosophy referred to as load factor design (LFD). During the period 1988 to 1993, the AASHTO LRFD Bridge Design Specifications was developed using statistically based probability methods. The load and resistance factor design (LRFD) philosophy makes use of load and resistance factors developed through statistical analyses.

The AASHTO LRFD Bridge Design Specifications, First (1994) and Second (1999) Editions, requires that each bridge component and connection satisfy all limit states in accordance with the relation

$$\eta \sum \gamma_i Q_i \leq \phi R_n \tag{8}$$

in which η is a factor related to a ductility factor η_D, a redundancy factor η_R, and an operational importance factor η_i in accordance with $h = \eta_D \eta_R \eta_i$, γ_i is a statistically-based load factor applied to force effect Q_i, and ϕ is a statistically-based resistance factor applied to the nominal resistance R_n. The numerical values to be used for these factors can be found in the LRFD Specifications (AASHTO LRFD, 1994 and 1999).

The value of Q_i for that value of i representing an extreme seismic event, designated as *EQ*, is found using the same procedure described above for Standard Specifications, Fifteenth (1992) and Sixteenth (1996) Editions.

An additional bridge classification, "Critical," has been added to the LRFD Specifications; and the number of substructure response modification factors *R*, have been increased to cover all three classifications, "Critical," "Essential," and "Other" as indicated in Table 3 below.

Table 3 - Response Modification Factors (*R*)

Substructure	Importance Category		
	Critical	Essential	Other
Wall-type piers-larger dimension	1.5	1.5	2.0
Reinforced concrete pile bents			
♦ vertical piles only	1.5	2.0	3.0
♦ with batter piles	1.5	1.5	2.0
Single columns	1.5	2.0	3.0
Steel or composite steel and concrete pile bents			
♦ vertical piles only	1.5	3.5	5.0
♦ with batter piles	1.5	2.0	3.0
Multiple column bents	1.5	3.5	5.0

DUAL STRATEGY OF SEISMIC DESIGN

The design of transportation structures to perform satisfactorily under expected seismic conditions requires that realistic earthquake loadings during their life times be specified and that the structural components be proportioned to resist these and other combined loadings within the limits of certain expected performance requirements. In regions of high seismicity, earthquake loading is often critical among the types of loading that must be considered because a great earthquake will usually cause greater stresses and deformations in the various critical components of a structure than will all other loadings combined; yet, the probability of such an earthquake occurring within the life of the structure is very low. On the other hand, a moderate earthquake is very likely to occur during the same period of time having the potential to produce damage unless controlled. Considering both types of earthquake, a dual-criteria strategy of two-level design is usually adopted for Ordinary Bridges as follows:

Functional Evaluation Earthquake (FEE) - A functional evaluation earthquake is defined as one, which has a relatively high probability of occurrence during the lifetime of a bridge structure. The structure should be proportioned to resist the intensity of ground motion produced by this event without significant damage to the basic system, thus allowing it to remain functional immediately following the FEE event.

Safety Evaluation Earthquake (SEE) - A safety evaluation earthquake is defined as the most severe event which can reasonably be expected to ever occur at the site. Because this earthquake has a very low probability of occurrence during the life of a bridge structure, significant structural damage is permitted; however, collapse and serious personal injury or loss of life should be avoided.

The challenge is to set seismic design criteria which will satisfy this dual-criteria strategy in a cost-effective manner.

Important bridges located on major, heavily traveled, routes, where no convenient alternative routes exist, are now being designated as LIFELINE BRIDGES. These bridges are expected to remain functional immediately following an SEE event; therefore, they must be proportioned to resist the intensity of this event without experiencing significant damage. Because of this specified high-level of performance during an SEE event, response under the FEE condition, as defined above, is relatively of minor concern.

CHARACTERIZATION OF SEISMIC GROUND MOTIONS

It is the authors' contention that at least one-half of the bridge earthquake engineer's overall problem, in either designing a new bridge or developing retrofit measures for an existing bridge, lies in establishing appropriate design ground motions which, along with other specified design criteria, will satisfy the dual-criteria design strategy described above. In the past, it has been common practice to represent the design ground motions using acceleration response spectra developed through statistical averaging of such spectra generated for families of recorded accelerograms representative of different site conditions. A deficiency of these spectra has been that they do not represent the same probability of exceedance, for a specified period of time, over the full spectral period (or frequency) range of interest. Further, the probability of exceedance of the spectral value at any specified period is not well known.

Because of these deficiencies, probabilistic risk assessment (PRA) methodologies have emerged having the objective of providing uniform hazard response spectra for a given site with each spectrum curve representing the same numerical probability of exceedance over the entire spectral period range of interest for a specified duration of time. Usually, these spectra are generated for the "rock-outcrop" condition at the site and then modified either through explicit site response analyses, using a computer program such as SHAKE, or by applying published site amplification factors.

Figure 1 shows a set of uniform hazard curves generated recently by Geomatrix Consultants which represents a single horizontal component of "rock-outcrop" motion at the base of a marl layer resting on hard rock at the site of the planned Cooper River Bridges in Charleston, South Carolina (Geomatrix Consultants, 2000).

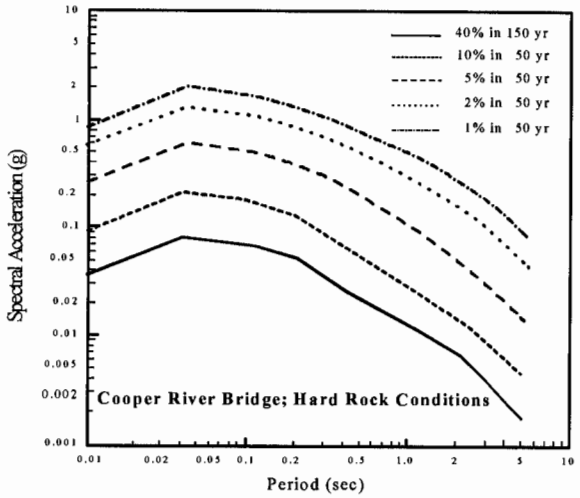

Fig. 1 Equal-hazard response spectra for hard rock (5% damped) (Source: Geomatrix Consultants, 1999)

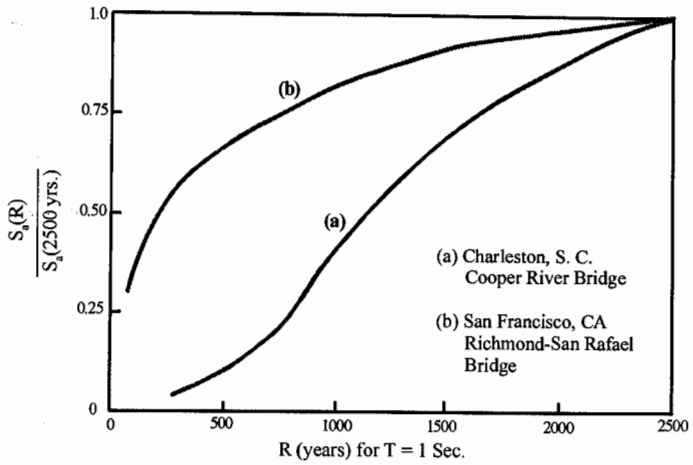

Fig. 2 Acceleration response spectral ratio $S_a(R)/S_a(2500\ \text{yrs.})$ vs. mean return period R

Once a set of uniform hazard response spectra have been generated for a specific site, a decision must be made as to which two probabilities of exceedance in a specified period of time (or mean return periods, T_R, in years) are the proper choices to represent the FEE and SEE events in satisfying the dual-criteria strategy of design previously discussed. The proper choices will, of course, depend upon the nature of the uniform hazard spectra generated. When considering a site in the eastern part of the U.S., one finds the uniform hazard spectral values for a mean return period equal to the life of a structure, say 150 years, will be very low in comparison with the corresponding values having a mean return period of say 2,500 years; see Fig. 1. On the other hand, when considering a site in the western part of the U.S., the 150-year mean-return-period spectral values will usually be high in comparison with and much closer to the corresponding 2,500-year values. To illustrate these differences, consider the acceleration response spectrum ratio $S_a(T_R)/S_a(2{,}500\ \text{years})$ for a fixed spectral period, say T =1.0 sec where the response spectral ratios are plotted as a function of mean return period T_R in years for two specific sites: namely, the Charleston, S.C. Cooper River Bridge site and the Richmond-San Rafael Bridge site in the San Francisco Bay Area (Geomatrix Consultants, 1993; see Fig. 2).

If a mean return period, T_R, equal to 2,500 years should be specified to represent the SEE event in designing a bridge for the Cooper River Bridge site using the AASHTO response modification factors shown in Table 3, the structural response due to this event will be extremely high in comparison with the response of an *FEE* event having an assigned mean return period T_R equal to say 300 years. Therefore, in this case, the SEE event will totally control the design. On the other hand, in designing a bridge for the Richmond-San Rafael site using the same mean return periods for the two events and the same response modification factors applied to the SEE event, the FEE event for which limited damage is specified would most likely control the design since the ratio $S_a(300\ \text{years})/S_a(2{,}500\ \text{years})$ is approximately 0.6. The above comparisons show the importance of assessing the performance of a final bridge design under both the FEE and SEE conditions to insure that the specified dual performance criteria have been met.

In addition to setting "rock-outcrop" response spectra representing the FEE and SEE events at a specific site, corresponding response-spectrum-compatible time histories of motion are usually generated for use in the design of bridges expected to experience inelastic deformations. These motions should be obtained by modifying "rock-outcrop" recorded time

histories using the time-domain procedure of adjustment, rather than the frequency-domain procedure, since it results in modified motions closely resembling the initial recorded motions (Lilhanand and Tseng, 1988). The recorded motions selected for modification should initially possess durations and peak ground accelerations, velocities, and displacements similar to those of the target design seismic event. For a near-field seismic event, e.g., within about 10 km of the site, the recorded motions selected should contain a definite velocity pulse or so-called "fling."

When generating components of motion to be used as seismic inputs at multiple-pier locations, they should reflect realistic spatial variations produced by wave-passage and wave-scattering effects and be response-spectrum-compatible. Thus, an appropriate wave-passage velocity (usually shown to have a speed in the range 2,000 to 3,000 m/sec by instrument-array recording data), an established set of coherency functions (Abrahamson et al, 1991) characterizing wave-scattering, and the initial response-spectrum-compatible time histories of motion should be used to generate the desired "coherency-compatible and response-spectrum-compatible" time histories of acceleration to be used as inputs at multiple-pier locations (Tseng and Penzien, 1999). Corresponding time histories of velocity and displacement should also be generated. The frequency-domain procedure should be used when interpolating motions at intermediate pier locations.

Standard site-response analyses using the above-described "rock-outcrop" motions as inputs to soil columns representing conditions at multiple-pier locations should be carried out to obtain corresponding soil motions at discrete elevations over the foundation depths. These motions are needed in order to allow an assessment of soil-foundation-structure interaction (SFSI) effects (Tseng and Penzien, 1999).

MODELLING AND DYNAMIC ANALYSIS

Over the years, finite element modelling and analysis, along with associated computer programs, have advanced greatly. Modelling can now include nonlinear elements such as nonlinear force-velocity and force-displacement hysteretic elements, and can account for nonlinear geometric effects. Much remains to be done, however, in defining elements which can realistically represent in three-dimensional forms the variety and mutual interaction of nonlinearities present in bridge structures, including those involved in soil-foundation interaction.

For determining low-level seismic response of complex or irregular bridge structures, the governing equations of motion used in evaluating seismically induced internal forces can be expressed in the linear time-domain matrix form

$$\begin{bmatrix} M_{ss} & M_{sf} \\ M_{sf}^T & \left[M_{ff}^s + \overline{M}_{ff}\right] \end{bmatrix} \begin{Bmatrix} \ddot{u}_s(t) \\ \ddot{u}_f(t) \end{Bmatrix} + \begin{bmatrix} C_{ss} & C_{sf} \\ C_{sf}^T & \left[C_{ff}^s + \overline{C}_{ff}\right] \end{bmatrix} \begin{Bmatrix} \dot{u}_s(t) \\ \dot{u}_f(t) \end{Bmatrix} + \begin{bmatrix} K_{ss} & K_{sf} \\ K_{sf}^T & \left[K_{ff}^s + \overline{K}_{ff}\right] \end{bmatrix} \begin{Bmatrix} u_s(t) \\ u_f(t) \end{Bmatrix} = \begin{Bmatrix} 0 \\ \left\{\overline{K}_{ff}\overline{u}_f(t) + \overline{C}_{ff}\dot{\overline{u}}_f(t) + \overline{M}_{ff}\ddot{\overline{u}}_f(t)\right\} \end{Bmatrix} \tag{9}$$

in which all of the M, K, and C letters denote mass, stiffness, and damping matrices, respectively, all u quantities denote time-dependent total-displacement vectors, subscript s denotes the number of DOF in the structure, excluding its f DOF located at the structure/foundation interface, and a bar placed above a letter indicates that the quantity applies to the f DOF of the foundations when isolated from the structure and subjected to the seismic free-field soil environment. For a bridge having multiple pile foundations, the

structure/foundation interface is normally specified to be at the lower surface of each footing having six degrees of freedom (three translations and three rotations). Thus, the footing masses are included in the structural system; however, to satisfy pile-head boundary conditions, rigid massless footings are included in the isolated foundation system. The total displacement vector $\bar{u}_f(t)$ in Eq. (9), and corresponding velocity and acceleration vectors, $\dot{\bar{u}}_f(t)$ and $\ddot{\bar{u}}_f(t)$, respectively, represent motions in the f DOF of the isolated foundations. These motions have been referred to in the literature as the "scattered" foundation motions (Tseng and Penzien, 1999).

The foundation stiffness, $\bar{K}_{ff}$, damping, $\bar{C}_{ff}$, and mass, $\bar{M}_{ff}$, matrices in Eq. (9) which have constant coefficients represent, collectively, approximations of the complex frequency-dependent foundation impedance matrices. These approximations have been made to remove frequency-dependent parameters in the equations of motion, thus allowing a time-domain solution of the equations of motion. If the same equations of motion were expressed in the frequency domain, then such approximations would not be necessary as the complex frequency-dependent impedance functions are fully compatible with a frequency-domain solution. The damping and mass terms on the right-hand side of Eq. (9) usually have small effects on the solution; however, their importance should be checked.

The full viscous damping matrix on the left hand side of Eq. (9) is usually expressed in Rayleigh (mass and stiffness proportional) form with two proportionality constants being assigned numerical values to limit the modal damping ratios to levels within acceptable bounds over the range of frequencies dominating seismic response. It is authors' opinion that this Rayleigh form of damping is too simplistic and unrealistic, and changes are needed to improve such a Rayleigh form of damping used in dynamic modelling, and that structure-analysis computer programs should be changed accordingly.

The above equations of motion have been expressed in the time domain, as it is necessary to do so when nonlinearities in the super-structure system, i.e., structural system above the foundations, are represented. These nonlinearities usually occur in the form of hysteretic force-displacement relations of individual components, thus requiring that the linear forms represented in the third term on the left-hand side of Eq. (9) be changed to the appropriate nonlinear hysteretic forms. Special damping devices having nonlinear viscous properties will require modifications to the second term in this equation. Having established all nonlinear forms, the corresponding coupled equations of motion can be solved for total displacements $u_s(t)$ and $u_f(t)$ using step-by-step numerical integration procedures. The use of total, rather than relative, displacements is required to avoid superposition of solutions, which is invalid when treating nonlinear systems. To complete the dynamic analysis of the overall bridge system, the time histories in vector $u_f(t)$ must be applied as inputs to each isolated soil/foundation model in a separate "feed-back" analysis (Tseng and Penzien, 1999).

Since the low-level seismic response produced by the FEE event remains essentially elastic, the linear equations of motion, Eq. (9), can be used directly yielding reliable results, even for structures having very large numbers of DOF; however, when these equations are modified to represent the variety of nonlinear component behaviors occurring under SEE conditions, the predicted response results are much less reliable. These less reliable results are due primarily to the lack of realistic modelling of the nonlinear components under their three-dimensional time-dependent deformation conditions.

It should be realized that increasing the number of degrees-of-freedom in modelling a particular structure does not necessarily improve the accuracy and reliability of global

response results obtained therefrom, especially when nonlinearities develop in the system. Often better predictions of global response can be obtained using wisely chosen generalized "super elements" resulting in fewer degrees-of-freedom.

ASSESSMENT OF SEISMIC PERFORMANCE

The procedure one should use in assessing seismic performance of a transportation structure depends upon (1) type of structure, regular or irregular, (2) level of seismic excitation, FEE or SEE, and (3) stage of the design process, preliminary or final. Because of lack of space in this paper, only the irregular structure will be discussed herein. The performance of a regular structure can be treated similarly; however, due to its simplicity, a less rigorous assessment of performance is usually adopted.

When assessing the SEE performance of an irregular structure, i.e., one having abrupt changes in mass, stiffness, and/or geometry, a separate linear response-spectrum modal analysis of a multi-degree-of-freedom (MDOF) finite element model is usually carried out first for each of three (x, y, and z) rigid-boundary inputs as defined by their corresponding acceleration response spectra. Maximum values of internal force components are evaluated and divided by their corresponding strength capacity values to establish force demand/capacity ratios for members of the initial design. Demand/capacity ratios greater than unity are, of course, fictitious since they cannot occur; however, they do provide an indication of where inelastic deformations are likely to occur first and, to a limited extent, some measure of the magnitudes of these inelastic deformations. The accuracy of this information depends very much on the amount of redundancy in the structural system. If the system is highly redundant, the distribution of internal forces will change each time an individual component undergoes inelastic deformation, which will continue until a collapse mechanism is reached. Nevertheless, the results of the linear response spectrum analysis will provide guidance toward making effective modifications to the initial design, leading to an improved (preliminary) design in terms of meeting the SEE performance criteria.

A seismic performance assessment of the preliminary design of an irregular structure under the SEE condition should focus primarily on evaluating global displacements and deformations in those individual components which experience inelastic deformations. A response-spectrum modal analysis, along with response modification factors, is invalid and should not be used at this stage of the design process. Rather, nonlinear modelling of the overall system, including foundations, should be established and nonlinear time-history analyses should be carried out to determine maximum values of component deformations, which can be compared with their corresponding deformation capacities. Deformation capacity of a component is defined as that deformation level at which the component's intended performance starts to exceed its acceptable level with increasing deformation.

In carrying out these nonlinear time-history analyses, simultaneous three-dimensional (x, y and z) response-spectrum-compatible time-histories of seismic input should be used, since superposition of separate solutions is no longer valid due to the nonlinear character of response. Further, for long, strongly coupled structures along its alignment, multiple-span segments of the total structure should be modelled; and, simultaneous three-component time histories of seismic input should be applied at each pier location. From pier-to-pier, these inputs should possess appropriate spatial characteristics reflecting realistic wave-passage, wave-scattering, and local site-response effects; and, as mentioned previously, if located in the near field to a controlling seismic source, each input should possess an appropriate velocity pulse (or fling). The critical nonlinear response of a transportation structure in such a location will most likely be dominated by its response to such velocity pulses.

In assessing the performance of a final design under the SEE condition, it is recommended that a minimum of three independent sets of three-component seismic inputs be applied to the nonlinear model separately and that the largest of the resulting maximum values of any critical response be used in assessing performance. This recommendation is made because of the large variations, which usually occur due to nonlinear effects, in critical response values.

When conducting a nonlinear time-history analysis as described above, approximations in the modelling of the structural elements are usually made, e.g., assuming idealized hysteretic force-displacement relations or, even simpler, using equivalent linear relations along with increased hysteretic damping. While these approximations are usually acceptable in conducting a demand analysis of the global system; they are not suitable for an assessment of member capacities. To evaluate such capacities, it is now standard practice to conduct inelastic static (pushover) analyses under controlled monotonic displacement and/or force conditions, noting the formation of inelastic deformations as they take place up to the point of maximum allowable performance. If the bridge structural system can be modelled adequately with only one independent degree-of-freedom, e.g., a transverse frame supporting a single deck, then the pushover analysis is straightforward. However, if the structure is irregular requiring more than one degree-of-freedom, it is difficult to perform a meaningful pushover analysis for the complete structure. The more independent degrees-of-freedom contributing to seismic response of the structure, the more difficult it is to perform a meaningful pushover analysis for the structure system. In such cases, pushover analyses for local elements and/or subsystems will be more meaningful. Special focus on improving capacity analyses is needed in order to improve one's ability to assess seismic performance.

REFERENCES

AASHTO, 1996, "*Standard Specifications for Highway Bridges*", Sixteenth Edition, American Association of State Highway and Transportation Officials.

AASHTO, 1994, "*LRFD Bridge Design Specifications*", First Edition, American Association of State Highway and Transportation Officials.

Abrahamson, N.A., Schneider, J.E., and Stepp, J.C., 1991, "Empirical spatial coherency functions for application to soil-structure analyses", *Earthquake Spectra*, **7**, 1.

ATC-6, 1981, "Seismic Design Guidelines for Highway Bridges", Applied Technology Council, funded by Federal Highway Administration.

Geomatrix Consultants, Inc., 1993, "Seismic Ground Motion Study for Richmond-San Rafael Bridge, Contra Costa and Marin Counties, CA", Prepared for Caltrans, Division of Structures.

Geomatrix Consultants, Inc., 2000, "Final Report, Cooper River Bridges Replacement Project Ground Motion Hazard Analysis, Charleston County, S.C.", Prepared for Parsons Brinckerhoff Quade & Douglas, Inc. and South Carolina Department of Transportation.

Lilhanand, K. and Tseng, W.S., 1988, "Development and application of realistic earthquake time histories compatible with multiple-damping design response spectra", *Proceedings, 9th World Conference on Earthquake Engineering*, Tokyo-Kyoto, Japan.

Tseng, W.S. and Penzien, J., 1999, "Soil-Foundation-Structure Interaction", Chapter 42, *Bridge Engineering Handbook*, Edited by Chen, W.-F. and Duan, L., CRC Press.

SYSTEM IDENTIFICATION AND MODELING OF BRIDGE SYSTEMS FOR ASSESSING CURRENT DESIGN PROCEDURES

Y. Arici[1] and K. M. Mosalam[2]

Department of Civil and Environmental Engineering
University of California Berkeley

ABSTRACT

The recorded motions by California Strong Motion Instrumentation Program (CSMIP) for seven different bridge systems are analyzed using parametric and non-parametric system identification methods. The results of these analyses include identification of modal frequencies, mode shapes and damping ratios. An excellent fit of the recorded motion in time domain is obtained using parametric methods. Utilizing the results from the identification study, the paper evaluates commonly used bridge design provisions in California.

INTRODUCTION

Identification of structural systems has been a major tool in the last two decades to verify and determine vibration characteristics. Numerous works have been conducted on building systems. In this paper, no attempt is made to review literature on buildings. Instead, the focus of the following concise literature review is on the identification and evaluation techniques performed on bridge structures.

Prior to 1999, there were 54 instrumented bridges in California, 47 of which were instrumented in the last decade. Complete list of instrumented bridges can be found in Hipley (1998). One of the older extensively instrumented bridges is El Centro Highway 8/Meloland Overpass. Several researchers, e.g. Werner et al. (1987, 1994) and Wilson and Tan (1990) have studied this bridge. Modal properties were determined using single-input/single-output and multi-input/multi-output methods. Levine and Scott (1989) used the ground motion recordings for verification of the bridge foundation model they established. Wilson (1986) used the recordings from San Juan Bautista 156/101 Overpass to evaluate the seismic response. Goel and Chopra (1995) studied Rio Dell-Hwy 101/Painter Street Overpass to estimate stiffness of abutments. McCallen and Romstadt (1994) performed detailed finite element modeling to evaluate the same structure. Saadeghvaziri and Foutch (1989) investigated the effects of vertical earthquake motions on highway bridges using data from Rio Dell-Hwy101/Painter Street Overpass. Safak (1994) used data from this bridge subjected to small earthquakes to predict the larger earthquake response. Fenves and Desroches (1994) evaluated the response of Interstate 5/Route 14 interchange using non-parametric and parametric identification

[1] Doctoral Student
[2] Assistant Professor

techniques. Hayward BART elevated section was studied by Tseng et al. (1992) producing results of coupling effects. Dumbarton Bridge has been studied by Fenves et al. (1992) pointing out the importance of articulations and longitudinal constraints at hinges. Abdel-Ghaffar et al. (1993) estimated the modal properties of Vincent Thomas Suspension Bridge from ambient vibration and Whittier earthquake recordings. Lus et al. (1999) used Eigen System Realization Algorithm and observer/Kalman filter identification approach to evaluate the same bridge system. Tsai et al. (1993) studied Caltrans seismic evaluation procedures on bridge structures using five different short bridge over-crossings concluding consistency with observed performances.

Several studies for analyzing recorded bridge data around the world are published in the literature. Chaudhary et al. (2000) used ground motion recordings from Kobe earthquake to determine vibration properties of two base-isolated bridges. Loh and Lee (1997) assessed the properties of New Lian River Bridge in Taiwan using weak and strong ground excitations by conducting multi-input/single-output identification.

The present paper covers the application of System Identification (SI) techniques on representative seven bridges out of the 54 instrumented ones in California. The primary aim of the study is to determine fundamental frequencies of these bridges to form the knowledge through which design recommendations are assessed. In addition, it is possible through SI methods to determine modal shapes and damping ratios. In this paper representative examples of such analysis concentrating on the evaluation of the first few modes of a complex curved bridge system is also presented. Note that, throughout the paper, extensive use of reports by Safak (1991), Fenves and Desroches (1994) and Glaser (1998) is made. These reports provide valuable information for performing parametric analysis using discrete time filters for structural systems.

After this introduction, the paper presents a concise information on the selected bridges. This is followed by a brief insight into the used system identification methods. Subsequently, the results of the data analysis, with detailed presentation on selected two bridges, namely, Truckee I80/Truckee River Bridge and Sylmar I5/14 Interchange Bridge are presented. Afterwards, the results from analytical modeling of the considered bridge systems using finite element method including comparison with the identified properties from the data analysis are given. Finally, the paper ends with concluding remarks and proposed future work.

SELECTED BRIDGES

The selected bridges and relevant information including earthquake data are listed in Tables 1 and 2. The criterion for choosing these bridges was to have a representative sample of commonly used systems in California. The selected bridges had different characteristics including: material (reinforced concrete versus prestressed concrete), bent types (single-column versus multiple-columns), number of spans (2 to 9), section types (box girders with different cell numbers), soil properties (soft versus stiff), structural

systems (continuous versus simply supported), and orientation (straight, skewed, and curved). Moreover, availability of sufficient sensors governed the choice of the bridges.

Table 1: Selected Bridge Information

Bridge	*Structural System*	*Built*	*Instr.*	*Spans*	*Chan.*
Hayward BART elevated section	Simply supported P/C twin beams on R/C single columns with double cantilevers	1967	1986	3 instrum. @ 77' each	19
Lake Crowley-Hwy 395	Continuos R/C 5-cell box girder on abutments and a 2-column bent	1969	1995	2 @ 104' & 99'	9
El Centro Hwy 8/Meloland Overpass	Monolithic continuous R/C 3-cell box girder on abutments and a single column bent	1971	1978	2 @ 104'	32
Rio Dell–Hwy 101/Painter St. Overpass	Continuous R/C 6-cell box girder on abutments and a 2-column bent	1976	1977	2 @ 119' & 146'	20
Ridge Crest-Hwy 580/13 Interchange	Continuos R/C 5-cell box girder on abutments and a 2-column bent	1966	1996	4 @ 62', 83', 83' & 54'	9
Truckee-I80/Truckee River Bridge	Continuos R/C 3-cell box girder on inverted A-column bents	1989	1995	3 @ 185', 192' & 185'	8
Sylmar I5/14 Interchange	Continuous R/C 3-cell box girder on single column bents with an expansion joint	1994	1995	9 from 135' to 198'	38

Table 2 Earthquake data investigated

Bridge	*Earthquake Date*	*Max. Free Field Acc.(g)*	*Max. Structure Hrz. Acc. (g)*
Hayward BART	10/17/1989	0.160	0.508
Lake Crowley-Hwy 395	06/08/1998	0.200	0.244
	06/14/1998	0.231	0.405
	05/15/1999	0.092	0.270
El Centro Hwy 8/Meloland Overpass	04/09/2000	0.043	0.174
	06/14/2000	0.013	0.044
	06/14/2000	0.011	0.038
Rio Dell–Hwy 101/Painter St. Overpass	07/31/1987	0.141	0.335
	11/21/1986	0.432	0.399
	04/25/1992	0.543	1.089
Ridge Crest-Hwy 580/13 Interchange	05/06/1997	0.005	0.016
	03/05/1998	0.019	0.077
Truckee-I80/Truckee River	10/30/1998	0.088	0.172
Sylmar I5/14 Interchange	04/11/1999	0.011	0.066
	10/16/1999	0.019	0.052

METHODOLOGY

The total displacement of the structure is represented as follows,

$$\ddot{u}_T = \ddot{u} + r\,\ddot{u}_g \tag{1}$$

where, $\ddot{u}_T$, $\ddot{u}$, and $\ddot{u}_g$ are the total structural acceleration, the relative structural acceleration, and the ground acceleration, respectively and r is the influence matrix. Using modal equations (Chopra, 1995) and classical damping, $\ddot{u}$ can be expressed by superposition of different modes as follows.

$$\ddot{u}(t) = \sum_{j=1}^{J} \phi_j \, \ddot{X}_j(t) \tag{2}$$

where ϕ_j is the j^{th} mode shape with modal coordinate $\ddot{X}_j(t)$ which can be obtained from the solution of the following differential equation.

$$\ddot{X}_j(t) + 2\xi_j \omega_j \dot{X}_j(t) + \omega_j{}^2 X(t) = -\frac{1}{M_j} L_j{}^T \ddot{u}_g{}^T \tag{3}$$

where ξ_j, ω_j, M_j are the j^{th} modal damping, frequency, and mass, respectively and L_j is the j^{th} vector of generalized influence factors for support motion. In the frequency domain, the solution of equation (3) is written using Laplace transform as follows.

$$\overline{X}(s) = -\frac{1}{s^2 + 2\xi_j \omega_j s + \omega_j{}^2} \frac{1}{M_j} L_j{}^T \, \overline{\ddot{u}}_g(s) \tag{4}$$

From the above equations, one obtains,

$$\overline{\ddot{u}}_T(s) = H(s) \; \overline{\ddot{u}}_g(s) \tag{5}$$

where,

$$H(s) = \sum_{j=1}^{J} \left(\frac{2\xi_j \omega_j s + \omega_j{}^2}{s^2 + 2\xi_j \omega_j s + \omega_j{}^2} \right) \frac{\phi_j{}^T L_j}{M_j} \tag{6}$$

<u>Non-Parametric Evaluation</u>

Transfer functions are used as for estimating system modal frequencies. For stationary input signals the transfer function may be defined in one of the following two ways.

$$H_1(i\omega) = S_{yx}(\omega) / S_{xx}(\omega) \tag{7}$$

$$H_2(i\omega) = S_{yy}(\omega) / S_{xy}(\omega) \tag{8}$$

where, S_{xx} and S_{yy} are the auto-power spectra, Fourier transform of the autocorrelations of input signal x and output signal y, respectively. S_{yx} and S_{xy} are the cross-power spectra, Fourier transform of the cross-correlations between x and y. It is known that H_1 estimate is more prone to input noise, whereas H_2 estimate is more prone to output noise. The square root of the ratio between H_1 and H_2, (Equation (9)), i.e. coherency (γ), gives an important quantity for evaluating the noise in the measurements.

$$\gamma = \sqrt{H_1(i\omega) / H_2(i\omega)} \tag{9}$$

In general, CSMIP data has bandwidth of 0.1 to 50 Hz. Since 50 Hz is much larger than the subject frequencies, the data is first low pass filtered (Ljung, 1997). In addition, the data is decimated to one-fourth the size after the filtering. Note that for older data, where the frequency resolution is not adequate, decimation is performed to one-half the size. The data is processed also by Welch method (Ljung, 1997) for estimating spectral densities using 3 to 5 data windows. Frequency resolution and windowing selection is chosen different for each earthquake record considering the quality of the data and the required resolution.

Parametric Identification

Transfer function provides accurate identification of the frequency and the mode shape information for the first few modes. A more accurate alternative would be the use of linear discrete time models, which yield both frequency and damping information. Typical single-input/single-output discrete time filter is defined as follows.

$$y_t = b_0 x_t + b_1 x_{t-1} + \cdots + a_1 y_{t-1} + a_2 y_{t-2} \tag{10}$$

where y_t and x_t are the output and input of the system at time t, respectively. The input series "b" coefficients are the causal Moving Average (MA) process, and the output series "a" coefficients are the non-causal Auto-Regressive (AR) process. Taking the Fourier transform of the above expression and applying the Z-transform gives the transfer function for this discrete system.

$$H(\omega) = \frac{Y_\omega}{X_\omega} = \frac{b_0 + b_1 z + b_2 z^2 + \cdots}{1 + a_1 z + a_2 z^2 + \cdots} \tag{11}$$

Various forms of the method exist in terms of modeling the error of the system. General format of a multi-input/single-output system can be given in a polynomial form as in Equation (12).

$$A(z)\, y(t) = \sum_{i=1}^{NI} [B_i(z)/F_i(z)]\, x_i(t - \delta_i) + [C(z)/D(z)]\, e(t) \tag{12}$$

where A, B, C, D, and F are polynomials in terms of the shift operator (z) to define various system properties and $e(t)$ is the prediction error in the model. δ is the time delay in the input. The summation in Equation (12) is performed for the number of inputs (NI).

The output error and the Auto-Regressive eXtended (ARX) model are selected in this study as best fits are acquired with these methods. In Equation (12), the output error models correspond to the case of A, C, and D being ones, while the ARX models correspond to the C, D, and F being ones. The parameters of the polynomials A, B, and F are estimated using least square minimization of the prediction error (e) (Ljung, 1997).

The modal frequencies of the dynamic system can be acquired from the poles of the transfer function between the different inputs and the output. The poles are the roots of the denominators, which exist in n/2 complex conjugate pairs where n is the order of

the auto-regressive part of each model. These can be transformed to the poles of the transfer function defined in Equation (6) using the transformation,

$$s_j = \ln(z_j)/\Delta t \tag{13}$$

where Δt is the sampling interval. Subsequently, one obtains the following relation

$$s_j, s_j^* = -\xi_j \omega_j \pm i\omega_j \sqrt{(1-\xi_j^2)} \tag{14}$$

Finally, the modal frequencies and damping ratios for the considered n/2 modes can be determined as follows.

$$\omega_j = \sqrt{(s_j \; s_j^*)} \tag{15}$$

$$\xi_j = -\mathrm{Re}(s_j)/\omega_j \tag{16}$$

The simulated and recorded outputs are compared to assess the quality of the model. This is conducted using the normalized mean square error, *J*, defined in (Werner et al., 1985).

$$J = \sum_{i=1}^{N} (y_i - y_i^M)^2 \Big/ \sum_{i=1}^{N} (y_i)^2 \tag{17}$$

where y_i *and* y_i^M are original recording from the structure and model output, respectively and *N* is the total number of time steps. A value of *J* less than 0.1 is defined to be excellent, whereas *J* in the range of 0.1 to 0.5 is considered adequate. Time history fits with *J* more than 0.5 are poor and disregarded in the analysis.

Most of the selected bridges are analyzed using multi-input/single-output error model. In part of the selected bridges, the sensor numbers and locations did not permit such analysis. The orientation of the sensors used in the SI is according to Figure 1 where the input sensors are denoted A, B, and C whereas the output sensor is denoted D.

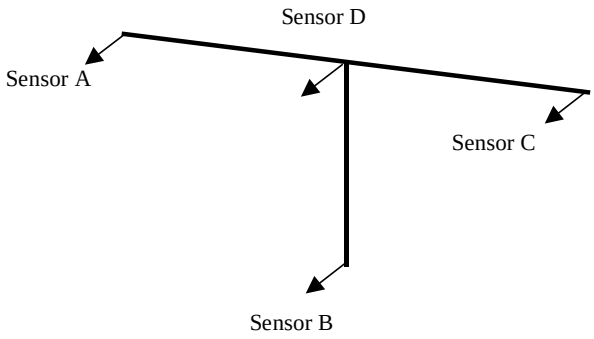

Figure 1 Selected pattern of sensors for identification

For the output error models, the acquired frequencies and damping ratios are for each of the input/output pairs. As three inputs and single output are used in this study, the frequency and damping values between the ground input and the superstructure output are selected to be the best candidate for estimating the system vibration characteristics. For the ARX models, single group of frequencies and damping ratios are acquired from the whole structure using the same sensor arrangement.

SYSTEM IDENTIFICATION

Hayward BART Elevated Section

The structural configuration of Hayward BART elevated section is illustrated in Figure 2. The SI results are given in Tables 3 and 4 for the longitudinal and transverse directions, respectively. Although the fundamental frequency in the longitudinal direction is 1.00 Hz, the third mode corresponding to 3.50 Hz is the dominant mode because of the high coupling provided by BART station nearby and the railing on structure. For the transverse direction, the fundamental frequency is found to be 1.67 Hz.

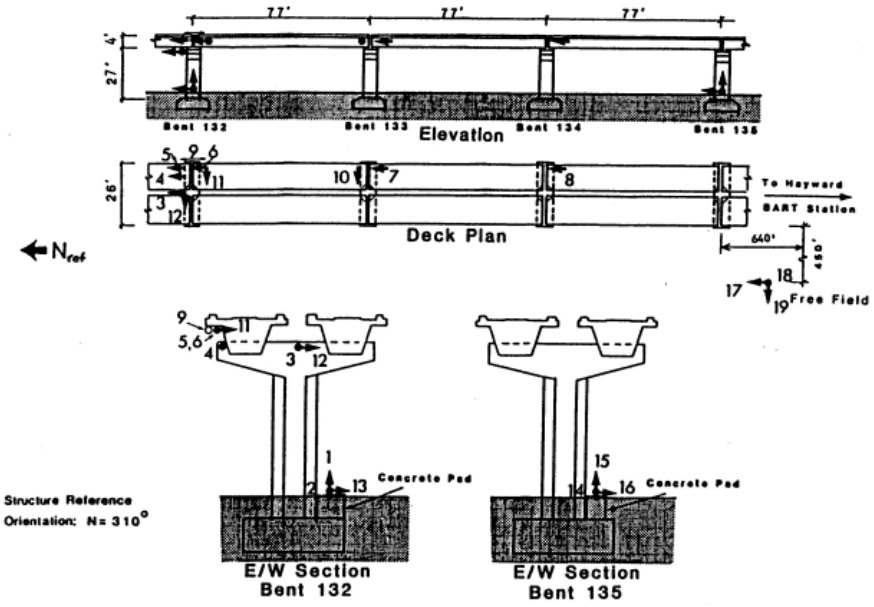

Figure 2 Hayward BART Elevated Section

Table 3 SI of Hayward BART Elevated Section (Longitudinal)

EQ. Date	*Mode #*	*TFE*	*OUTPUT ERROR*	
		Frequency	*Frequency*	*Damping*
10/17/1989	1	1.00	-	-
	2	2.10	2.07	2.12
	3	3.50	3.61	1.08

Table 4 SI of Hayward BART Elevated Section (Transverse)

Eq. Date	*Mode #*	*TFE*	*OUTPUT ERROR*	
		Frequency	*Frequency*	*Damping*
10/17/1989	1	1.80	1.67	6.20
	2	3.60	3.60	39.49

Lake Crowley–Highway 395 Bridge

The structural configuration of Lake Crowley-Highway 395 Bridge is illustrated in Figure 2. The SI results are given in Table 5. The fundamental frequency of the structure is found to be 4.6 Hz. For the second earthquake, as shown in Table 5, the first frequency was not identified since the ground motion has a very high peak of 4.9 Hz in the frequency domain, exciting the structure primarily in the corresponding mode.

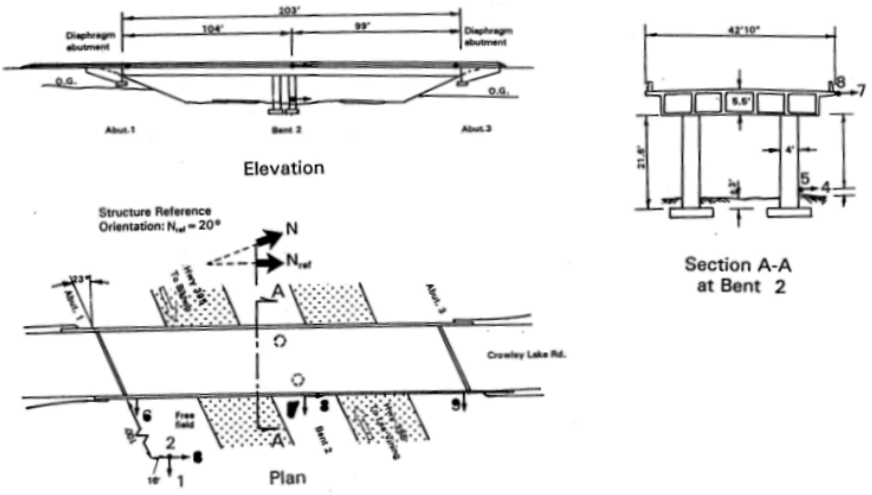

Figure 3 Lake Crowley-Highway 395 Bridge

Table 5 SI of Lake Crowley-Hwy 395 Bridge

EQ. Date	*Mode #*	*TFE*	*OUTPUT ERROR*		*ARX*	
		Frequency	*Frequency*	*Damping*	*Frequency*	*Damping*
06/08/1998	1	4.60	4.49	5.62	-	-
	2	4.99	-	-	-	-
	3	5.90	5.91	1.21	-	-
06/14/1998	1	-	-	-	-	-
	2	4.90	4.98	0.56	4.80	8.74
	3	6.06	6.37	4.04	6.15	4.38
05/15/1999	1	4.70	4.49	6.24	4.74	8.92
	2	4.98	4.94	1.21	-	-
	3	6.50	6.29	6.81	5.64	3.86

El Centro–Highway 8/Meloland Overpass

The structural configuration of El Centro–Highway 8/Meloland Overpass is illustrated in Figure 2. The SI results are given in Table 6. The fundamental frequency of the structure was deemed to be 3.25. As the bridge is monolithic with the abutments, the mode shapes involve embankment movements. Werner et al. (1987) determined modal frequencies of 2.50 and 3.20 for the case involving embankment movements, and 3.70 for

the case involving only superstructure. Note that there is significant difference between the amplitude of the bridge motion in the current study compared to that by Werner et al. (1987).

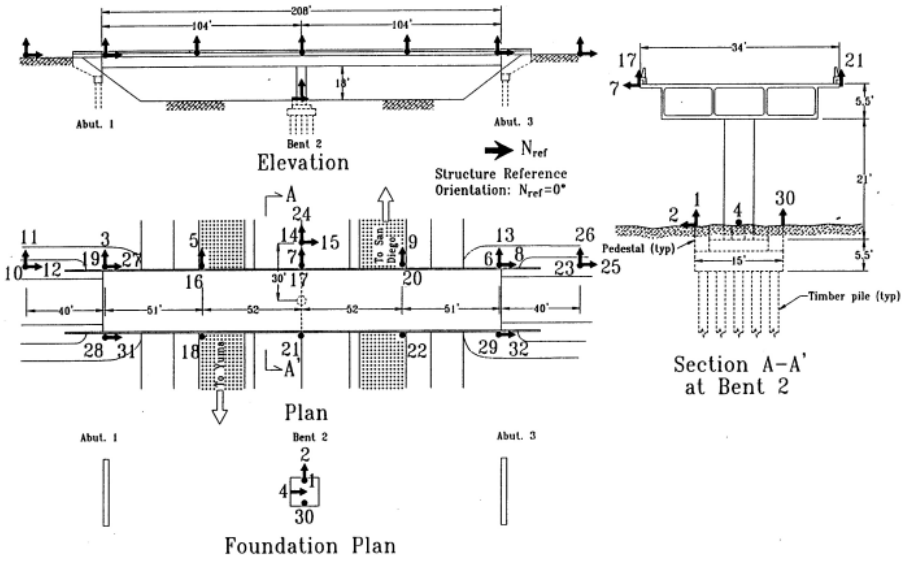

Figure 4 El Centro-Highway 8/Meloland Overpass

Table 6 SI of Meloland Overpass

EQ. Date	*Mode #*	*TFE*	*OUTPUT ERROR*		*ARX*	
		Frequency	*Frequency*	*Damping*	*Frequency*	*Damping*
04/09/2000	1	3.15	3.08	4.36	3.24	7.72
	2	3.77	-	-	3.73	5.20
06/14/2000	1	3.18	3.33	24.27	3.27	35.81
	2	3.91	3.86	5.18	3.82	3.59
06/14/2000	1	3.28	3.30	3.12	3.23	14.67
	2	3.90	3.96	5.21	3.99	2.83

Rio Dell–Highway 101/Painter Street Overpass

The structural configuration of Rio Dell–Highway 101/Painter Street Overpass is illustrated in Figure 5. The SI results are given in Table 7. The fundamental frequency of the system is determined to be 3.5 Hz. For the third earthquake, the SI results are significantly different from the first two earthquakes. This is expected since the maximum acceleration of the superstructure reaches 1.09 g during the third earthquake indicating high chance of change in the system properties.

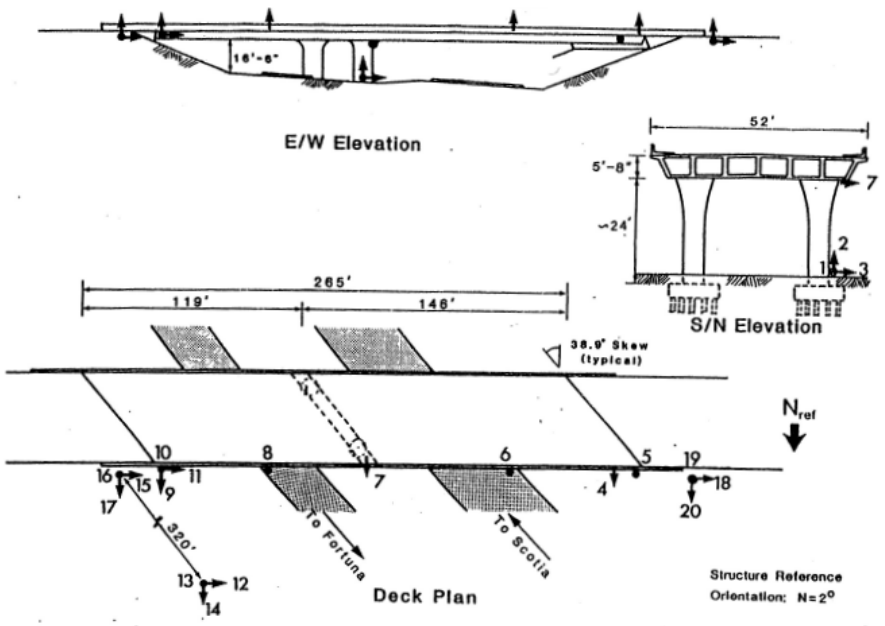

Figure 5 Rio Dell-Highway 101/Painter Street Overpass

Table 7 SI of Rio Dell-Hwy 101/Painter Street Overpass

EQ. Date	*Mode #*	*TFE*	*OUTPUT ERROR*		*ARX*	
		Frequency	*Frequency*	*Damping*	*Frequency*	*Damping*
07/31/1987	1	3.56	3.33	0.66	3.45	10.04
	2	4.74	4.86	2.1	4.82	4.11
11/21/1986	1	3.51	3.50	13.79	3.27	35.81
	2	-	-	-	4.74	6.18
04/25.1992	1	2.95	-	-	3.09	33.12
	2	4.15	-	-	4.15	7.31

Ridgecrest–Highway 395/Brown Road Bridge

The structural configuration of Ridgecrest–Highway 395/Brown Road Bridge is illustrated in Figure 6. The SI results are given in Table 8. The fundamental frequency is determined to be 3.22 Hz for this bridge. The results from the output error model using the second earthquake for this bridge is decided as more representative results. On the other hand, the ARX model inaccuracy for the second earthquake is evidenced by the relatively high error of this model for this particular case.

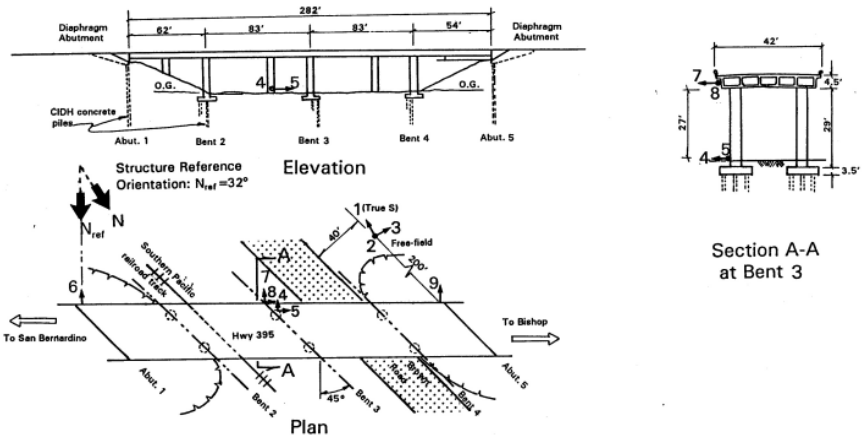

Figure 6 Ridgecrest-Highway 395/Brown Road Bridge

Table 8 SI of Ridgecrest-Hwy 395/Brown Road Bridge

EQ. Date	*Mode #*	*TFE*	*OUTPUT ERROR*		*ARX*	
		Frequency	*Frequency*	*Damping*	*Frequency*	*Damping*
05/06/1997	1	3.57	3.36	1.88	3.68	1.76
03/05/1998	1	3.21	3.22	1.80	3.39	5.34

Truckee-I80/Truckee River Bridge

The structural configuration of Truckee-I80/Truckee River Bridge is illustrated in Figure 7. The SI results are given in Table 9. The fundamental mode for the bridge is determined to be 1.19 Hz. The output error model did not identify some of the higher modes whereas ARX model was successful in that respect.

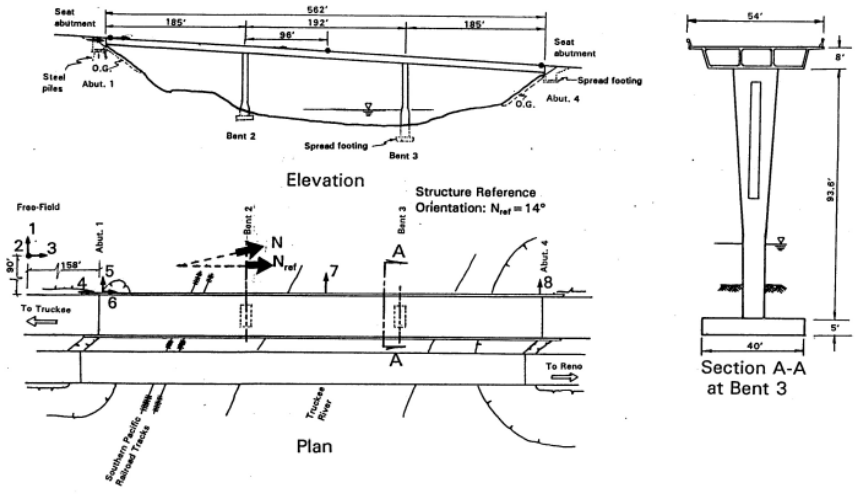

Figure 7 Truckee-I80/Truckee River Bridge

Table 9 SI of Truckee-I80/Truckee River Bridge

EQ. Date	*Mode #*	*TFE*	*OUTPUT ERROR*		*ARX*	
		Frequency	*Frequency*	*Damping*	*Frequency*	*Damping*
10/30/1998	1	1.12	1.19	2.30	1.19	2.82
	2	2.27	-	-	2.12	10.33
	3	3.13	-	-	3.02	2.48
	4	4.15	4.18	1.31	4.22	2.68
	5	6.54	6.36	0.45	-	-

Figure 8 represents a comparison for transverse acceleration at the middle of the deck (Channel 7 as shown in Figure 7) between the recorded and simulated (using ARX model) time histories. This figure illustrates excellent fit as also evidenced from the normalized mean square error (J = 0.022).

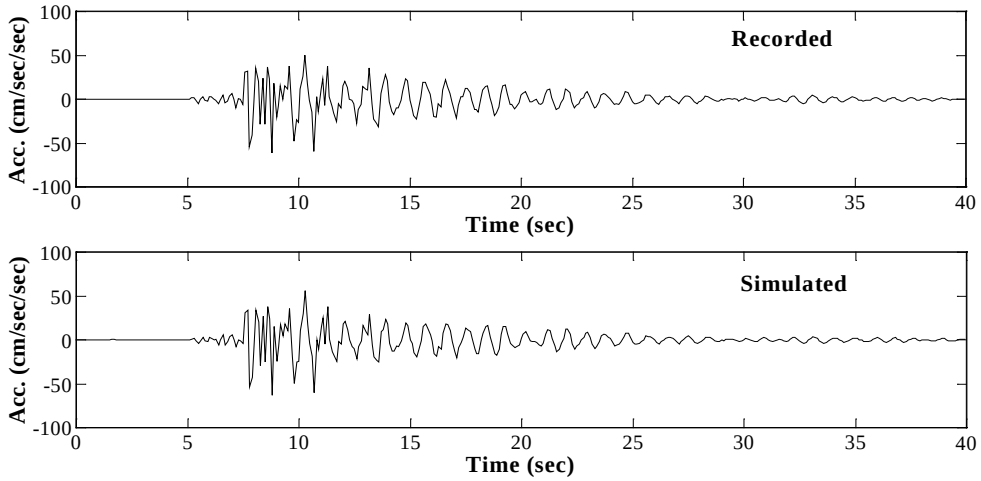

Figure 8 Time History Comparison, ARX Model versus Recording

Sylmar-I5/14 Interchange Bridge

The structural configuration of Sylmar-I5/14 Interchange Bridge is illustrated in Figure 9. The large size and geometrical configuration (e.g. the expansion joint in the middle of the bridge) of the bridge system led to the analysis of the bridge in two parts, namely the North and South substructures (left and right of the expansion joint). The SI results are given in Tables 10 and 11 for the South and North substructures, respectively.

The fundamental frequency in the first earthquake for the bridge system is identified to be 0.78 Hz from the North substructure. On the other hand, it is identified that the lowest frequency from the South substructure is 0.97 Hz corresponding to the second (anti-symmetric) mode of the whole bridge system. From Tables 10 and 11, it is noticed that the higher frequencies (> 1 Hz) are equally identified from both the North and South substructures.

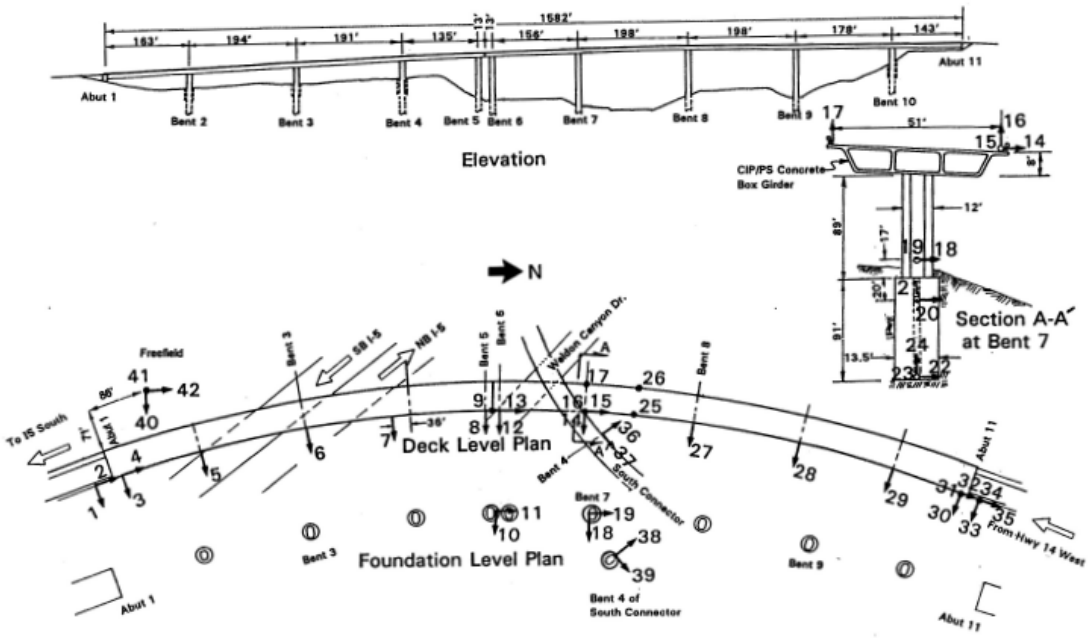

Figure 9 Sylmar-I5/14 Interchange Bridge

The fundamental frequency and the higher ones are lower based on SI using data from the second earthquake. This observation is attributed to the shear key at the expansion joint binding in the second earthquake, which is not the case during the first one. The maximum displacements near the expansion joint in the first and the second earthquakes are 0.05 cm and 2.91 cm, respectively. From the visual inspection of the displacement time histories, significant differences are observed in the structural response near the expansion joint for the two earthquakes (refer to Figure 10).

Table 10 SI of Sylmar-I5/14 Interchange Bridge (South Substructure)

EQ. Date	*Mode #*	*TFE*	*OUTPUT ERROR*		*ARX*	
		Frequency	*Frequency*	*Damping*	*Frequency*	*Damping*
04/11/1999	1	0.97	1.01	3.03	-	-
	2	1.25	1.33	3.22	-	-
	3	1.61	-	-	-	-
	4	1.76	-	-	-	-
	5	2.22	2.21	3.79	-	-
	6	2.73	-	-	-	-
10/16/1999	1	0.90	0.84	57.16	0.88	22.76
	2	1.06	1.04	13.50	-	-
	3	1.32	-	-	1.4450	8.94
	4	1.54	1.64	7.26	-	-
	5	-	2.05	7.88	2.0209	2.35
	6	2.63	2.39	1.13	2.6537	2.53

Table 11 SI of Sylmar-I5/14 Interchange Bridge (North Substructure)

EQ. Date	*Mode #*	*TFE*	*OUTPUT ERROR*		*ARX*	
		Frequency	*Frequency*	*Damping*	*Frequency*	*Damping*
04/11/1999	1	0.78	0.77	0.94	0.74	9.06
	2	0.97	-	-	-	-
	3	1.27	1.20	3.95	1.20	14.43
	4	-	-	-	1.86	2.08
	5	2.27	2.07	1.37	-	-
	6	-	2.60	0.32	2.52	18.19
10/16/1999	1	0.71	0.70	3.76	0.69	81.65
	2	0.90	-	-	-	-
	3	1.04	-	-	-	-
	4	-	1.30	5.96	1.32	21.15
	5	1.56	-	-	1.84	7.16
	6	-	2.07	9.16	2.15	7.42

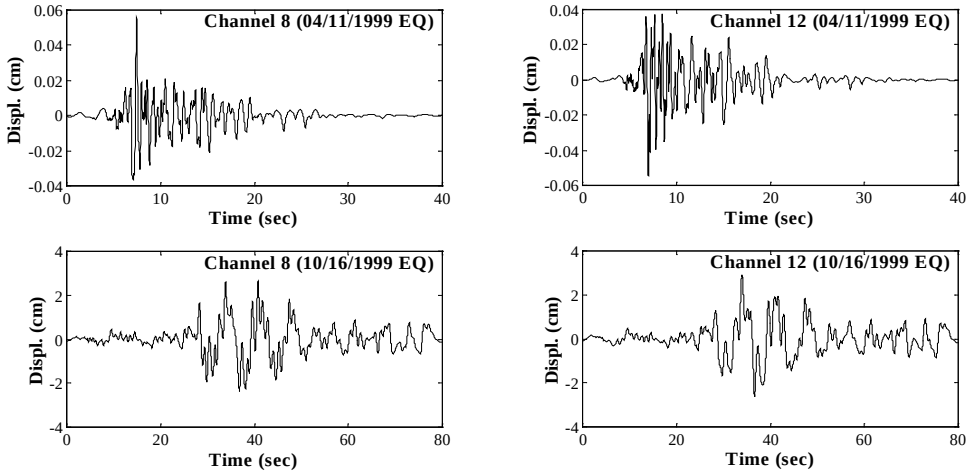

Figure 10 Displacement Time Histories at Sylmar Expansion Joint

The transverse acceleration time histories from the North substructure (channel 14 from Figure 9) from the first earthquake are compared in Figure 11 for the recorded data and simulated output using ARX model. From this figure, it is evidenced that the fitting is excellent (J = 0.025).

Assessment of Error in the SI Models

The errors for the SI models are within acceptable limits. Apart from the single analysis on Ridgecrest, all the multi-input/single-output error values are about or under 0.04. For BART, only single-input/single-output analysis is performed. The error, although significantly more than the multi-input approach, is better compared with the

results of the single-input/single-output analysis performed on the other bridges in this study. The errors of the multi-input/single-output analysis with respect to each of the selected bridges and with respect to the maximum acceleration recorded at the output sensors are given in Figures 12 and 13.

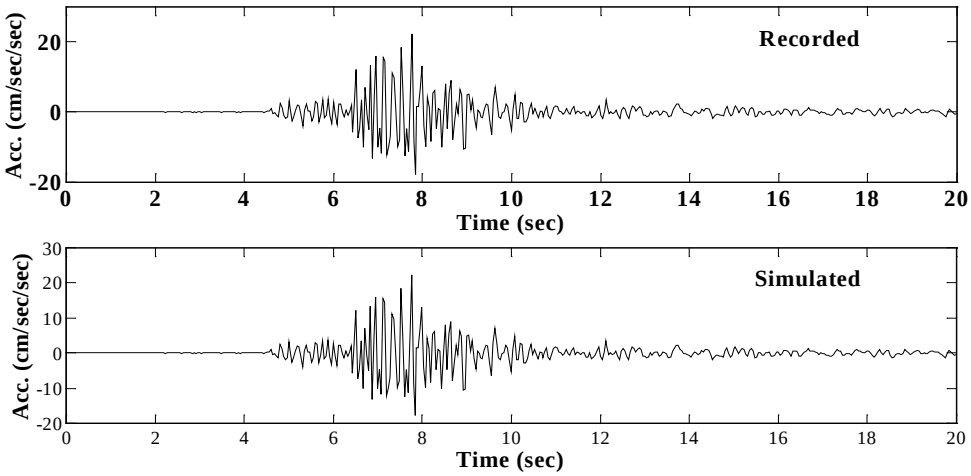

Figure 11 Time History Comparison, ARX Model versus Recording

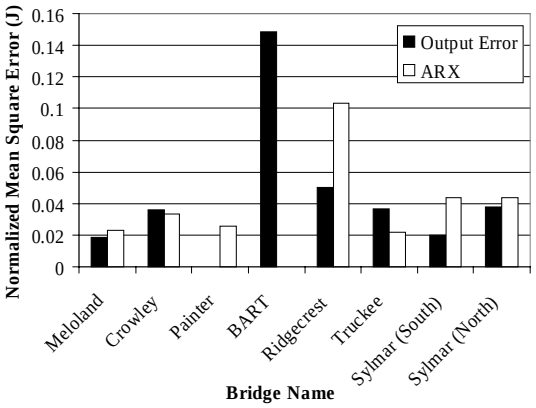

Figure 12 NMSE for SI of Bridges

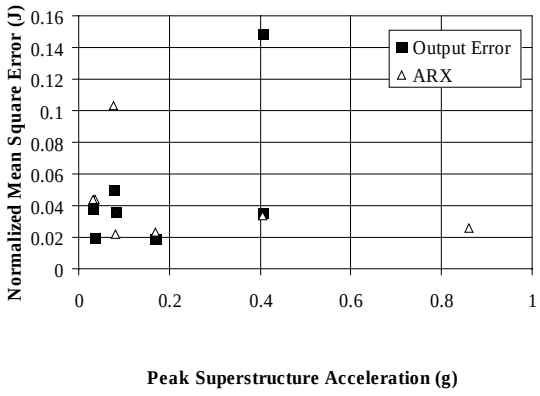

Figure 13 NMSE versus Peak Acceleration

FINITE ELEMENT ANALYSIS

Six of the selected seven bridges were analyzed using Finite Element Analysis (FEA) where Eigen analyses were conducted. The analyses are performed using the finite element package DIANA (Witte and Feenstra, 1998). The results of these FEA compared with those from the SI are given in Table 12. The analysis of Hayward BART elevated segment required high mass and stiffness coupling to match the SI results. In this way,

the fundamental frequencies in the longitudinal and transverse directions were determined. In the case of Lake Crowley-Highway 395 Bridge, Caltrans design abutment stiffness provisions (Caltrans, 1999, Priestley et al., 1996) did not lead to reasonable results compared to the SI. When the boundary conditions of the system was treated as fixed, the fundamental frequency was accurately determined. Caltrans abutment stiffness gave a perfect match with the acquired frequency from the SI for El Centro Hwy 8/Meloland Overpass. Rio Dell- Highway 101/Painter Street Overpass had the same problem as Lake Crowley-Highway 395 Bridge. Caltrans abutment stiffness estimation for the analysis of Rio Dell- Highway 101/Painter Street Overpass led to significantly lower frequencies whereas assuming the boundary condition for the abutment fixed led to the value of the fundamental frequency from SI.

Table 12 Comparison between FEA and SI

Bridge	f_1 *(Hz) SI*	f_1 *(Hz) FEM*	*Remarks*
Hayward BART	1.67	1.95	High mass and stiffness coupling
Lake Crowley-Hwy 395 Overpass	4.50	4.46	Fixed Boundaries
El Centro Hwy 8/Meloland Bridge	3.20	3.25	Excellent agreement using abutment stiffness based on Caltrans
Rio Dell–Hwy 101/Painter Street Overpass	3.50	3.55	f_1 =2.53 using Caltrans abutment stiffness, improved results with fixed east boundary
Truckee-I80/Truckee River Bridge	1.09	1.15	Caltrans abutment stiffness with cracked column section (I_{eff}/I_{gross}=0.35)
Sylmar I5/14 Interchange	0.71	0.72	Intermediate hinge at expansion joint with cracked column section (I_{eff}/I_{gross}=0.45)

The FEA of the two taller bridges, namely Truckee-I80/Truckee River Bridge and Sylmar I5/14 Interchange, required the use of cracked column cross sections for better match with the SI results. Caltrans design aids for the effective moment of inertia of cracked column sections (based on the axial load and the longitudinal reinforcement ratios) (Caltrans, 1999) were followed. Moreover, Caltrans abutment stiffness provisions were adequate for modeling Truckee-I80/Truckee River Bridge (refer to Figure 14).

Sylmar-I5/14 Interchange is modeled with the expansion joint in between the North and South substructures as an intermediate hinge (refer to Figure 15). It can be deduced that the first mode of the system is a local mode of the flexible North substructure, which is weak in the South substructure. This behavior, first determined from the SI of the system, is also captured using FEA. The second mode which appears to

be the dominant mode in the South substructure is actually the second (anti-symmetric) mode for the whole bridge system with a node existing in the North span.

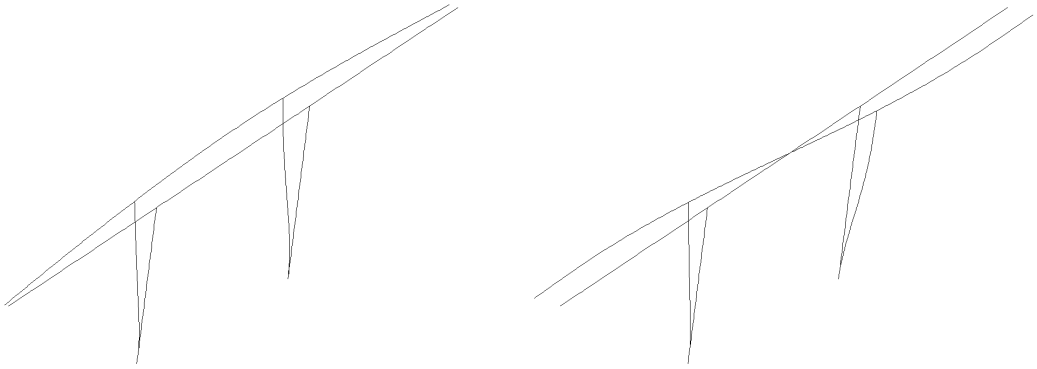

First Mode (f_1 = 1.15 FEA, 1.09 SI) Second Mode (f_2 = 1.95 FEA, 2.15 SI)

Figure 14 Modal Shapes of Truckee-I80/Truckee River Bridge

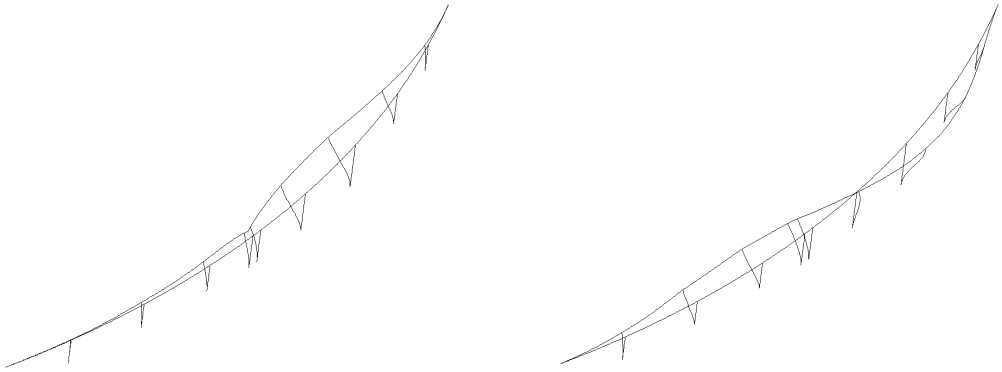

First Mode (f_1 = 0.72 FEA, 0.71 SI) Second Mode (f_2 = 1.00 FEA, 0.90 SI)

Figure 15 Modal Shapes of Sylmar I5/14 Interchange

CONCLUDING REMARKS

From the above results and discussions, the following conclusions may be inferred:

1. The selected seven bridges form a representative sample of common bridge systems in California. They accounted for different materials, section shapes, soil conditions, and structural configurations. Moreover, the data from several earthquakes was examined.
2. The utilized system identification methods are shown to be powerful techniques in identifying frequencies, mode shapes, and damping ratios for the available number and orientation of sensors.
3. The model errors (using the normalized mean square error) for both output error and ARX methods are within acceptable limits. It is worth mentioning that the ARX method is more robust and capable of accurately identifying more modes than the

output error method. In general, ARX identified higher damping ratios than the output error method.

4. The fundamental frequencies based on Eigen analysis using the finite element method reproduced the system identification results with reasonable accuracy. This was achieved with proper boundary conditions and column cross section properties.
5. Caltrans design aids for the effective moment of inertia when used for tall column cross sections led to reasonable analytical predictions of the fundamental frequency. On the contrary, the Caltrans provisions for the abutment stiffness require further refinement particularly for short span bridges, e.g. Lake Crowley-Hwy 395 Bridge.

ACKNOWLEDGMENTS

The authors gratefully acknowledge the financial support provided by the California Strong Motion Instrumentation Program under the Contract No. 1098-714 with funding from the California Department of Conservation. The contents of this paper do not necessarily represent the policy of the funding agency. The technical support of Dr. Moh Huang and Mr. Patrick Hipley was instrumental for the completion of the research.

REFERENCES

1. Abdel-Ghaffar, A.M., Niazy, A.M., and Masi, S.F. (1993) “Analysis of the seismic records of a suspension bridge,” Proceedings of the ASCE structural congress ’93, New York, 2, 1509-1514.
2. Caltrans (1999) “Caltrans Seismic Design Criterion,” Version 1.1, July.
3. Chaudhary, M.T.A., Abe, M., Fujino, Y., and Yoshida, J. (2000) “System identification of two base-isolated bridges,” Accepted for Journal of Engineering Mechanics, ASCE.
4. Chopra, A. K. (1995) “Dynamics of Structures,” Prentice Hall, New Jersey.
5. Goel, R.K. and Chopra, A.K. (1995), “Seismic response study of the Hwy 101/ Painter Street Overpass near Eureka using strong-motion records,” Data Utilization Report CSMIP/ 95-01.
6. Fenves, G.L. and Desroches, R. (1994) “Response of the northwest connector in the Landers and Big Bear earthquakes,” Report No. 94/12, Earthquake Engineering Research Center, University of California, Berkeley, CA.
7. Fenves, G.L., Filippou, F.C., and Sze, D. (1992) “Response of the Dumbarton Bridge in the Loma Prieta earthquake,” Report No. 92/02, Earthquake Engineering Research Center, University of California, Berkeley, CA.
8. Glaser, S.D. (1998) “ System identification and its application to soil dynamics,” Report No. 98/01, Geotechnical Engineering, University of California, Berkeley, CA.
9. Hipley, P, Huang., M., and Shakal, A. (1998) “ Bridge instrumentation and post-earthquake evaluation of bridges”, Proceedings SMIP98 seminar on utilization of strong motion data, 53-71.

10. Levine, M.B. and Scott, R.F. (1989) “Dynamic response verification of simplified bridge-foundation model,” Journal of Geotechnical Engineering, 115, 2, 246-260.
11. Ljung, L. (1997) “System Identification Toolbox Users Guide,” The Math Works Inc.
12. Loh, C.H. and Lee, Z.K. (1997) “Seismic monitoring of a bridge: Assessing dynamic characteristics from both weak and strong ground motions,” Earthquake Engineering and Structural Dynamics, 26, 269-288.
13. Lus, H., Betti, R., and Longman, R.W. (1999) “Identification of linear structural systems using earthquake induced vibration data,” Earthquake Engineering and Structural Dynamics, 28, 1449-1467.
14. McCallen, D.B. and Romstadt, K.M. (1994) “Dynamic analysis of a skewed short span box girder overpass,” Earthquake Spectra, 10(4), 729-755.
15. Priestley, M.J.N., Seible, F., and Calvi, G.M. (1996) “Seismic Design and Retrofit of Bridges,” John Wiley & Sons, Inc., New York.
16. Saadeghvaziri, M.A., and Foutch, D.A., (1989) ” Effects of vertical motion on the inelastic behavior of highway bridges,” Structures Congress '89: Seismic engineering: research and practice, ASCE, New York, 51-61.
17. Safak, E. (1991) “Identification of linear structures using discrete-time filters,” Journal of Structural Engineering, ASCE, 117(10), 3064-3085.
18. Safak, E. (1994) “Use of structural response data from small earthquakes and aftershocks,” NIST SP 871, Wind and Seismic Effects, Proceedings of the 26th Joint Meeting of the U.S.-Japan Cooperative Program in Natural Resources Panel on Wind and Seismic Effects, NIST, Gaithersburg, Maryland, 613-623.
19. Tsai, N.C., Firouz, A., Sedarat. H., Nisar, A., and Werner, S.D. (1993) “ Application of Caltrans current seismic evaluation procedures to selected short bridge overcrossing structures,” Technical Report, Dames & Moore.
20. Tseng, W.S., Yang, M.S., Penzien, J. (1992) “Seismic performance investigation of the Hayward BART elevated section,” Data Utilization Report CSMIP/ 92-02.
21. Werner, S.D., Beck, J.L., and Levine, M.B. (1987) “Seismic response evaluation of Meloland Road Overpass using 1979 Imperial Valley earthquake records,” Earthquake Engineering and Structural Dynamics, 15, 249-274.
22. Werner, S.D., Crouse, C.B., Katafygiotis, L.S., and Beck, J.L. (1994) “Use of strong motion records for model evaluation and seismic analysis of a bridge structure,” Proceedings of the Fifth U.S. National Conference on Earthquake Engineering, 1, 511-520.
23. Wilson, J.C. (1986) “Analysis of the observed seismic response of an highway bridge,” Earthquake Engineering and Structural Dynamics, 14, 339-354.
24. Wilson, J. C. and Tan, B.S. (1990) “Bridge abutments: assessing their influence on earthquake response of Meloland Road Overpass,” Journal of Engineering Mechanics, 116, 8, 1838-1856.
25. Witte, F.C. and Feenstra, P.H. (1998) “DIANA – Finite Element Analysis. User’s Manual: Release 7.2,” TNO Building Construction and Research, Delft, The Netherlands.

COSMOS VIRTUAL STRONG MOTION DATA CENTER

Ralph Archuleta

Institute for Crustal Studies
& Department of Geological Sciences
University of California, Santa Barbara

ABSTRACT

The COSMOS virtual data center http://db.cosmos-eq.org/ is a web accessible relational database for strong motion data. This database was designed to make it simple for a user to retrieve strong motion data that are most relevant to the needs of the user. At the same time it gives primary responsibility for quality control of the original data to the agencies that collected and processed the data. The virtual data center has information on 95 earthquakes, 3180 accelerograms, and 570 station descriptions. For each earthquake the data center has tried to include all the available accelerograms.

INTRODUCTION

As the number of strong motion accelerograms increases with each major earthquake, it has become imperative that the data be organized such that the user can easily access the data most relevant to his/her needs. When the number of significant accelerograms could be counted on two hands, each engineer or scientist could easily find the most appropriate data for his/her needs. That situation has changed dramatically in the past decade with more instruments recording strong motion. The COSMOS virtual strong motion data center has been designed to allow the user to find the data most appropriate to the problem at hand.

The COSMOS virtual data center was organized around three basic principles. First, the user must be able to search the database easily on the worldwide web. Second, the user must be able to retrieve the data without difficulty. Third, the agencies collecting the data would be the primary source of the data. These basic principles defined the basic construct. Thus the COSMOS virtual data center is the relational database with the tables and parameters to be searched; the agencies are the data repositories holding the accelerograms at their respective institutions.

The virtual data center was organized with a typical www shopping cart approach. Based on a wide range of search parameters, the user can specify criteria that will be used to select the appropriate strong motion acceleration time histories. Once selected the user can preview the acceleration time histories and their relevant attributes, such as peak acceleration, closest

distance to the fault, geological conditions at the site, etc. If the records are acceptable, the user puts them into his shopping bin. Multiple searches can be done. When all the searches are finished, the user can download the data (using ftp) directly from the agency that collected the data. This download is completely transparent to the user. The data are in the format of the agency that collected the data.

At present the virtual data center has information on 95 earthquakes, 3180 accelerograms, and 894 station descriptions. For each earthquake the data center has tried to include all the available accelerograms. The data center will soon expand to 159 earthquakes, 5287 accelerograms and 1387 station descriptions.

The database has fields in seven parameter tables related to the earthquake, station, local geology, region, instrument, owner, network and acceleration time histories. This allows the user to search for records based on many different combinations of criteria. In addition to the general search on basic parameters, the user can use an advanced search or a point-and-click search using a map of the earthquake and recording stations. In addition there is a bibliography associated with the parameters such that a user can find the reference for a magnitude or for the processing of the data—a useful feature when writing papers or reports.

USING THE COSMOS DATABASE

The COSMOS virtual data center is accessed through the web either by going to the COSMOS home page http://www.cosmos-eq.org/ and clicking on the COSMOS virtual data center or by addressing it through http://db.cosmos-eq.org. A user will find the home page that allows one to logon/logoff with his/her email address. The user will then find a heading and the primary networks that have made available their data to the database. The user will see headings that can serve as starting points for the search.

The basic search page illustrates the operation with the most common search parameters (Figure 1). A critical feature of the database is that only the field(s) the user wants to search have to be specified. The user can leave the other fields blank and the database will supply the values based on the search. For example, suppose a user wants all the records that have peak acceleration between 500 and 600 cm/s/s recorded at a distance closest to the fault between 15 and 20 km. These values are input into the search and the following results are returned (Figure 2). At this point the user can look the list of stations or the list of earthquakes that satisfied the criteria. For each record the user can 1) click on a description of the earthquake to see its magnitude, location and other source parameters, 2) examine the station to see its local geology, site conditions, and other records recorded at this station, 3) look at a map to see the epicenters of the earthquake and the locations of the station, 4) view the accelerograms. Note that the results indicate the location of the sensor within structures or in an instrument shelter at ground level (free field). Such descriptions are possible when using the advanced search.

The search routine is versatile. Each record is associated with a station. By simply clicking on the station name the database will return information about that station, and it will

show all other records that have been recorded at the site (Figure 3). In Figure 3, the Castaic Old Ridge Route site is described. The records include those obtained with the search criteria—1971 San Fernando CA earthquake—but it also includes five other earthquakes (only two are shown in Figure 3). By clicking on the "View Plot of Data" the user will immediately see plots of the accelerograms (Figure 4) that include relevant information about the earthquake, the site and the time histories.

One of the more useful features of the database is to find data using "Map." As one searches the database, the user will often find the ability to create a simplified map of the station locations and the earthquake epicenter. In Figure 5 a map is drawn after selecting the 1979 Imperial Valley earthquake. The epicenter is shown as a diamond (orange on color monitors) and the stations are shown as white squares. By simply pointing and clicking on a station, the user can find the accelerograms for that station. Or by pointing and clicking on an epicenter, the information about the earthquake will appear and all of the data associated with that event (Figure 6). Thus one can interactively move between stations and earthquakes to find data.

Naturally all of the data are listed in tables so that the user can find either stations or earthquakes grouped by region. A partial listing of the earthquakes is shown in Figure 7. The station list, 570, is too large to show. However, what the user will find in the database are scroll bars that allow the user to easily find a station for different regions. Both the earthquake and station lists have clickable scroll bars that allow the user to jump into a particular region without having to scroll through unwanted data.

All of the searchable parameters can be viewed by clicking on the advanced search option (Figure 8). The user first selects those parameters that will be part of the criteria in finding the appropriate data. Once the parameters are selected, the user proceeds to the search page. In Figure 9 there are six parameters that could be searched in this example. However, only two are actually used, instrument location and peak ground acceleration. The database can search on both numerical values and text strings and the types are clearly labeled. Also Figure 9 illustrates that the user does not have to fill in all the boxes. The data found using this search are shown in Figure 10. A point to note is that if any one of the three components satisfy the search criteria, all three components of acceleration are returned.

All during the search of the COSMOS database the user has the opportunity to add the data to his shopping bin. At some point the user will proceed to the download bin with a list of accelerograms that the user would like to retrieve (Figure 11). In doing so the user will finally reach the point where the data can be downloaded to the user's computer. By simply clicking on the "Download" the data are transferred to the user's computer in a format supplied by the agency that processed the data. It is also possible to delete items from the bin. Each user will have had to log in by giving an email address to reach this point. The database keeps track of previous shopping bins for the user. So that a user could go back and retrieve data that was previously downloaded and then discarded. With the COSMOS database the user will not have to store countless records on his/her own computer; the user can simply retrieve them whenever they are needed.

LOOKING TO THE FUTURE

The COSMOS database is evolving. There are simple features that can be improved such as showing closest distance to the fault instead of epicentral distance. More substantial improvements are nearly ready for implementation. In the near future the database will have the ability to search for acceleration records that have response spectral ordinates at particular periods, e.g., 0.1, 0.3, 1.0, 3.0 s. At the same time the database will show plots of response spectra similar to its presentation of the three components of acceleration. All of these features are being considered so that the user will be able to select the most appropriate data and download what is necessary. At present the data are downloaded in the format determined by the agency that collected the data. In the future, there will be a standard format for all the strong motion data that are downloaded so that the user does not have to keep several different translators working.

The amount of strong motion data is rapidly increasing. The usefulness of the data depends on its accessibility to the user. The COSMOS virtual data center was created to insure that all users have equal access to the data. Moreover it increases the efficiency of the users by allowing each one to select the data most appropriate to his/her needs. By trying to be complete in that all records for the significant earthquakes are included, the database eliminates biases that might arise because a user was unaware of some critical data that are relevant to the study being done. One of the major efforts will be to update the database. The data center will soon expand to 159 earthquakes, 5287 accelerograms and 1387 station descriptions not including recent earthquakes.

ACKNOWLEDGMENTS

The COSMOS virtual data center was built on the foundation of the Southern California Earthquake Center strong motion database. That database and the COSMOS virtual data center were crafted by the superior computer expertise of Dr. Grant Lindley. The contents of this report were developed under Contract No. 1098-716 from the California Department of Conservation, Division of Mines and Geology, Strong Motion Instrumentation Program. However, these contents do not necessarily represent the policy of that agency nor endorsement by the State Government. This report was also supported by the U.S. Geological Survey Cooperative Agreement No. 99WRAG0016.

COSMOS VIRTUAL DATA CENTER

Consortium of Organizations for Strong-Motion Observation Systems

Home · Login/Logoff · Download · About Us · Contact · Mirror Sites
Earthquakes · Stations · Search · Map · Adv. Search

Database Search

To search on database parameters not found on this page, use the advanced search.

Note: Leave blank any fields that do not apply to your search.

Event Name: [ ] (e.g. North Palm Springs)

Station Identifier: [ ] (Station location or number assigned by the station owner.)

Enter minimum and/or maximum values:

Earthquake Magnitude:	from [ ] to [ ]
Peak Ground Accel. (cm/s/s):	from [300] to [350]
Closest Distance to Fault (km):	from [20] to [25]
Epicentral Distance (km):	from [ ] to [ ]

(•) Return earthquake, station, and accelerogram information
( ) Return station information only
( ) Return earthquake information only

Station Owner:
(•) Any
( ) Army Corps of Engineers
( ) California Strong Motion Instrumentation Program
( ) California Institute of Technology
( ) Private owner of building or structure
( ) United States Bureau of Reclamation
( ) United States Geological Survey
( ) Department of Veterans Affairs

Region:
(•) Any
( ) Alaska
( ) Central and Eastern United States
( ) Mexico
( ) Northern California
( ) Pacific Northwest
( ) Southern California

[Search] [Reset Form]

Home + Login + Download + About Us + Contact + Mirror Sites
Earthquakes + Stations + Search + Map + Advanced Search

Figure 1. COSMOS basic search page. Here only the peak acceleration and closest distance to the fault are specified in a rather narrow range. Any parameter can be specified. Note one can restrict the region of the earthquake.

COSMOS VIRTUAL DATA CENTER

Consortium of Organizations for Strong-Motion Observation Systems

Home · Login/Logoff · Download · About Us · Contact · Mirror Sites
Earthquakes · Stations · Search · Map · Adv. Search

Search Results

Event Name: Any
Magnitude: Any
Region: Any
PGA: 300 to 350 cm/s/s

Station Identifier: Any
Epicentral Distance: Any
Closest Distance to Fault: 20 to 25 km
Station Owner: Any

Jump within page to:
[Choose an earthquake]

Jump within page to:
[Choose a station]

☐ Add all data on this page to the download bin

Go to Download Bin View Map

NORTHRIDGE CA 1994 01 17 0430 PST
14.9 km: TOPANGA - FIRE STATION
USGS station 5081

Structure: 1-STORY BLDG
Instrument: GROUND

Summary Page for this Station View Plot of Data

☐ Add all of this station's data to the download bin Go to Bin

Component:	360	**PGA (cm/s/s):**	326.9	☐ Add this trace to download bin
Component:	270	**PGA (cm/s/s):**	191.7	☐ Add this trace to download bin
Component:	Up	**PGA (cm/s/s):**	188.7	☐ Add this trace to download bin

Return to top

NORTHRIDGE CA 1994 01 17 0430 PST
19.1 km: LOS ANGELES - 10751 WILSHIRE BLVD
USGS station 0663

Structure: 12-STORY BLDG
Instrument: ROOF 12TH LEVEL

Summary Page for this Station View Plot of Data

☐ Add all of this station's data to the download bin Go to Bin

Component:	252	**PGA (cm/s/s):**	385.3	☐ Add this trace to download bin
Component:	162	**PGA (cm/s/s):**	320.0	☐ Add this trace to download bin
Component:	Up	**PGA (cm/s/s):**	377.0	☐ Add this trace to download bin

Return to top

Figure 2. Search results (partial listing) for parameters specified in Figure 1.

COSMOS VIRTUAL DATA CENTER

Consortium of Organizations for Strong-Motion Observation Systems

Home · Login/Logoff · Download · About Us · Contact · Mirror Sites
Earthquakes · Stations · Search · Map · Adv. Search

CSMIP: CASTAIC
OLD RIDGE ROUTE

Agency Number: 24278 **Structure:** 1-STORY BLDG
Network: Unknown
Site Geology: SANDSTONE T
Owner: California Strong Motion Instrumentation Program (external link)
References

☐ Add all data on this page to the download bin

Go to Download Bin View Map

14.0 km: SOUTHERN CALIFORNIA 1965 07 15 2346 PST
Summary page for this earthquake View Plot of Data
☐ Add this station record to the download bin

Component:	Down	**PGA (cm/s/s):**	29.8	☐ Add this trace to download bin
Component:	90	**PGA (cm/s/s):**	42.6	☐ Add this trace to download bin
Component:	180	**PGA (cm/s/s):**	49.2	☐ Add this trace to download bin

Return to top Go to Bin

27.6 km: SAN FERNANDO CA 1971 02 09 0601 PST
Summary page for this earthquake View Plot of Data
☐ Add this station record to the download bin

Component:	Down	**PGA (cm/s/s):**	173.7	☐ Add this trace to download bin
Component:	21	**PGA (cm/s/s):**	327.6	☐ Add this trace to download bin
Component:	291	**PGA (cm/s/s):**	280.9	☐ Add this trace to download bin

Return to top Go to Bin

40.1 km: NORTHRIDGE CA 1994 01 17 0430 PST
Summary page for this earthquake View Plot of Data
☐ Add this station record to the download bin

Component:	Up	**PGA (cm/s/s):**	213.0	☐ Add this trace to download bin
Component:	90	**PGA (cm/s/s):**	557.1	☐ Add this trace to download bin
Component:	360	**PGA (cm/s/s):**	504.2	☐ Add this trace to download bin

Return to top Go to Bin

Figure 3. Clicking on the station summary for Castaic Ridge leads to this page (partial) showing the site characteristics as well as other accelerograms recorded at this station. These additional accelerograms will probably not satisfy the original search criteria.

COSMOS VIRTUAL DATA CENTER

Consortium of Organizations for Strong-Motion Observation Systems

Home · Login/Logoff · Download · About Us · Contact · Mirror Sites
Earthquakes · Stations · Search · Map · Adv. Search

Data Plot

Station: CASTAIC - OLD RIDGE ROUTE
Station Owner: California Strong Motion Instrumentation Program
Station Latitude & Longitude: 34.5600, -118.6400

Earthquake: SAN FERNANDO CA 1971 02 09 0601 PST

Epicentral Distance: 27.6 km

(Use the back button on your browser to return to the previous page)

Component: 291 GROUND LEVEL

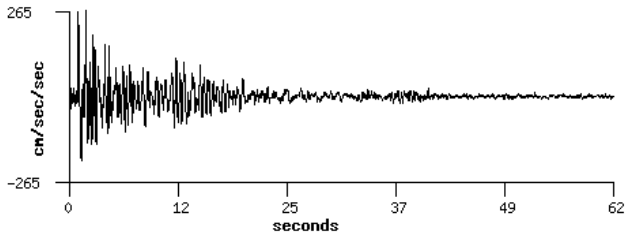

Component: 21 GROUND LEVEL

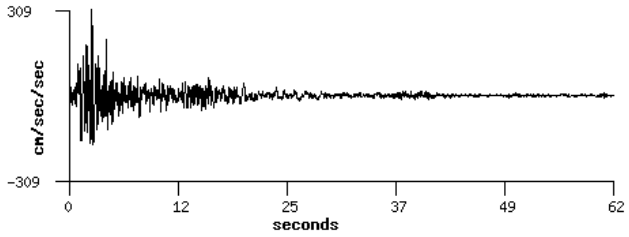

Component: Down GROUND LEVEL

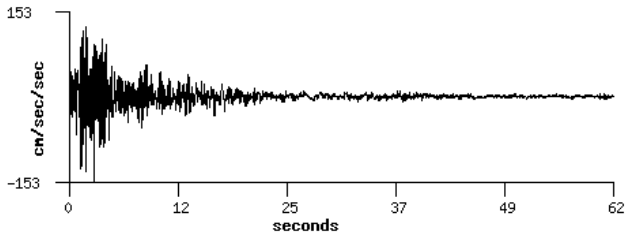

Home + Login + Download + About Us + Contact + Mirror Sites
Earthquakes + Stations + Search + Map + Advanced Search

Figure 4. Having clicked on the View Plot of Data the user sees the 3 components for the 1971 San Fernando earthquake recorded at Castaic Old Ridge Route.

COSMOS VIRTUAL DATA CENTER

Consortium of Organizations for Strong-Motion Observation Systems

Home · Login/Logoff · Download · About Us · Contact · Mirror Sites

Earthquakes · Stations · Search · Map · Adv. Search

IMPERIAL VALLEY CA 1979 10 15 2316

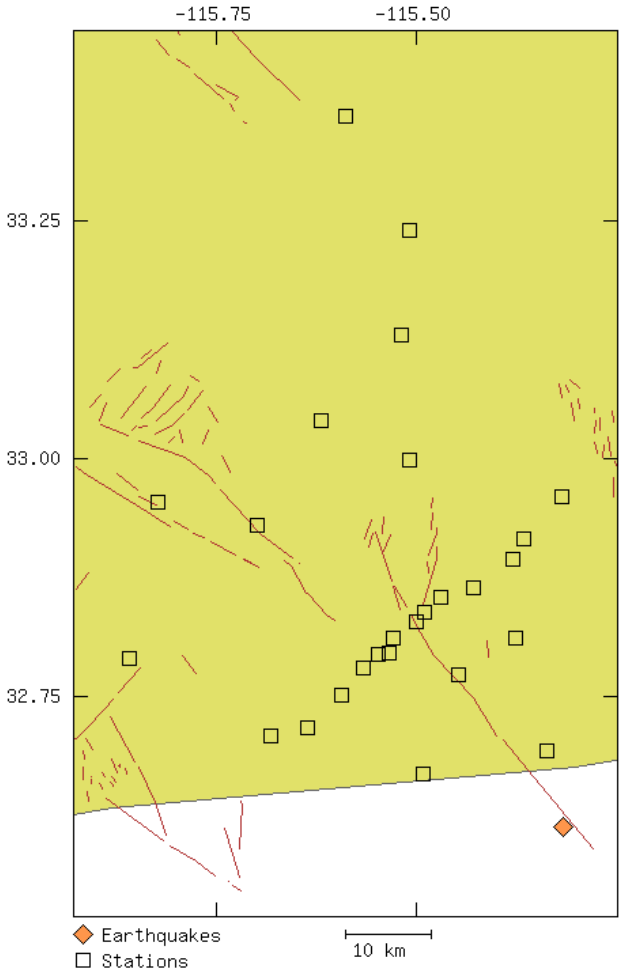

Click on the map to zoom in or to select a station or earthquake.

Zoom Out

Enter new latitude and longitude ranges:

Latitude:	32.52	to	33.45
Longitude:	-115.93	to	-115.25

Create New Map Reset Coordinates

Home · Login · Download · About Us · Contact · Mirror Sites
Earthquakes · Stations · Search · Map · Advanced Search

Figure 5. Using the map option for seeing the epicenter, station locations and nearby faults for the 1979 Imperial Valley earthquake. By pointing either to the epicenter (diamond) or the stations (squares) one can immediately retrieve information about the earthquake or the station.

COSMOS VIRTUAL DATA CENTER

Consortium of Organizations for Strong-Motion Observation Systems

Home · Login/Logoff · Download · About Us · Contact · Mirror Sites

Earthquakes · Stations · Search · Map · Adv. Search

IMPERIAL VALLEY CA 1979 10 15 2316

Region: Southern California
Event Latitude (North): 32.6140
Event Longitude (West): -115.3180
Event Depth (km): 12.10
Preferred Magnitude: 6.4
Moment Magnitude: 6.5
Surface Magnitude: 6.9
Local Magnitude: 6.6
Other Magnitude: 6.5
Seismic Moment (dyne-cm): 3.0E+25
Strike: 132
Dip: 90
Rake: 180
References

Jump within page to:
[Choose a Station]

Add all data on this page to the download bin

Go to Download Bin View Map

9.0 km: BONDS CORNER - HWYS 115 & 98

USGS station 5054
Site Geology: ALLUVIUM
Summary Page for this Station

Structure: 1-STORY BLDG
Instrument: GROUND LEVEL
View Plot of Data

Add all of this station's data to the download bin

Go to Bin

Component: 230	**PGA (cm/s/s):** 763.2	Add this trace to download bin
Component: 140	**PGA (cm/s/s):** 582.5	Add this trace to download bin
Component: Up	**PGA (cm/s/s):** 434.9	Add this trace to download bin

Return to top

Figure 6. Having clicked on the epicenter of the 1979 Impeiral Valley earthquake (diamond, Figure 5) the database retrieves the information about the earthquake and all of the records for that earthquake. Only Bonds Corner is shown here on this single page, but all records are retrieved and sorted by epicentral distance.

COSMOS VIRTUAL DATA CENTER

Consortium of Organizations for Strong-Motion Observation Systems

Earthquakes within each Region

Jump within page to:
[Choose a Region]

Alaska

Earthquake (most recent event is first)	Magnitude	Stations	Owners
SOUTHEASTERN ALASKA 1979 02 28 2127 UTC	7.1	3	USGS
ANCHORAGE ALASKA 1975 01 01 0355 UTC	5.9	4	USGS
ADAK ALASKA 1971 05 02 0608 UTC	7.1	1	USGS

Return to Top

Central and Eastern United States

Earthquake (most recent event is first)	Magnitude	Stations	Owners
ENOLA ARKANSAS 1982 07 05 0413 UTC	3.8	4	USGS
ENOLA ARKANSAS 1982 06 26 1556 UTC	3.0	7	USGS
NEW HAMPSHIRE USA 1982 01 19 0014	4.5	6	ACOE USGS

Return to Top

Mexico

Earthquake (most recent event is first)	Magnitude	Stations	Owners
BAJA CALIFORNIA MEXICO 1934 12 30 0552 PST	6.4	1	USGS

Return to Top

Northern California

Earthquake (most recent event is first)	Magnitude	Stations	Owners
PARKFIELD CA 94 12 20	5.0	2	CSMIP
SOUTH LAKE TAHOE CA 94 09 12	6.1	1	CSMIP
EUREKA CA 94 09 01	6.8	3	CSMIP
CAPE MENDOCINO/PETROLIA CA 1992 04 26 1118	6.6	8	USGS
CAPE MENDOCINO/PETROLIA CA 1992 04	6.6	8	USGS

26 0741			
CAPE MENDOCINO/PETROLIA CA 1992 04 25 1106 PDT	7.0	14	USGS CSMIP
LOMA PRIETA CA (SANTA CRUZ MOUNTAINS) 1989 10 18 0004	7.0	87	USGS CSMIP
MORGAN HILL CA 1984 04 24 2115	6.1	31	CSMIP USBR USGS
COALINGA CA AFTERSHOCK 1983 09 09 0916	5.3	2	CSMIP
COALINGA CA AFTERSHOCK 1983 07 25 2231	5.3	2	CSMIP
COALINGA CA AFTERSHOCK 1983 07 22 0343	5.0	2	CSMIP
COALINGA CA AFTERSHOCK 1983 07 22 0239	6.0	9	USGS CSMIP USBR
COALINGA CA AFTERSHOCK 1983 07 09 0740	5.4	9	USGS CSMIP
COALINGA CA AFTERSHOCK 1983 06 11 0309	5.2	3	USGS CSMIP
COALINGA CA AFTERSHOCK 1983 05 09 0249	5.3	20	USGS CSMIP USBR
COALINGA CA 1983 05 02 2342	6.5	48	CSMIP USBR
MAMMOTH LAKES CA 1980 05 27 0751 PDT	6.2	4	CSMIP
MAMMOTH LAKES CA 1980 05 26 1158 PDT	5.7	2	CSMIP
MAMMOTH LAKES CA 1980 05 25 1336 PDT	5.7	2	CSMIP
MAMMOTH LAKES CA 1980 05 25 1245 PDT	6.1	2	CSMIP
MAMMOTH LAKES CA 1980 05 25 0949 PDT	6.0	3	CSMIP
MAMMOTH LAKES CA 1980 05 25 0934 PDT	6.1	3	CSMIP
LIVERMORE CA 1980 01 27 0233	5.8	2	USGS
LIVERMORE CA 1980 01 24 1900	5.5	2	USGS
COYOTE LAKE CA 1979 08 06 1705	5.7	8	CSMIP
COYOTE DAM CA 1978 03 25 1627 PST	4.5	1	USGS
PARKFIELD CA 1966 06 27 2026 PST	6.1	7	USGS CSMIP
SAN FRANCISCO CA 1957 03 22 1144 PST	5.3	5	USGS CSMIP
SAN LUIS OBISPO CA 1952 11 21 2346 PST	6.0	1	USGS

Return to Top

Figure 7. A complete listing of all earthquakes in the database showing magnitude, number of recording stations and owner can be easily seen by clicking on the word "Earthquakes" at the top of any search page. From here all one has to do is click once more any earthquake to reach the accelerograms for that event. Shown in this figure is only a partial listing of all the events currently in the database.

COSMOS VIRTUAL DATA CENTER

Consortium of Organizations for Strong-Motion Observation Systems

Home · Login/Logoff · Download · About Us · Contact · Mirror Sites
Earthquakes · Stations · Search · Map · Adv. Search

Advanced Search: Choose Parameters

Select the database parameters that you wish to search on.

Event Parameters

☐ Event Code	☐ Earthquake Name
☐ Event Date (e.g. 15-JAN-2000)	☐ Event Latitude (North)
☐ Event Longitude (West)	☐ Event Depth (km)
☐ Preferred Magnitude	☐ Moment Magnitude
☐ Surface Magnitude	☐ Local Magnitude
☐ Other Magnitude	☐ Seismic Moment (dyne-cm)
☐ Strike	☐ Dip
☐ Rake	

Region Parameters

☐ Region

Station Parameters

☐ Station Name	☐ Agency Number
☐ Location	☐ Auxillary Location
☐ Address	☐ Geology
☐ Los Angeles Basin Geology	☐ California Geology
☐ S-wave Velocity Top 30m (m/s)	☐ Structure
☐ Status	☐ Outside Web Address

Station Owner Parameters

☐ Owner Name	☐ Web site
☐ FTP site	☐ Address
☐ Contact Person	☐ Contact E-mail
☐ Parent Agency	☐ Parent Agency Web Site
☐ Owner Acronym	☐ Data in COSMOS Data Center?

Figure 8. Searchable parameters in the COSMOS database.

Network Parameters

☐ Network Name	☐ Owner
☐ Network Web Site	☐ Network Acronym

Instrument Parameters

☐ Location	☐ Instrument Type
☐ Instrument Agency Number	☐ Latitude (North)
☐ Longitude (East)	☐ Outside Web Address

Accelerogram (Trace) Parameters

☐ Uncorrected Acceleration Download	☐ Corrected Acceleration Download
☐ Epicentral Distance (km)	☐ Hypocentral Distance (km)
☐ Closest Distance to Fault (km)	☐ Component Offset from Vertical
☐ Component Azimuth	☐ Peak Ground Acceleration

Proceed to Search Page Reset Form

Home + Login + Download + About Us + Contact + Mirror Sites
Earthquakes + Stations + Search + Map + Advanced Search

Figure 8 (continued). Searchable parameters in the database. There are plans to increase the parameter list to include others such as response spectral ordinates at selected periods.

COSMOS VIRTUAL DATA CENTER

Consortium of Organizations for Strong-Motion Observation Systems

Home · Login/Logoff · Download · About Us · Contact · Mirror Sites
Earthquakes · Stations · Search · Map · Adv. Search

Advanced Search: Parameter Input

Enter search values into the text boxes below. You may leave boxes empty.

Text input fields:

Type	Parameter	Value
Instrument	Location	Ground
Station	Geology	
Station	Structure	

Numerical input fields:

Type	Parameter	Min/Max Values	
Station	S-wave Velocity Top 30m (m/s)		
Trace	Closest Distance to Fault (km)		
Trace	Peak Ground Acceleration	900	

Proceed to Results Page Reset Form

Home · Login · Download · About Us · Contact · Mirror Sites
Earthquakes · Stations · Search · Map · Advanced Search

Figure 9. The parameters taken from the advanced search to find records with peak acceleration greater than 900 cm/s/s. Note that in the advanced search text can be used in descriptions, such as instrument location. Here "Ground" is used so that records from buildings at any floor level other than ground or from dams are not considered in the search.

COSMOS VIRTUAL DATA CENTER

Consortium of Organizations for Strong-Motion Observation Systems

Home · Login/Logoff · Download · About Us · Contact · Mirror Sites

Earthquakes · Stations · Search · Map · Adv. Search

Advanced Search: Results

Location: Contains the string **'Ground'**
Geology: No condition
Structure: No condition
S-wave Velocity Top 30m (m/s) Max.: No condition
S-wave Velocity Top 30m (m/s) Min.: No condition
Closest Distance to Fault (km) Max.: No condition
Closest Distance to Fault (km) Min.: No condition
Peak Ground Acceleration Max.: No condition
Peak Ground Acceleration Min.: 900

Jump within page to:
[Choose an earthquake]

Jump within page to:
[Choose a station]

☐ Add all data on this page to the download bin

Go to Download Bin View Map

NORTHRIDGE CA 1994 01 17 0430 PST

5.5 km: TARZANA - CEDAR HILL NURSERY

CSMIP station 24436
Site Geology: ALLUVIUM;9M;SILTSTONE
Summary Page for this Station

Structure: 1-STORY BLDG
Instrument: GROUND LEVEL
View Plot of Data

☐ Add all of this station's data to the download bin

Go to Bin

Component: 360	**PGA (cm/s/s):** 970.7	☐ Add this trace to download bin
Component: 90	**PGA (cm/s/s):** 1744.5	☐ Add this trace to download bin
Component: Up	**PGA (cm/s/s):** 1027.5	☐ Add this trace to download bin

Return to top

Figure 10. Records that satisfy the parameters in the advanced search. Note that text strings can be used in searching records that describe the station or instrument.

° NORTHRIDGE CA 1994 01 17 0430 PST °

7.3 km: ° SEPULVEDA VA HOSP - BLDG 40 °

USGS station 0637
Site Geology: ALLVM;1280M;SHALE
Summary Page for this Station

Structure: 1-STORY BLDG
Instrument: GROUND LEVEL
View Plot of Data

☐ Add all of this station's data to the download bin Go to Bin

Component: ° 360	**PGA (cm/s/s):** ° 922.7	☐ Add this trace to download bin
Component: ° 270	**PGA (cm/s/s):** ° 738.2	☐ Add this trace to download bin
Component: ° Up	**PGA (cm/s/s):** ° 466.5	☐ Add this trace to download bin

Return to top

° CAPE MENDOCINO/PETROLIA CA 1992 04 25 1106 PDT °

3.8 km: ° CAPE MENDOCINO - PETROLIA °

CSMIP station 89005
Site Geology: CRETACEOUS ROCK
Summary Page for this Station

Structure: INST SHLTR H
Instrument: GROUND LEVEL
View Plot of Data

☐ Add all of this station's data to the download bin Go to Bin

Component: ° 90	**PGA (cm/s/s):** ° 1019.4	☐ Add this trace to download bin
Component: ° Up	**PGA (cm/s/s):** ° 738.9	☐ Add this trace to download bin
Component: ° 0	**PGA (cm/s/s):** ° 1468.3	☐ Add this trace to download bin

Return to top

° IMPERIAL VALLEY CA 1979 10 15 2316 °

29.8 km: ° EL CENTRO ARRY STA 6 - 551 HUSTON RD °

USGS station 5158
Site Geology: ALLUVIUM;MORE THAN 300 M
Summary Page for this Station

Structure: INST SHLTR H
Instrument: GROUND LEVEL
View Plot of Data

☐ Add all of this station's data to the download bin Go to Bin

Component: ° 230	**PGA (cm/s/s):** ° 443.0	☐ Add this trace to download bin
Component: ° 140	**PGA (cm/s/s):** ° 444.3	☐ Add this trace to download bin
Component: ° Up	**PGA (cm/s/s):** ° 1703.6	☐ Add this trace to download bin

Return to top

° Home °+° Login °+° Download °+° About Us °+° Contact °+° Mirror Sites
Earthquakes °+° Stations °+° Search °+° Map °+° Advanced Search

Figure 10 (continued). Second page of results from the advanced search.

COSMOS VIRTUAL DATA CENTER

Consortium of Organizations for Strong-Motion Observation Systems

Home · Login/Logoff · Download · About Us · Contact · Mirror Sites
Earthquakes · Stations · Search · Map · Adv. Search

Download Bin

Start over with a new bin

Earthquake	Station	Instrument	Component	Corrected	Uncorrected
California Strong Motion Instrumentation Program stations:					
NORTHRIDGE CA 1994 01 17 0430 PST	TARZANA CEDAR HILL NURSERY	GROUND LEVEL	UP	Download	Not Available
			90	Same As Above	Not Available
			360	Same As Above	Not Available
United States Geological Survey stations:					
NORTHRIDGE CA 1994 01 17 0430 PST	SEPULVEDA VA HOSP BLDG 40	GROUND LEVEL	360	Download	Download
			UP	Download	Download
			270	Download	Download

Return to an old bin (bins kept for six months):

1. 2000-09-05 19:14:35.437 - 6 trace(s)
2. 2000-05-26 13:57:15.527 - 3 trace(s)
3. 2000-05-22 11:17:56.100 - 9 trace(s)

Home + Login + Download + About Us + Contact + Mirror Sites
Earthquakes + Stations + Search + Map + Advanced Search

Figure 11. Final stage will be transferring data from the respositories to your own computer. After selecting data that have been added to the bin and proceeding to the download, the user sees something like this. One feature is that the database keeps track of previous searches so the user can return and download data that was taken in the past 6 months.

TriNet Engineering Strong Motion Data Center

A.F. Shakal, California Strong Motion Instrumentation Program,
Calif. Dept. Conservation/Div. Mines & Geology
Sacramento, California
and

C.W. Scrivner, California Strong Motion Instrumentation Program,
Calif. Dept. Conservation/Div. Mines & Geology, and
Calif. Institute of Technology, Pasadena
(now at Central Washington University)

Abstract

The TriNet project greatly increases the number of strong motion recordings available after significant earthquakes. A means of communicating that data to the earthquake engineering community in the aftermath of major earthquakes is described, which can be viewed as an Internet based evolution of the customary Quick Reports and full data reports produced after significant earthquakes. A second evolution is that the post-earthquake data collection will be multi-agency. In parallel, the low-amplitude records obtained at modern strong motion stations will routinely be made available through the seismological data center of the Southern California Earthquake Center for seismological analysis.

Introduction

Effective means for disseminating strong motion data for engineering application after major earthquakes is an important goal of the TriNet project. Traditional methods of disseminating data in the aftermath of damaging earthquakes include Quick Reports and similar means. These methods can be significantly advanced by utilization of modern Internet technology, and by combining the data from several networks into one product that is convenient to the user while adequately crediting the source of the data. The data of the TriNet project is a central aspect of this effort, and as the consortium extends statewide, as presently projected, this product can be of even greater convenience for the engineering user of consortium data.

TriNet Project

TriNet is a cooperative effort of three agencies, the California Division of Mines and Geology, the California Institute of Technology and the Pasadena Office of the U.S. Geological Survey. The project was initiated after the 1994 Northridge earthquake with support by the Federal Emergency Management Agency through the Governor's Office of Emergency Service, with additional funds provided by the USGS, CDMG, and Caltech.

The initial station deployment period of the TriNet project will be completed at the end of 2001. By that time a total of 600 stations capable of recording strong motion will be installed in southern California, 200 of which will have real-time, broad-band recording capability, installed by Caltech/USGS Pasadena. The remaining 400 will be classic strong motion stations with near-real-time communication (i.e., communication-on-demand via conventional phone lines and similar means) installed by CDMG. Some additional strong motion stations will have been installed and/or upgraded by the USGS strong motion program.

After all earthquakes in southern California, small or large, the records recovered by the source networks will be transmitted to and made available through the Southern California Earthquake Center (SCEC) data center of Caltech, at http://www.scecdc.scec.org/, to allow seismological analysis. This includes the low amplitude records recorded by strong motion instruments, which will be passed to the SCEC data center and made available for seismological research through that data center. This requires conversion of conventional strong motion data files to the SEED format used in seismological research.

After major earthquakes, up to 600 strong motion recordings may be obtained from the TriNet network. These records, as well as being available through the SCEC data center, will also be available through the TriNet Engineering Strong Motion Data Center, described here, for earthquake engineering utilization and analysis. Use of records from the seismic networks in engineering applications requires conversion of the data from SEED to traditional strong motion formats. Software packages have been developed for the two conversions.

Dual Use of Ground Motion Recordings

A basic bridging concept in bringing together data from the classic seismic networks and strong motion networks is convenient use of the pooled data by both the seismological and the earthquake engineering data-user communities. These two communities customarily access and utilize the data in very different manners. To obtain the full benefit of the recorded data, it must be available to these two user communities in the manner to which they are accustomed.

In the dual-use model, the same ground motion recording is made available through two separate but linked Internet sites – one with products and data in formats customarily used in seismological research, the other with products and data in formats customarily used in earthquake engineering. A key feature of the TriNet inter-agency agreement that makes this practical is that the source agencies will still be credited as the original source of the data. Under this model, the user's task is much simpler, since it is no longer necessary to visit the web site of each agency to perform the needed searches. This paper describes one half of this parallel data-distribution structure.

Engineering Strong Motion Data Center

The TriNet Engineering Strong Motion Data center will share features of the seismological data centers and the COSMOS data center. The COSMOS data center (Archuleta, 2000; this volume) is a virtual data center, which is a key reason for its success. As Archuleta discusses in greater detail, the data center is virtual in that the actual records generally remain on the server of the agency that recorded the data and which is responsible for quality control of the data. This allows that agency to make any necessary corrections as the ongoing process of quality control continues after an earthquake, and relieves the data center of that responsibility. It also helps to ensure that the source agency receives appropriate credit, and is able to describe data usage and customer satisfaction during internal strategic planning and program reviews by the agency.

In a similar way, the TriNet engineering strong motion data center will provide a virtual data dissemination channel for data that resides at the three agencies, and provide appropriate source-agency credit. In addition, this vehicle will serve as an evolutionary electronic version of the "Quick Reports" often produced after major networks.

Northern California Outlook

Although TriNet is limited to southern California, a similar TriNet-like project has been under discussion for northern California for several years, the corresponding partners being the USGS at Menlo Park, UC Berkeley, and CDMG. In the absence of significant funding only limited progress has been possible. A current proposal is that TriNet and its developing northern California counterpart be drawn together into a single statewide network consortium, to be known as the California Integrated Seismic Network (CISN). Once this occurs, an Engineering Strong Motion Data Center would be part of the effort. That data center, like the seismological data centers, would be expanded to include statewide recordings, again with appropriate credit to the source networks. Thus, although the discussion here is focused on TriNet, because it is an element of that project, it is intended that northern California be included in the near future.

Relationship to Quick Reports

It has been customary in the last 15 years for CDMG and some other strong motion networks to produce what are known as Quick Reports after significant earthquakes. These brief reports are rapidly produced and distributed. They contain a tabulation of the peak acceleration values known up to that point and reproductions of images of the most important records, or the most important records that had been recovered since the previous Quick Report. For a major earthquake like Northridge, a series of Quick Reports would be produced, the earliest on the day of the earthquake and the last perhaps 10 days later (e.g., CSMIP, 1994a; 1994b). These reports are then followed by a comprehensive Full Report, containing all data, about 30 days after the earthquake (e.g., CSMIP, 1994c).

Quick Reports serve the information needs of the earthquake engineering community well in the immediate aftermath of an earthquake, and many users give high marks to the effectiveness of this approach. However, they have presented some drawbacks:

Distribution: It is somewhat difficult to distribute even brief reports rapidly to a large number of people (e.g., several hundred). Fax machines can be very slow, and reproduce copies of records poorly. Surface mailings provide good quality images but may take several days to reach a user. Distribution via email is effective, but transmitting a significant number of record images as attachments can present problems for some Internet providers and servers; in addition, delivery time for the email messages can be quite unpredictable.

Independence of Information Packets: Quick Reports are largely independent, in order to be kept small, and are not cumulative – the 4th Quick Report does not contain the records which were in the 3rd, and so forth. Until the Full Report, the information is therefore piecemeal, and users may have difficulty keeping a clear understanding of the earthquake unless they keep each Quick Report at hand.

The data center discussed here addresses these issues and takes the Quick Report concept forward into the electronic Internet world.

Description of Data Center

The main user interface page to the Data Center on the Internet is illustrated in Figure 1. This page will be linked from the TriNet/CISN web pages, and the "Latest Earthquake" link will lead to the electronic analog of the Quick Reports, in a manner similar to the way the most recent TriNet ShakeMap is accessed (e.g., see http://www.trinet.org/shake).

A central feature of Quick Reports, and Full Reports, is a table of peak acceleration values. The parallel to this table is shown in Figure 2 (for which the Hector Mine earthquake is used as an example). The key feature of the table is that it can be cumulative, and updated continuously. If users check the table on the 2nd day after an earthquake, the table will show all data recovered and quality-controlled as of that time. If they check later, they can see from the update time if new information has been added in the intervening time.

The graphic images available in Quick Reports are available from links on the main table in Figure 2. For example, a record image will be received if the user clicks on the "View" under Time Series, and spectra can similarly be requested in the next column. In the case of an analog record, just the image of the accelerogram would appear until the record has been digitized and processed.

Another advance beyond the previous means of releasing data is the ability to present more information about the station, including geology, site conditions, recording

housing, etc. Figure 3 illustrates station information for a ground response station; more information could easily be added. Figure 4 illustrates that, for structures, a photo of the structure will be available as well as an image of the sensor layout and details of the design, so that an engineer can study the location of the sensor relative to key elements of the structure, to analyze the drift, torsion and other aspects of the structural response. For bridges and dams, the sensor layout will similarly show the locations of the sensors on the abutments, bents, deck, crest, etc.

Multi-agency Quick Report through TriNet/CISN

Beyond changes in the means of report delivery through the use of new technology, a major change from previous Quick Reports is that this continuously-updated quick report will be multi-agency. Instead of CDMG reports or USGS reports, there will be a single joint report, which will be electronic. Caltech has for some years deployed strong motion sensors, and more in recent years under TriNet, and that data will be available through this channel. Similarly, UC Berkeley has recently deployed strong motion sensors, and that data can also be included as CISN becomes established.

Link to COSMOS Virtual Data Center

A major focus of TriNet/CISN is rapid information after an earthquake, ranging from the ShakeMap to dual distribution of the data. In contrast, the COSMOS Virtual Data Center has a library of strong motion data extending back to the first records obtained in 1933, and includes data from around the world. The COSMOS data center will link to, and build necessary database tables for, the data in the TriNet/CISN data centers during the days and weeks after the event; it will virtually link to that data as it links to the data maintained by its other contributing agencies (Archuleta, 2000). The COSMOS and TriNet sites will be linked to, and complement, each other. The extensive information needed to do structural analysis of records will not be available in the COSMOS data center, while the extensive search engine and world wide database will not be available in the TriNet data center.

Summary

The TriNet Engineering Strong Motion Data Center is an important product of the TriNet project and is an evolutionary step in several ways. The Data Center:

- Provides access by the earthquake engineering user community to strong motion records of engineering importance recorded by all three agencies in TriNet (CDMG, USGS, Caltech). In a corresponding way, CDMG records for all events will be available through the seismological data center at SCEC.

- Provides an evolutionary path for the Quick Report product to transition into the electronic web environment, providing greater user convenience and more rapid access. This electronic Quick Report product will be continuously updated, so it

is always comprehensive at the time accessed; the user need only download the specific graphic images needed.

- Provides a smooth transitional path for access to records through the long-term COSMOS data center, which has a powerful search engine capability and comprehensive data set from around the world.

- Provides a complete presentation of structural records, including structure descriptions, sensor layouts, and structural design information.

References

Archuleta, R. (2000). "COSMOS Virtual Data Center"; this volume.

CSMIP (1994a). "First Quick Report on CSMIP Strong-Motion Data from the San Fernando Valley Earthquake of January 17, 1994," *Report OSMS 94-01*, Calif. Div. Mines and Geology, Strong Motion Instr. Program, January 17, 1994, 10 pp.

CSMIP (1994b). "Fifth Quick Report on CSMIP Strong-Motion Data from the Northridge/San Fernando Valley Earthquake of January 17, 1994," *Report OSMS 94-05*, Calif. Div. Mines and Geology, Strong Motion Instr. Program, January 25, 1994, 8 pp.

CSMIP (1994c). "CSMIP Strong-Motion Records from the Northridge, California Earthquake of January 17, 1994," *Report OSMS 94-07*, Calif. Div. Mines and Geology, Strong Motion Instr. Program, February 18, 1994, 308 pp.

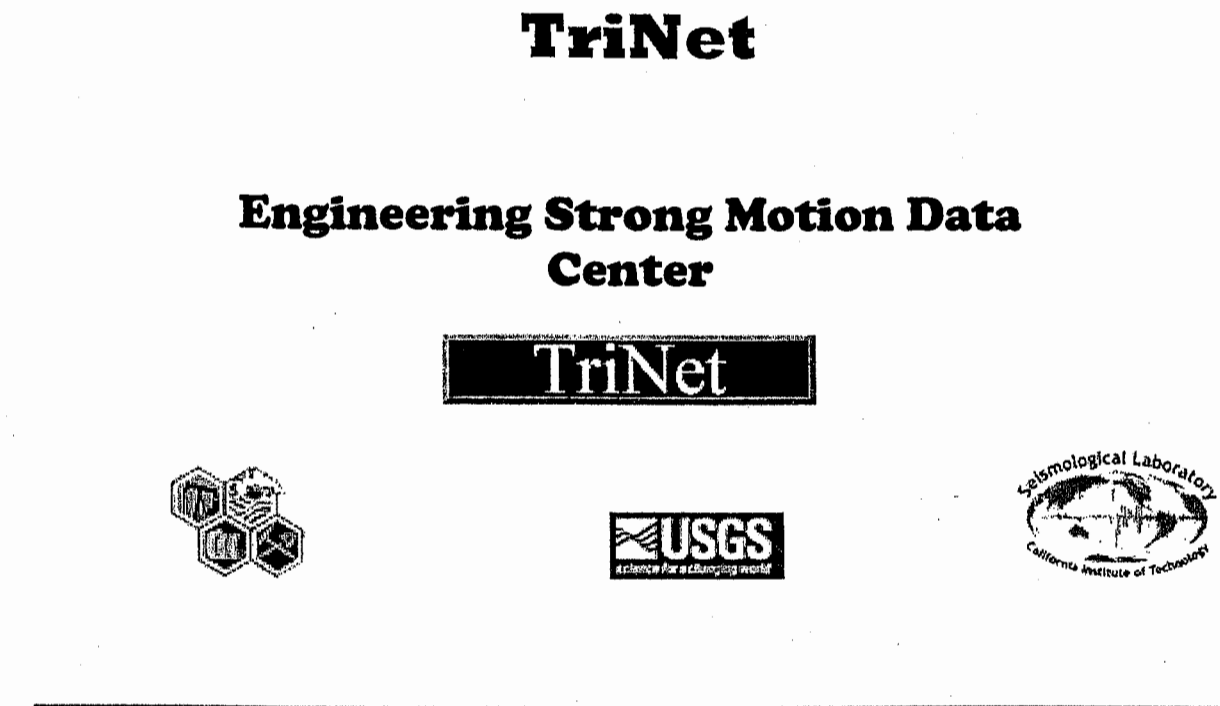

Figure 1. Illustration of main interface to the TriNet Engineering Strong Motion Fata Center, linked from the TriNet home page.

Pooled TriNet Strong-Motion Data Set

-- Data from stations of CDMG, USGS, and Caltech--

(SCSN is a cooperative network of Caltech and the USGS)

M7.1 Hector Earthquake of Oct 16, 1999

For information on Hector Earthquake: Location, magnitude and TriNet ShakeMap

Stations listed in **Increasing Epicentral Distance** (Alternatively, select alphabetical listing)

Stations <100km *100-185km 185-230km*	Station No./ID	Network	Site Type	Dist. (km)	Horiz Apk (g)		Time Series	Spectra	Down-load
					Ground	Struct.			
HEC, Hector	HEC	SCSN		26.1	0.328	--	View	View	Download
Amboy	21081	CDMG	1-story	48.6	0.185	--	View	View	Download
Joshua Tree - Fire Station	22170	CDMG	1-story	52.3	0.191	--	View	View	Download
Morongo Valley - Fire Sta	5071	USGS		66.8	0.086	--	View	View	Download
Big Bear Lake - Fire Station	22791	CDMG	1-story	68.2	0.174	--	View	View	Download
Twentynine Palms - Joshua Tree N.M.	22161	CDMG	1-story	68.6	0.072	--	View	View	Download
Heart Bar State Park	22T04	CDMG	T-hut	68.8	0.082	--	View	View	Download
Los Angeles - 52-story Office Bldg	24602	CDMG	52-story	70.0	0.20	0.71	View	View	Download
Desert Hot Springs - Fire Station	12149	CDMG	1-story	74.1	0.082	--	View	View	Download
Fun Valley - Reservoir	5069	USGS		75.0	0.088	--	View	View	Download
Joshua Tree N.M. - Keys View	12647	CDMG	T-hut	75.4	0.088	--	View	View	Download
Whitewater Canyon	5072	USGS		75.8	0.057	--	View	View	Download
Baker - Fire Station	32075	CDMG		76.7	0.131	--	View	View	Download
Barstow - Vineyard & H St.	23559	CDMG		78.0	0.082	--	View	View	Download
Whitewater Canyon	5295	USGS		79.0	0.063	--	View	View	Download
DAN, Danby	DAN	SCSN		81.6	0.132	--	View	View	Download
Forest Falls - Post Office	5075	USGS		82.0	0.061	--	View	View	Download
Fort Irwin	32577	CDMG		83.2	0.127	--	View	View	Download
Snow Creek	12630	CDMG		87.7	0.029	--	View	View	Download
Cabazon - Post Office	5073	USGS		89.0	0.040	--	View	View	Download

Figure 2. Peak acceleration table, analogous to the acceleration tables in paper reports (e.g., CSMIP 1194a,c). Besides listing peak acceleration the table allows the user to obtain more information about the station (linked through the first column), or view the time series or spectra, or download a zipped file of the data (right columns). Note that the source network is clearly indicated (second column).

Big Bear Lake - Fire Station	Sta.No. 22791
Network:	CDMG/CSMIP

Latitude	34.241N
Longitude	116.872W
Elevation	2100 m
Site Geology	Shallow alluvium over granite bedrock

Return

Figure 3. Example of station information for a ground station, obtained through a link from Fig. 2, for Big Bear station.

Los Angeles - 52-story Office Building, No. 24602

Instrumented by: CDMG/SMIP

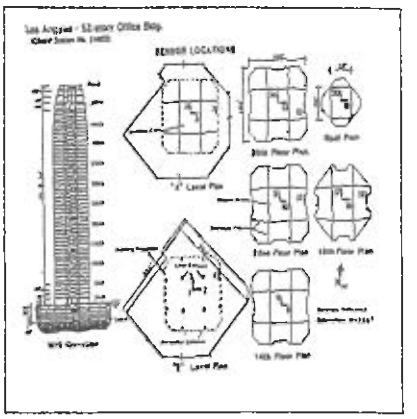

(Sensor Layout - click to enlarge)

Los Angeles - 52-story Office Building **(CSMIP Station No. 24602)**

No. of Stories above/below ground	52 / 5
Plan Shape	Square with clipped corners
Base Dimensions	274 x 263 ft (83.5 x 80.2 m)
Typical Floor Dimensions	156 x 156 ft (47.5 x 47.5 m)
Design Date	1988-90
Instrumentation	20 accelerometers, on 7 levels

Vertical Load Carrying System	3 - 7 in. (7.6 -17.8 cm) concrete slabs on steel deck supported by steel frames.
Lateral Force Resisting System	Concentrically braced steel frame at the core with moment resisting connections and outrigger moment frames in both directions.
Foundation Type	Concrete spread footings, 9 to 11 ft (2.7 - 3.3 m) thick.

Return to Home Page

Figure 4. Example of station information for an instrumented building. The sensor layout can be enlarged for study and printing.